University of Potsdam
Institute of Physics and Astronomy
Applied Condensed-Matter Physics

Three-dimensional Polarization Probing in Polymer Ferroelectrics, Polymer-Dispersed Liquid Crystals, and Polymer Ferroelectrets

Dissertation
in partial fulfillment of the
requirements of the degree of
Doctor of Natural Sciences (Dr. rer. nat.)

submitted to the
Faculty of Science
of the University of Potsdam

presented by Rosaura Flores Suárez

Potsdam, December 2011

Published online at the
Institutional Repository of the University of Potsdam:
URL http://opus.kobv.de/ubp/volltexte/2012/6017/
URN urn:nbn:de:kobv:517-opus-60173
http://nbn-resolving.de/urn:nbn:de:kobv:517-opus-60173

Statement

Rosaura Flores Suárez,
student matric. no. 729003

I, Rosaura Flores Suárez, formally submit my thesis "Three-dimensional Polarization Probing in Polymer Ferroelectrics, Polymer-Dispersed Liquid Crystals and Polymer Ferroelectrets" in fulfillment of the requirements set forth by the regulations for awarding the title "doctor rerum naturalium" (Dr. rer. nat.) in the Science Faculty of the University of Potsdam.

I declare that the work presented in this thesis has not been submitted as an exercise for a degree to any other university.

The work described herein is entirely my own, except for the assistance mentioned in the acknowledgments and collaborative work mentioned in the list of publications. The present thesis work was completed within the "Applied Condensed-Matter Physics" (ACMP) group at the Institute of Physics and Astronomy in the University of Potsdam.

December 2011

Abstract

A key non-destructive technique for analysis, optimization and developing of new functional materials such as sensors, transducers, electro-optical and memory devices is presented. The Thermal-Pulse Tomography (TPT) provides high-resolution three-dimensional images of electric field and polarization distribution in a material. This thermal technique use a pulsed heating by means of focused laser light which is absorbed by opaque electrodes. The diffusion of the heat causes changes in the sample geometry, generating a short-circuit current or change in surface potential, which contains information about the spatial distribution of electric dipoles or space charges. Afterwards, a reconstruction of the internal electric field and polarization distribution in the material is possible via Scale Transformation or Regularization methods. In this way, the TPT was used for the first time to image the inhomogeneous ferroelectric switching in polymer ferroelectric films (candidates to memory devices). The results shows the typical pinning of electric dipoles in the ferroelectric polymer under study and support the previous hypotheses of a ferroelectric reversal at a grain level via nucleation and growth. In order to obtain more information about the impact of the lateral and depth resolution of the thermal techniques, the TPT and its counterpart called Focused Laser Intensity Modulation Method (FLIMM) were implemented in ferroelectric films with grid-shaped electrodes. The results from both techniques, after the data analysis with different regularization and scale methods, are in total agreement. It was also revealed a possible overestimated lateral resolution of the FLIMM and highlights the TPT method as the most efficient and reliable thermal technique. After an improvement in the optics, the Thermal-Pulse Tomography method was implemented in polymer-dispersed liquid crystals (PDLCs) films, which are used in electro-optical applications. The results indicated a possible electrostatic interaction between the COH group in the liquid crystals and the fluorinate atoms of the used ferroelectric matrix. The geometrical parameters of the LC droplets were partially reproduced as they were compared with Scanning Electron Microscopy (SEM) images. For further applications, it is suggested the use of a non-strong-ferroelectric polymer matrix. In an effort to develop new polymer-ferroelectrets and for optimizing their properties, new multilayer systems were inspected. The results of the TPT method showed the non-uniformity of the internal electric-field distribution in the shaped-macrodipoles and thus suggested the instability of the sample. Further investigation on multilayers ferroelectrets was suggested and the implementation of less conductive polymers layers too.

Zusammenfassung In dieser Arbeit wird eine zerstörungsfreie Technik zur Analyse, Optimierung, und Entwicklung neuer funktioneller Materialien für Sensoren, Wandler, Speicher und elektrooptische Anwendungen vorgestellt. Die Wärmepuls-Tomographie (Thermal-Pulse Tomography, TPT) liefert dreidimensionale Abbildungen hoher Auflösung von elektrischen Feldern und Polarisationsverteilungen eines Materials. Bei dieser thermischen Methode wird ein fokussierter, gepulster Laserstrahl durch eine undurchsichtige Oberflächenelektrode absorbiert, welche sich dadurch aufheizt. Die einsetzende Wärmediffusion führt – aufgrund der Wärmeausdehnung des Materials – zu Änderungen der Probengeometrie, welche in pyroelektrischen Materialien einen Kurzschlussstrom oder eine Änderung des Oberflächenpotentials zur Folge hat. Diese wiederum enthalten wichtige Informationen über die räumliche Verteilung elektrischer Dipole und Raumladungen im untersuchten Material. Aus dem gemessenen Kurzsschlussstrom kann anschließend das interne elektrische Feld und die Polarisationsverteilung im Material mittels verschiedener Skalentansformations- und Regularisierungsmethoden rekonstruiert werden. Auf diese Weise ermöglichte die TPT-Methode erstmals die Darstellung inhomogener ferroelektrischer Schaltvorgänge in polymeren ferroelektrischen Filmen, welche mögliche Materialien für die Datenspeicherung sind. Die Ergebnisse zeigen eine typische Haftschicht im ferroelektrischen Polymer und unterstützen die Hypothese einer ferroelektrischen Umpolung auf einer der Korngröße äquivalenten Längenskala über Keimbildung und anschließendes Wachstum. Um die Lateral- und Tiefenauflösung zu untersuchen, wurden sowohl die TPT-Methode als auch die äquivalente Methode in der Zeitdomäne (Focused Laser Intensity Modulation Method, FLIMM) auf ferroelektrischen Filme mit Gitterelektroden angewendet. Die Ergebnisse beider Techniken zeigen nach der Datenauswertung mit unterschiedlichen Regularisierungs- und Scale-Methoden eine vollkommene Übereinstimmung. Des weiteren stellte sich heraus, dass bisherige Untersuchungen der lateralen Auflösung von FLIMM diese möglicherweise überschätzen. Damit behauptet sich TPT als effiziente und verlässliche thermische Methode. Nach einer Optimierung der Optik wurde die TPT-Methode in polymerdispergierten Flüssigkristallen (Polymer-Dispersed Liquid Crystal,PDLC), welche in elektrooptischen Anwendungen von Interesse sind, angewendet. Die Ergebnisse deuten auf eine mögliche elektrostatische Wechselwirkung zwischen den COH-Gruppen des Flüssigkristalls und den Fluoratomen der verwendeten ferroelektrischen Matrix hin. Die durch rasterelektronenmikroskopische Aufnahmen (scanning electron microscopy, SEM) gewonnenen geometrischen Parameter der Flüssigkristalltröpfchen konnten mittels TPT reproduziert werden. Für weitere Anwendungen werden schwach ferroelektrische Polymermatrices vorgeschlagen. Im Bestreben neue polymere Ferroelektrete zu entwickeln und deren Eigenschaften zu optimieren, wurden neuartige Mehrschichtsysteme untersucht. Die Ergebnisse aus der TPT-Methode zeigen eine Abweichung der Uniformität der inneren Verteilung des elektrischen Feldes in den geformten Makrodipolen, was auf eine Instabilität der Probe hindeutet. Ebenfalls wurden weitere Untersuchungen an Mehrschicht-Ferroelektreten und die Anwendung von halbleitenden Polymerschichten vorgeschlagen.

Acknowledgements

I would like to thank Prof. Dr. Reimund Gerhard and Prof. Dr. Axel Mellinger for their scientific support during my PhD studies. Thanks to ACMP group members from the department of Physics and Astronomy, at the Potsdam University. Dipl. Ing. Werner Wirges thank you for being the technical soul of my experiments and for cheering me up whenever I needed. Likewise to Dr. L. Meena Ganesan for her scientific collaboration during the studies on polymer dispersed liquid crystal (PDLC) samples. Thanks to Dr. Xunlin Qiu and Dipl. Phys. L. Holländer for the scientific collaboration related on the new multilayer ferroelectrets. Thanks to Marco Schreiber for the experimental help on ferroelectric switching. Sandra Zeretzke helped on many bureaucratic moments and Dr. Denis Mc Carthy corrected some chapters of this Thesis. Thanks to Prof. Dr. Anca Petre, Dr. Cong-Duc Pham and Dr. Laurent Berquez for the scientific collaboration and stimulating discussions at the Paul Sabatier University, Toulouse. A special thank to Prof. Dr. Sigfried Bauer and Dr. Simona Bauer-Gogonea for their fruitful discussions and the high-energy "injections".

Deseo agradecer a mis padres Elena y Roberto por el apoyo incondicional a casi todos mis proyectos. Su amor y dedicación son base de mi vida. Dedico este trabajo también a mis hermanos Rosalba, Ricardo, Roberto y Raúl. Por supuesto, agradezco a mi adorado esposo Ronald por confiar en mi y por motivarme a terminar con la escritura. Gracias explicitas a Dr. R. Schwein and Dr. habil. M. de Kee por *convivir juntos* estos años en Potsdam. Mi admiración a las mujeres y hombres que pese a tantas millas de distancia, me siguen brindado su amistad: Claudia, Laura, Lili, Dianis, Gerardo, Danny, Cuauhtli, Oscarín, Pedrito, Ildaura, Norma, Charo, Tere, Prof. Dr. Lulú, Prof. Dr. José, Monsita, Alberta, Antonia, Flores Mexicanas y amigos de la misión en Berlín.

Last but not least, many thanks for the lovely support to Terris group (*specially to Meena*), Francisco, *JASM* and Familie Göbel.

Contents

Chapter 1

Introduction

Most of the electronic devices to which we have access in our daily life are manufactured with polymers, not only as packing but also as functional materials. Most of these polymers are synthetic. The advantage of using them is based on their flexibility and relatively low cost. Their mechanical and chemical properties can be enhanced during the synthesis by adding other monomers. Depending on the structural unit, the polymers or copolymers can be polar or non-polar. The former ones contain dipole moments and the stability of the polymer is dependent on its configuration. The stereoisomerism dictates whether the bulk presents a neat polarization or neutrality. A certain configuration can be modified by mechanical drawing and poling (application of high electric fields) at certain temperature and pressure conditions. This process may lead to orientation of domains in the bulk.

Application of mechanical stress in some of the polar polymers produces an electric displacement. The phenomenon is known as piezoelectricity. Other polymers generate an electrical current when they are thermally stimulated [1]. These materials are known as pyroelectric. All pyroelectric materials are also piezoelectric, since the polarization in the material not only depends on temperature (pyroelectricity) but also on pressure (piezoelectricity) [2]. Since pyroelectricity and piezoelectricity refer to 2nd derivative of the free energy of the material, there are two more effects that should be mentioned: The electrocaloric effect and inverse piezoelectricity [3]. Some of the pyroelectric polymers can reverse the direction of the spontaneous polarization after application of sufficient high electric fields. These materials are known as ferroelectrics.

One of the most studied ferroelectric polymers (because of its many applications in memory devices, sensors, ultrasound, large area spacecraft, etc) is polyvinylidene fluoride (PVDF) [4]. This polar polymer has several configurations, known as α-, β-, γ- and δ-phase. The α-phase is thermodynamically stable, but non-polar. The β-phase is polar and provides the ferroelectricity in PVDF. The γ-phase is polar, but the ferroelectric activity is not as high as for the β-phase. Copolymers with trifluoroethylene are usually more crys-

talline than the homopolymer PVDF. The β-phase is stable and depending on the TrFE content a rich phase transition sequence is a well documented in the literature [5]. P(VDF-TrFE) is the material of choice in memory devices [6], sensors and actuators [7, 8, 9, 10].

Ferroelectrics have also been used as matrix in Polymer-Dispersed Liquid Crystals (PDLCs). These new materials are of interest in electro-optical applications [11]. The characteristics of the former can be tailored by means of mechanical- or electrical stress. In the case of a ferroelectric matrix, the electrical stress causes an alignment of dipoles in the bulk [12,13]. A polarization profiling of the system, for instance liquid crystal droplets immersed in PVDF-TrFE, would provide information not only about the droplet parameters, but also about their influence on the polymer matrix.

Ferroelectrets also show a hysteresis-like loop when the applied electric field exceeds a threshold value [14]. These materials are based on non-polar polymers and present pyro- and piezoelectric activity after charging [15]. The magnitude of the pyroelectric effect is lower than that of PVDF, but the piezoelectric effect can be one or two order of magnitude higher than in PVDF [16]. The clue in ferroelectrets is their cellular nature. After charging the voids in the foam, macroscopic dipoles are formed which can be deformed by mechanical stimulation, resulting in piezoelectricity [17]. Cellular polymers are applied in thermal and/or electrical insulation, packaging vibration damping, etc, and after charging as piezoelectrets. In the last two years efforts to achieve stable multi-layer ferroelectrets have been carried out [18]. Some systems were built up using laser-perforated voids in fluoropolymer films. Information about the piezoelectric and the pyroelectric coefficients of those systems is needed in order to find suitable materials and void geometries.

Ferroelectric polymers, PDLCs and ferroelectrets need to be electrically poled or charged to be used as functional materials. To learn more about the poling or charging process, it is desirable to have a look on the polarization distribution in the thickness and lateral dimension of these materials. This work contributes to the progress in the understanding of charge- and polarization-distribution in ferroelectric polymers, PDLCs and ferroelectrets.

Several techniques based on acoustic or thermal stimulation are available to study the space-charge and polarization distribution in dielectrics [19]. The acoustic method uses a discontinuous pressure that propagates in the sample causing a deformation [20, 21]. The dimensional changes originate a current or voltage due to an electric displacement. The acoustic methods have been applied for thick samples in the millimeter range. Some of these methods are, however, destructive and modify the chemical and physical properties of the sample during the experiment. Several non-destructive thermal methods use sinusoidal thermal waves [22] or pulses [23] to vary the temperature inside the dielectrics. The first technique is known as Laser-Intensity Modulation Method (LIMM) and the latter method

as Thermal-Pulse (TP). LIMM is implemented in the frequency domain, while TP works in the time domain. The thermal expansion causes a decrease in the dipole density and an electric displacement is generated as well. The measured signal in acoustic and thermal methods, either current or voltage, contains the information of the space-charge or polarization distribution. The acoustic and thermal methods complement each other because, while the former techniques offer a constant resolution in the whole sample, the latter methods have a high resolution near the irradiated surface of the sample. More recently the thermal techniques have been updated to measure distributions in three dimensions. They are known as Focused LIMM (FLIMM) [24] and Thermal-Pulse Tomography (TPT) [25]. The tomography on a dielectric gives an extended view of the poling process and it may help to assess the mobility of space charges.

The measured electrical signal needs to be deconvolved, since it is related to the charge and polarization distribution via a Fredholm integral equation of the first kind. This is an ill-posed problem and therefore has many different solutions. In the 1970s, solutions were approximated by De Reggi et al. [26] and Von Seggern [27] using Fourier coefficients. In the 1980s, Lang and Das-Gupta carried out the data analysis by using ordinary least squares [28]. In the beginning of the 1990s, a simple method was introduced by Emmerich and co-authors known as the Scale Transformation (ST) [29]. The advantage of the ST over the previous methods is that a polarization profile can be obtained from the raw data and it is very fast in computational terms. Some other regularization methods have been used. One of the most implemented is the Polynomial Regularization L-Curve Method (PRMLC), first published by Lang in 2004 [30]. In this method, an eighth-degree polynomial is calculated and then introduced on the Fredholm integral. After calculating the weight parameter from the L-Curve method, the polarization distribution inside a dielectric can be found by minimizing an equation containing a data fit residual and a roughness residual. In 2005 the Monte Carlo technique was presented by Tuncer and Lang as a promising method to solve the ill-posed problem [31]. This method needs to solve a least-squares problem in terms of a matrix and vectors. The variation of the temperature with the time is represented by a matrix and the pyroelectric current is written as a vector. The polarization distribution, which is averaged after many cycles, is also expressed as a vector. The MC method requires more computation time than regularization and scale transformation techniques.

The resolution of all methods is a matter of discussion [19, 32]. Many publications do not specify whether the reported resolution is on the sample thickness direction, or on the sample surface direction. The former is also known as depth resolution and the latter as lateral resolution. Some reviewers defined resolution as *the width of the smallest feature in the distribution accurately represented in the measured profile.* Thermal techniques like LIMM, reported 1 µm resolution in the thickness direction, while FLIMM claimed a lateral

resolution down to 10 µm. The TPT setup offers a depth resolution of 0.5 µm. Its lateral resolution, defined as the width of the transition between poled and unpoled areas in a dielectric, was similar to the smallest spot size, around 38 µm. The lateral resolution of TPT is limited due to a faster thermal diffusivity of the thermal pulse on the metal electrode than in a polymer. The diffusivity of the metal electrodes is three orders of magnitude higher than the diffusivity of a polymer like PVDF. Another limitation to focus the laser spot size to smaller diameters than 30 µm is the simple lenses used in the TPT setup, which suffer of spherical aberration.

In this thesis, several polarization profiles on polyvinylidene fluoride copolymer with trifluoroethylene P(VDF-TrFE), on a liquid crystal dispersed in P(VDF-TrFE), and on a three-layer system built up by a cover lid of polycarbonate (PC), and an adhesive tape as middle layer and a bottom layer of PC were measured by means of the Thermal-Pulse Tomography.

Chapter 2

Concepts and materials

2.1 Pyroelectricity

The phenomenon of pyroelectricity was probably first observed by the Greek philosopher Theophrastus [2]. In his account, the property of attracting straw and bits of wood by a stone (most probably the mineral tourmaline) was described. In other words, he observed electrostatic charges produced by temperature changes. Pyroelectricity was also described in the Middle Ages, though quantitative studies did not start until the nineteenth century [33]. Pyroelectricity is a property of anisotropic solid materials defined as the temperature dependence of the spontaneous polarization, P_{s}, in the bulk. The spontaneous polarization in a pyroelectric material refers to its dipole moment per unit volume. If the material is subjected to changes of temperature, then the dipole moment will change and so will the spontaneous polarization. A temperature change in a pyroelectric material will generate a current flow if the ends are metallized and short-circuited. This current, called the pyroelectric current, is a consequence of the redistribution of free charges on the electrodes after the dipole moment changed [2]. As its Greek name describes the phenomenon, pyro: heat and electricity, this effect is only observed on variation of the temperature. Mathematically, the pyroelectric coefficient is defined by

$$p = (\partial P_{\mathrm{s}}/\partial T)_{\sigma,E} \tag{2.1}$$

where p is the pyroelectric coefficient (with units $\mu\mathrm{C/m^2K}$), P_{s} the spontaneous polarization, T the temperature, and σ, E represent the constraints of constant elastic stress and constant electric field, respectively. After an increment of temperature, a material expansion occurs which produces a strain that affects the electric displacement, in other words a piezoelectric effect is generated. This is known as the secondary pyroelectric effect. Experimentally, primary and secondary effect are measured together.

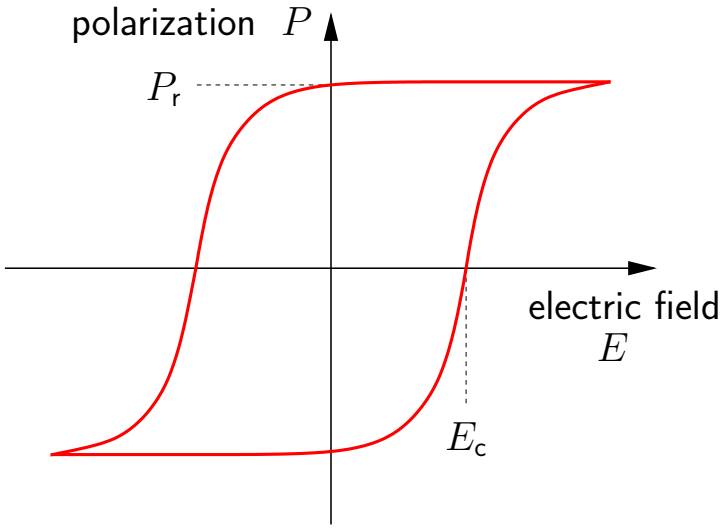

Figure 2.1: Polarization/electric field hysteresis loop. The remanent polarization P_r and the coercive field E_c are shown.

2.2 Ferroelectric materials

Among the main application of these materials are IR detectors and thermal imaging. The first trials on IR detectors were based on ceramics. During the 1960's thermal imaging using pyroelectric materials was possible and ten years later they were employed on spacecrafts. Ferroelectrics are pyro- and piezo-electric materials that can reverse the direction of their spontaneous polarization via high electric field, yielding a polarization/electric field hysteresis loop (Fig. 2.1). The remanent polarization P_r is defined as the amount of polarization remaining after the poling field is removed [34]. The coercive field E_c is the field required to switch half of the already induced remanent polarization. The ferroelectricity is restricted to temperatures below the Curie temperature, T_c , above which the materials become paraelectric. The most frequently used ferroelectrics are ceramics like lead-zirconate-titanate (PZT) or barium titanate ($BaTiO_3$). Semi-crystalline polymers have also found their way into diverse applications. Polyvinylidene fluoride (PVDF) and its copolymers with trifluoroethylene (TrFE) are an example of these new materials. The homopolymer does not show the Curie point (T_c) because the ferroelectric phase melts below this temperature. On the other hand, the Curie temperature of the copolymer P(VDF-TrFE) is shifted linearly towards lower temperatures with increasing TrFE concentration [35].

2.2.1 Polyvinylidenefluoride (PVDF) and its copolymers with trifluoroethylene

These ferroelectric polymers are the most preferred sensors for applications in the MHz range. They are also used as actuators in pharmaceutical, chemical, electrical, and architectured areas among others. The sensors made from PVDF and P(VDF-TrFE) have a great impact in medical applications because of the similarity in acoustic impedance between PVDF and water. Thus, medical ultrasound imaging of mammals and living tissue can be performed [7,8]. Moreover, PVDF is a biocompatible polymer that makes it attractive for producing prostheses, artificial tissues and bone healing. Piezoelectric PVDF films have been employed as sensors in space [9, 10]. When hypervelocity dust particles impact these sensors, an induced depolarization charge is detected.

PVDF polymers are synthesized either by emulsion or suspension polymerization and therefore the physical, mechanical, thermal and chemical properties vary. The piezoelectricity of this polymer was reported for first time by Kawai [4]. In his work, it was stressed that a stretching process at temperatures higher than the glass transition temperature T_g , followed by the application of high voltages, is needed in order to observe piezoelectricity. Fukada and Sakurai [36] published the changes of the complex piezoelectric constant of PVDF in a temperature range between (-150 °C to 150 °C). The authors concluded that the piezoelectricity is a result of variation of the spontaneous strain due to orientation of dipoles after the application of an electric field, which is known as the inverse piezoelectric effect.
PVDF has different crystalline phases which are present in the sample depending on the preparation conditions. The high piezoelectric activity depends on the crystalline polar phase named β. The best known crystalline phases are called α, β and γ [37, 38]. The α phase has a certain degree of polarity; however, on a macroscale the phase with a trans gauche trans gauche conformation (TGT$\overline{G}$) is non-polar (Fig. 2.2b). The most important phase is β, since it is polar and shows the highest ferroelectric activity. The origin of this property comes from the slightly deflected planar zigzag conformation, known as trans trans (TT). Therefore all the dipole moments are pointed in the same direction (Fig. 2.2a). The dipole moment, μ, of a monomer is approximately $7 \cdot 10^{-30}$ C·m. The γ phase is a polar phase, which favors a parallel packing and, in comparison to β phase, offers low piezoelectric activity. The conformation is known as trans gauche trans gauche ($T_3GT_3\overline{G}$) (Fig. 2.2c). A PVDF polymer film normally presents the non-polar α phase. In order to obtain the polar β phase, the polymer film must be stretched, poled by means of very high electric fields and annealed at temperatures higher than the glass-transition temperature. Vibrational spectroscopy have been used to study the transitions from $\alpha \rightarrow \beta$ phase [38].

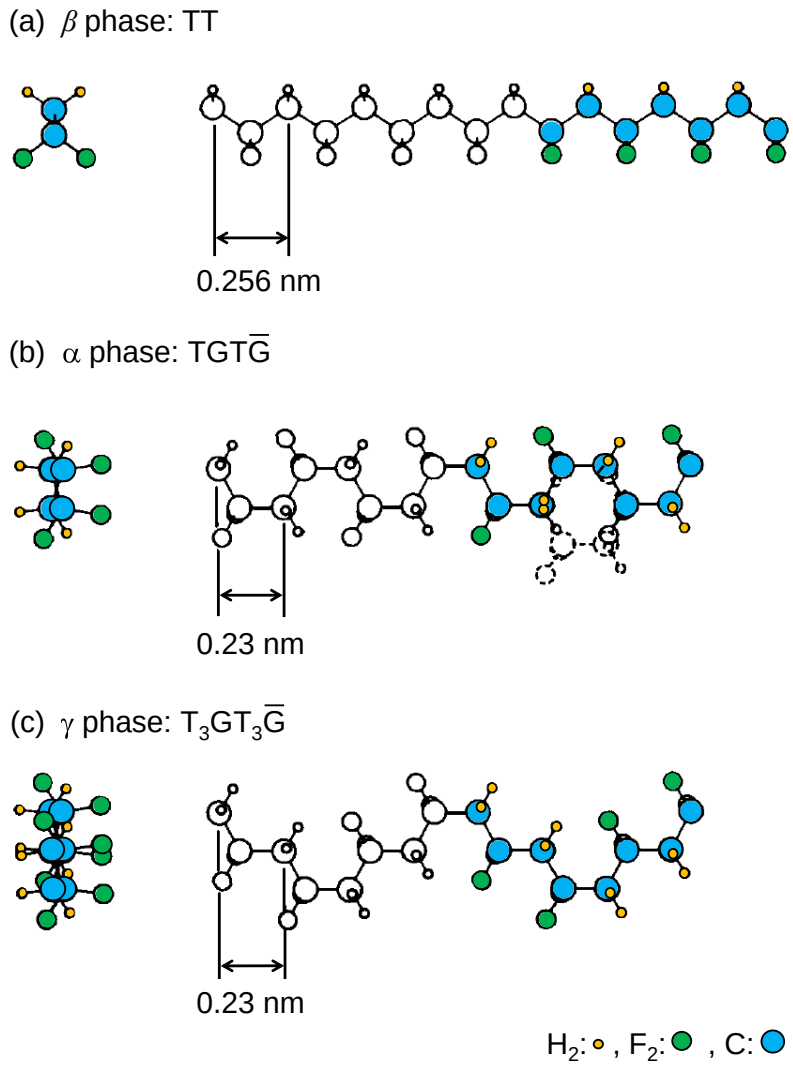

Figure 2.2: PVDF crystalline phases,(a) β or TT conformation,(b) α or TGT$\overline{G}$ conformation and (c) γ or $T_3GT_3\overline{G}$ conformation [5].

The copolymers of PVDF are synthesized by suspension or emulsion polymerization. The polyvinylidene fluoride with trifluoroethylene P(VDF-TrFE) is a random copolymer and has excellent mechanical properties (high elasticity), chemical resistance, high temperature capabilities and is easily processed by extrusion. The copolymer exhibits greater thermal stability than the homopolymer. The interesting properties appear when the TrFE content is higher than 11%. If this requirement is fulfilled, then a polar phase similar to β phase (Fig. 2.2a) forms upon cooling from melt, without the need for mechanical stretching. In table 2.1 there is a comparison of the most important parameters of the homopolymer and the copolymer with TrFE.

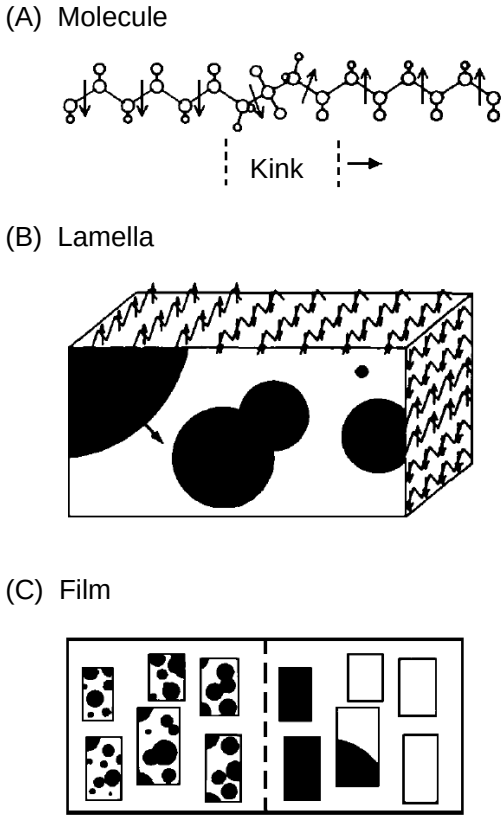

Figure 2.3: Mechanism of the polarization reversal on PVDF [5].

2.2.2 Switching phenomena

The dipole reorientation of the homopolymer has been detected with X-ray diffraction. The shape of the hysteresis loop shown in Fig 2.1 depends on the crystallinity and, in the case of copolymers, on the comonomer content. In copolymers with TrFE, the polarization reversal is evident whenever the VDF content is above 50%. According to Furukawa [5], this might be related with the loss of ferroelectricity, i.e. the dipole moment of TrFE is smaller than VDF. The mechanism of the ferroelectric polarization reversal has been described as a nucleation-growth process (Fig. 2.3),

(A) Reversal of some dipoles is propagated along a single chain molecule,

(B) Chains rotate their dipoles along a plane in the lamella,

(C) The new reversed crystalline lamellas aggregate in the bulk.

The switching process in PVDF and its copolymers needs a higher electric field than in ceramics [39]. The factors influencing this process are divided between structural and

electrical factors. Crystallinity, thickness of the films and electrode material belong to the first group. In order to increase the crystallinity, Furukawa group annealed their samples at 145 °C [6, 40, 41]. Films from few micrometers down to 100 nm thickness are preferred. Gold electrodes are commonly used instead of aluminum, since the latter oxidizes and hinders the polarization reversal. The second category considers mainly the field strength and number of cycles applied during the poling process. The typical values of coercive field and remanent polarization for PVDF and its copolymer with TrFE are presented for comparison with a ceramic known as lead zirconate titanate (PZT):

Table 2.1: Electric parameters of the most known ferroelectrics.

Ferroelectric	Dipole moment	Coercive field	Remanent polarization	Piezoelectric coefficient	Pyroelectric coefficient
	μ	E_c	P_r	d_{33}	p_3
	(C· m)	(MV/m)	(mC/m^2)	(pC/N)	(µC/m^{2}K)
PVDF	$7 \cdot 10^{-30}$	50 to 100	60	-20	20
P(VDF-TrFE) 65/35	$5.7 \cdot 10^{-30}$	60	60 to 100	-38	35
$Pb(Zr_{0.95}Ti_{0.05}O_3)$	–	≥1.5	340	360	270

More recently Sakai et al. [40] mentioned the phenomenon of fatigue, which is the decrease of the remanent polarization P_r after repetitive application of electric field cycles. This behavior is of importance when the films are to be used in memory devices. Fatigue may result in breakdown as well. In their publication, Sakai et al. investigated films after 10^4 cycles and concluded that fatigue is linked to a nonuniform polarization distribution on the films. They proposed the existence of pinned layers on the top and bottom electrodes and a mechanism for the evolution of the polarization reversal. The metal-ferroelectric-semiconductor (MFS) capacitor is very attractive because of its application in nonvolatile memory devices. MFS containing PVDF-TrFE films are prepared by means of spin-coating. In 2009, Furukawa et al. investigated the polarization reversal in the copolymer and its correlation with accumulation-depletion-inversion on silicon (Si) substrates [41].

2.2.3 Polymer-Dispersed Liquid Crystals (PDLCs)

Liquid crystals (LCs) are a state of matter with properties between those of a conventional liquid and those of a solid crystal. Their main applications are flat panel displays. Dispersions of liquid crystals have an impact on electro-optical applications. Dispersions of LC droplets in a polymer matrix are called polymer-dispersed liquid crystals (PDLC) and they are more flexible than the conventional LC [11]. The studies on these dispersions have reported improved properties after a pre-alignment of the LC in the PDLC film by means of mechanical or electrical stress [12]. The application of the pre-orientation allows

fast switching in ferroelectric LC in PDLC displays. More recently the interfacial effect of the LC molecules and the ferroelectric polymer matrix (P(VDF-TrFE)) was reported [13].

2.3 Ferroelectrets

The novel cellular space-charge electret polymers have applications in sensors and actuators. Ferroelectrets are internally charged cellular polymer electrets that show piezo- and pyroelectricity [17, 15, 42, 43, 44]. The main difference between this type of materials and the well-known ferroelectrics like PVDF is that their piezo- and pyroelectricity do not originate from symmetry breaking at a nanoscopic level but on a macroscopic level. The first cellular polymers with piezo- and pyro-electric properties were prepared using polypropylene (PP) [45, 46]. The ferroelectrets were charged by means of corona discharge, direct contact charging and electron-beam poling. Paschen breakdown occurs inside the voids; this is evidenced by light emission (Fig.2.4) [47, 48]. The result is a film with internally charged voids which are macroscopic dipoles. The threshold voltage V_{th} for breakdown is an analogue to the coercive field in common ferroelectrics [14]. The piezoelectricity originates from the deformation of these dipoles under mechanical stress (known as the direct piezoelectric effect) or electrical stress (known as the inverse piezoelectric effect). Likewise, the increment of temperature causes a thermal expansion and so an expansion of the voids, which results in an increment of film volume. Thus, there is an increment of the macroscopic dipole moments of the voids which originates the pyroelectricity. The typical values of pyroelectric coefficients in ferroelectret foams are quite small, ca. two orders of magnitude smaller than those for conventional polar polymers like PVDF [16].

One of the first studies on the polarization distribution in porous electrets was performed by van Turnhout et al. [49]. The authors used the thermal-wave method (see section 3.2.2) and the approximation method to obtain and analyze the data, respectively. A more recent study on cellular polypropylene by means of thermal techniques was reported by Neugschwandtner et al. [16]. They found out that the thermal-pulse response contained electromechanical oscillations. The vibrations were correlated with the piezoelectric thickness, width and length resonances. A quantitative calculation of the pyroelectric coefficient $p = 0.25$ µC/m^{2}K was done. The stability of the pyroelectric effect was investigated as well. The typical electrical parameters that characterized the PP foams are given in the following table:

Table 2.2: Electrical parameters of the most known ferroelectret.

Ferroelectret	Threshold voltage	Effective charge density	Piezoelectric coefficient	Pyroelectric coefficient
	V_{th}	σ_{eff}	d_{33}	p_3
	(kV)	(mC/m^2)	(pC/N)	(µC/m^{2}K)
cellular PP	3.0	0.5	$\geq$400	0.25

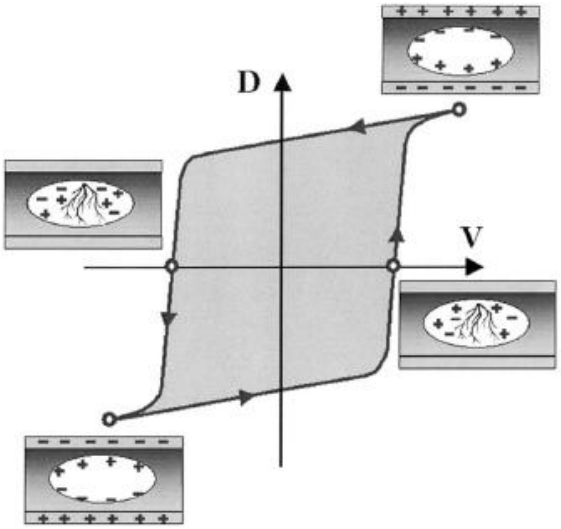

Figure 2.4: Hysteresis-like loop in cellular polymers [17]

An attempt to obtain ferroelectrets from different dielectric materials was performed by Basso et al. [18] using a multilayer ferroelectret system. This consisted of three layers, top and bottom lids (fluorinated ethylene-propylene (FEP)) were thermally fused to a perforated (either laser- or mechanically drilled) polytetrafluoroethylene (PTFE) film. The resulting sandwich system was 160 µm thick. The charging process above the threshold for Paschen breakdown [50] generates a micro-plasma discharge. To generate macroscopic dipoles, the charges have to be separated and then deposited on the internal surfaces of the voids. The piezoelectric response of the multilayer system depends on the deformation of the voids.

Chapter 3

Methods to measure polarization and space-charge profiles

Many techniques have been developed to obtain information about polarization and charge distribution in dielectric materials. Examples of these are: acoustic methods and thermal methods. It is known that acoustic and thermal methods complement each other because of the constant resolution in the whole sample thickness and the high resolution near the irradiated surface of the electret, respectively. Therefore, acoustical methods are suitable for relatively thick films (<1 mm) and thermal methods are optimal for thin samples (up to 200 µm) [19, 51]. The resolution of these techniques was referred to that in the sample thickness direction. In a recent review of the advances in the measurement of space-charge and polarization profiles, Fleming [32] discussed the definition of spatial resolution. According to the author, an intuitive definition would be "the width of the smallest feature in the distribution accurately represented in the measured profile". The acoustic and thermal methods are discussed in further sections taking this definition into account. However, the discussion will be focused on the thermal techniques.

3.1 Acoustic techniques

These methods, first suggested in the late 1970s and beginning of the 1980s, use a discontinuous pressure which is generated by means of laser or voltage pulses in the bulk or at the sample surface [52](Fig.3.1 left). The methods are known as Laser-Induced Pressure-Pulse (LIPP) [53, 20], Piezoelectrically generated Pressure-Step (PPS) [21, 54] and Pulsed Electro-Acoustic (PEA) techniques [55, 56]. This pressure propagates in the sample with the velocity of longitudinal sound waves. The resulting deformations generate a current due to charge displacement, changes in dielectric permittivity or the piezoelectric effect. The current or voltage contains the information of the space-charge or polarization distribution. The spatial resolution (thickness direction) was reported to range from 1 to 3 µm [57].

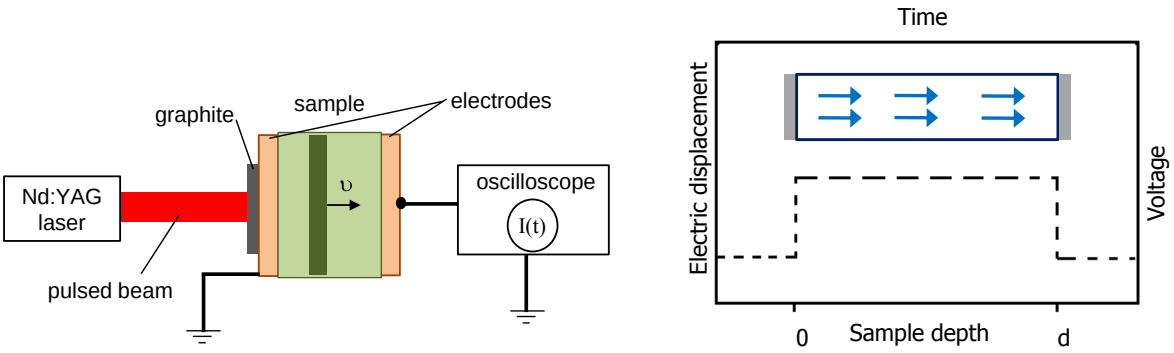

Figure 3.1: Laser-Induced Pressure-Pulse (LIPP) setup for two-sided metallized samples (left) [58] and schematic response of a homogeneously poled sample using PPS method (right) [63]

.

These values are calculated as the product: rise-time of the pressure pulse × the speed of sound in the material. Initially, the resolution of the LIPP method raised to 30 µm [53]. This value was calculated considering a laser pulse duration of 5 ns FWHM (Full Width at Half Maximum), i.e. the duration of the pressure pulse in the material was higher than 15 ns, and a 2 km/s pressure-pulse speed in polymer samples. In view of these limitations, Sessler et al. [20, 58] used light pulses of 70 ps duration i.e. the detected rise time in the sample was better than 0.5 ns, then an optimal resolution of 1 to 3 µm was reached. Later, the Piezoelectrically generated Pressure-Step (PPS) Method was introduced [21, 54]. Voltage pulses are generated by a cable discharge generator, these excite a piezoelectric quartz plate and the pair of pressure steps can be efficiently coupled to the sample by using silicone oil. The result in a charged or poled sample is the generation of a piezoelectric current. The electrical signal is converted to a voltage by a pre-amplifier and monitored by an oscilloscope. The resolution of the PPS method is ca. 2 µm and depends on optimal electronics and the velocity of the sound in the sample. A homogeneously poled sample produces a step signal (Fig.3.1 right.) The PEA technique [55, 56] first implemented in 1985, used a voltage-pulse duration ranging from 5-40 ns, then the best achievable resolution was 80 µm due to the longer time for the pressure pulse to propagate to the transducer [59]. The resolution was later improved to ca. 2 to 3 µm by using a FFT deconvolution [60, 61].

In conclusion, the advantage of the acoustic methods is that the distribution of the space charges and the polarization is easily obtained from the measured electric response. They are non-destructive methods, designed mainly for planar geometries. Even though studies on polarization depth profiles in piezoelectric sensor cables were performed with acoustic methods, the geometry was modified and the resulting profile was an average over the angular coordinate [62].

3.2 Thermal techniques

The Laser-Intensity Modulation Method (LIMM) and the Thermal-Pulse (TP) method are the best known non-destructive thermal techniques. The techniques are performed in the frequency domain and in the time domain, respectively. The variation of temperature with time inside the material is caused by the absorption of a periodically modulated laser beam (LIMM) or a short light pulse (TP). The measured signal, either current or voltage contains information about the spatial distribution of the spontaneous polarization in a ferroelectric material. In order to carry out the data analysis, the thermal diffusivity of the sample should be known. The strong non-uniform spatial resolution through the material should be remarked; this is caused by the diffusive nature of heat. The determination of the polarization distribution from the measured electrical signal is rather complicated, since a deconvolution process is needed. The resolution is high near the irradiated electrode, but it decreases rapidly, as will be discussed in the next section. Due to the limited resolution, thermal techniques are most suitable for thinner samples.

3.2.1 Thermal-Pulse Technique

In 1975, Collins introduced the Thermal-Pulse method (Fig.3.2) which allowed him to study the charge distribution in materials containing both fixed charges and permanently aligned dipoles [23]. In his work, a non-uniform temperature on a copolymer film of tetrafluoroethylene and hexafluoropropylene (FEP) was generated with a short light pulse (<100 µs), produced with a gas discharge tube. One year later, Collins suggested that a deconvolution procedure would have to be performed to obtain information on the charge distribution. The non-uniqueness of the charge and polarization distributions is also mentioned. At the same time, the author points out the high depth resolution of this thermal technique near to the heated electrode.

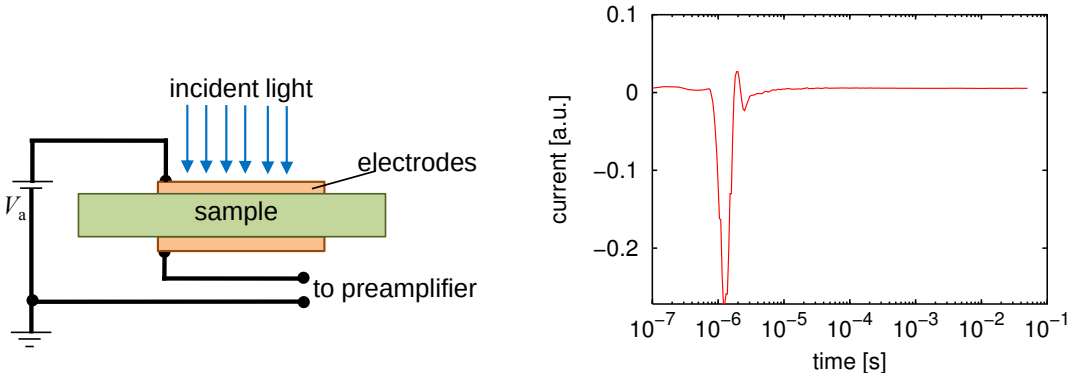

Figure 3.2: Thermal-Pulse setup for two-sided metallized samples [64] and raw spectrum of the measured electric signal [65].

Many attempts have been focused to yield a unique solution. For instance, De Reggi et al. [26] established that the charge or polarization distribution can be approximated by Fourier coefficients which can be determined by using graphical analysis or numerical calculations. They could obtain up to fifteen coefficients from Collins' experimental data. Later, Collins [64] reported several details about the experimental procedure of the Thermal-Pulse technique. For example, he mentioned an equivalent circuit for an electret in TP experiments as well as the need of either a voltage or charge amplifier to enhance the signals generated by the electret. The author associated the thickness of the samples with the resolution. It was found that the electrodes should be thinner than the sample, however extremely thin electrodes increase noise in the signal. Collins discussed the work of De Reggi et al., emphasizing that the shape of voltage pulse is still a good indicator of the existence of a surface charge distribution.

At the same time, von Seggern [27] studied the effects of the signal-to-noise ratio to determine the charge distribution in an electret using the thermal-pulse technique. The results he obtained showed that the maximum number of numerically significant Fourier coefficients was six to eight. In the same manner, Mopsik and De Reggi [66] measured the short-circuit charge in PVDF as a function of time. The contribution of charge and polarization distribution was described with a Fourier analysis. However, the total charge on the sample could not be measured. The relative charge distribution in a sample with permanent polarization could be calculated if its distribution is compensated by free charge. The acquisition of data from top and bottom electrodes is recommended in order to have a resolution of the order of one tenth the sample thickness.

3.2.2 Laser-Intensity Modulation Method (LIMM)

Even though LIMM is a technique that was proposed a few years later than TP, the analysis of LIMM data matured faster. Lang and Das-Gupta were the pioneers of the laser-intensity modulation method in 1981 [22]. The authors used the technique to determine the polarization distribution of a polymer electret. In 1984, the same authors presented an extended version of their previously discussed method [28], called the Laser-Intensity Modulation Method (LIMM) (Fig.3.3). As its name describes, the intensity of the laser is sinusoidally modulated. The complex pyroelectric current is measured over a range of frequencies (100 Hz to 100 kHz). Experimental and simulated data of PVDF films were presented. Two years later, a more complete theory is suggested to convert the pyroelectric current data to a spatial polarization distribution as well as a description of the laboratory implementation of this technique. The data analysis was carried out using a linear least-squares fit [67].

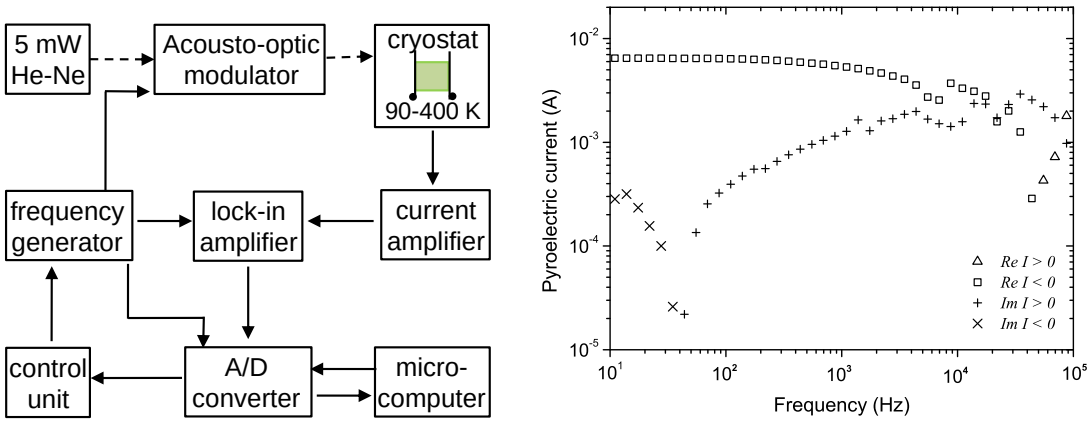

Figure 3.3: Laser-Intensity Modulation Method setup [67] and frequency spectrum of pyroelectric current measured in a PVDF film [68].

At the beginning of the 1990s, two new methods were published for analyzing experimental data from the LIMM technique. One widely used method was published by Bauer and Ploss [69]. The pyroelectric current could be measured on one side of a thin metallized polymer film with a modulated laser. The transient current and temperature were measured as a function of the modulation frequency of the laser light. Using thin-film bolometers, the temperature was recorded. In this way, the pyroelectric coefficient p and the thermal diffusivity were determined in thin PVDF films. Later, Das-Gupta and Hornsby [70] faced the problem of the deconvolution by assuming the space charge was constant in a limited layer of the sample and a normal Gaussian distribution of the polarization. Both statements were considered suitable for their material which possessed spatially distributed space charges and dipolar concentrations. The parameters involved in the integrals they obtained were chosen by minimizing the sum of squared errors. They proved that the analysis fit very well the experimental results from a low-density polyethylene (LDPE) sample.

In 1992, Ploss and coworkers introduced a new method for the analysis of pyroelectric spectra from LIMM experiments [71]. The method is known as the Scale Transformation (ST) method. Another important contribution regarding methods for solving the LIMM equation was made by Lang [30] who introduced the Polynomial Regularization Method (PRM). The most used methods and their accuracy will be described in section 3.5.

3.3 Three-dimensional profiling

Acoustic and thermal techniques are widely used in the determination of polarization distributions. Nevertheless, the yielded distributions from both groups of methods do not precisely give the position of the charges inside the material because the data analysis is constrained to one dimension. The first maps of polarization distributions at only two different depths were published in 1998 by Ploss et al. [72]. They used LIMM to investigate lead zirconate titanate-lead magnesium niobate (PZTPMN) material. Another attempt to determine a three-dimensional space-charge distribution in a thick polymethylmetacrylate (PMMA) layer was performed in 1999 by Qin et al. [73]. They used an acoustic lens and thus established the focused pressure wave propagation (PWP) method; the acquisition time for the profile in the z-direction at a given (x, y) position was 3 s. The resolution in the $x - y$ plane and in the z-direction were ± 1 mm^2 and ± 60 µm respectively. Later, in 2001, Maeno [74] developed a three-dimensional PEA technique after attaching an acoustic lens to the detector of the 1-D setup. When using a 5 ns voltage-pulse duration and averaging more than 1000 pulses (acquisition time of 2 s), the time to scan an area of 5 mm×5 mm using a 0.5 mm mesh took 200 s. A spatial resolution of 12 µm in the thickness direction and a lateral spatial resolution $\leq$0.5 mm were reported.

3.3.1 Focused Laser-Intensity Modulation Method (FLIMM)

In 2002, Marty-Dessus et al. [24] developed a point-to-point detection technique called Focused Laser-Intensity Modulation Method or FLIMM (Fig. 3.4). The authors modulated the intensity of a laser diode, and by means of a positive lens the spot size can be varied down to 1 µm. The pyroelectric current was measured on polyethylene (PE) films recording 256 frequency values between 10 Hz and 10 kHz. The data acquisition for a single point took about 45 min. A three-dimensional model of temperature was required for the data analysis. The deconvolution process needed to obtain the space charge density cartographies was performed by means of regularization methods (see section 3.5.1 and [75, 76]).

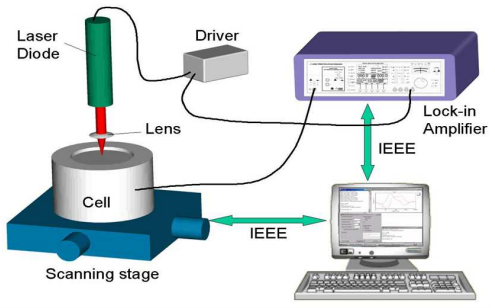

Figure 3.4: Focused LIMM experimental setup [24]

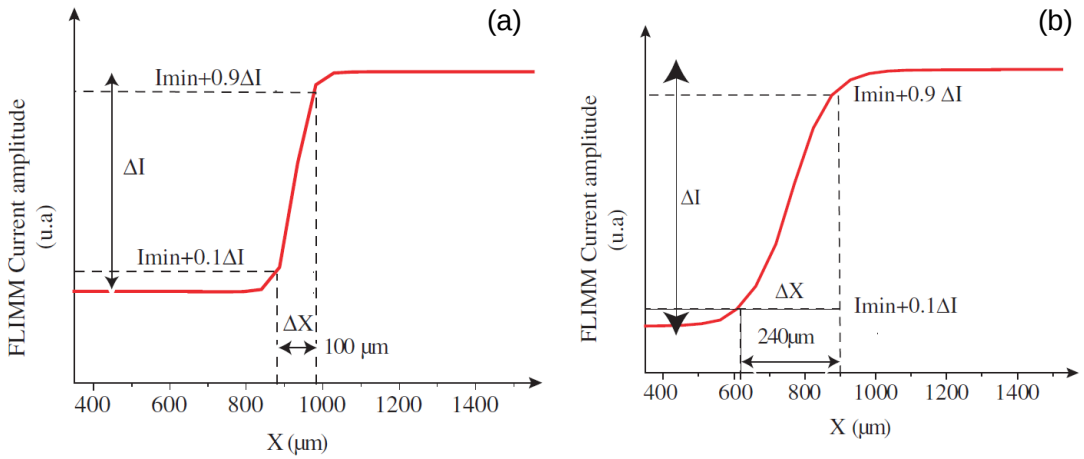

Figure 3.5: Pyroelectric current profile measured in a PE films at f =1 kHz using FLIMM with spot sizes of (a) 5 µm and (b) 20 µm [24].

The lateral resolution was measured using a 20 µm laser beam spot size and a similar step size on a PE film. The films were mechanically stretched, therefore the thickness is a function of the X coordinate. The thickness on the film varies from 20 to 26 µm and the transition zone ranges from 80 to 100 µm. The pyroelectric current reached its maximum at the thinner parts of the film however, the authors do not clarify whether the laser spot size was kept constant. The lateral resolution of this technique was calculated at f =1 kHz ($Z \approx$ 4 µm) and between 10% and 90% of the pyroelectric current in the X coordinate (Fig. 3.5a). From the profile, the lateral resolution value is $\approx$ 240 µm, however the authors claimed 150 µm. Likewise, the space charge profile on the PE film was obtained using a 5 µm laser spot size. The lateral resolution is seen to be 100 µm (Fig. 3.5b), but the authors claimed 10 µm. The resolution in the thickness direction was reported as 1 µm. In summary, FLIMM is a technique that provides a three-dimensional mapping in dielectrics using small laser beam spot sizes and better spatial resolution than 3D acoustic methods. Due to the longer data acquisition time, significant information on the space charge or polarization distribution may change. In case of small polarization or space charge densities in a sample, the sensitivity of the thermal methods can be increased by enhancing the laser power and the absorption coefficient of the irradiated electrode. Mellinger et al. [65] suggested that if cw lasers were focused as in FLIMM, the bulk temperature in free-standing samples may rise to values that lead to damage or even destruction of the polymer sample. Sample damage is not exclusively found with FLIMM, however. When using pulsed lasers above a threshold laser fluence, ablation of the irradiated metal electrode and possibly damage to a thin surface layer of the polymer may occur [65].

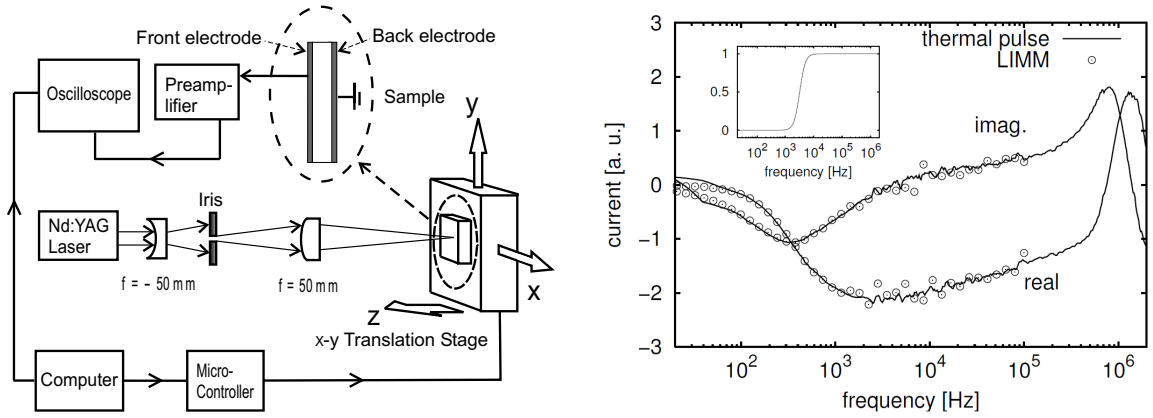

Figure 3.6: The TPT setup and the measured pyroelectric current showing good agreement with the LIMM technique. [25, 65].

3.3.2 Thermal-Pulse Tomography (TPT)

Based on the clear limitations of FLIMM, and the need for a technique that can obtain polarization distribution maps at different depths in shorter periods of time, Mellinger et al. [25] reported the first work on focused thermal pulses. This new method helps to determine a three-dimensional mapping of polarization profiles in a polymer electret. The samples were stretched PVDF films. The electrical poling of the samples, well above the coercive field, was performed with "T"-shaped aluminum electrodes on the top of the film, while full-area metallization was applied on the bottom. Afterwards, a copper coating was applied to the surface of the samples; the 'T"-structure electrode was not removed.

The laser-beam spot size was varied from 1 mm down to 30 µm. In order to avoid ablation of the films, the energy of the laser per unit area, i.e. the fluence was kept below 0.1 J/cm^2. The samples could be scanned either free-standing or fixed to a substrate. The generated pyroelectric current was analyzed in the same way as the LIMM data (Fig.3.6); the current was divided by the gain spectrum and later Fourier transformed. The deconvolution process was performed using the method proposed by Lang [30]; the regularization parameter was selected by using the L-curve method [77]. The results clearly showed the shaped electrode after scanning with a laser spot size of 200 µm.

The resolution in the thickness direction was approximately 0.5 µm. The lateral resolution of the TPT method was measured using one-dimensional scans along one of the spatial coordinates at different z depths across the edge of the shaped electrode using the smallest available laser spot size (Fig.3.7). The resolution was defined as the "width of the transition region measured between 20% and 80% of the plateau height" or in other words the width of the transition between the unpoled and poled area. The reported spatial lateral resolution near the irradiated surface (z =1 µm) was 38 µm using a spot size of 30 µm,

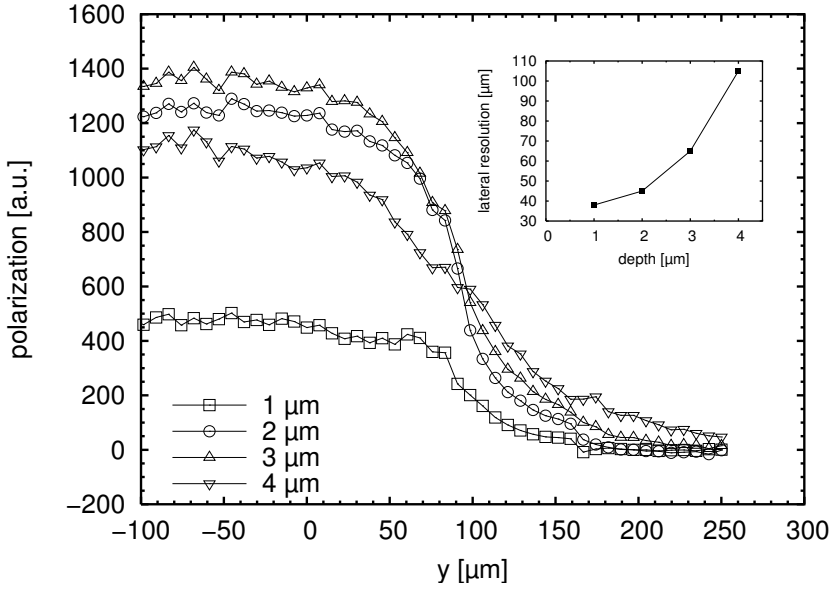

Figure 3.7: One dimensional polarization profile measured from TPT method. The resolution tendency is shown in the inset [25].

and it decreases as the laser spot size is increased. The resolution is limited due to the fast thermal diffusivity of the metal electrode, which is three orders of magnitude higher than in the polymer. The advantage of using TPT instead of FLIMM is the fast data acquisition, up to 40 times faster. More over, we have implemented the TPT for investigating samples with cylindrical geometry (see page 23). The resulting polarization distribution in the piezolectric sensor cables suggested an optimization of the corona poling. In table 3.1 the characteristics of acoustic and thermal techniques (PWP, PEA, FLIMM and TPT) that have been developed to achieve three-dimensional cartographies of space charge and polarization in dielectrics are highlighted.

Table 3.1: Most used techniques for three-dimensional mapping.

Method	depth-resolution	space-resolution	spot-size	data acquisition	comments
PWP	60 µm	1000 µm	-	fast (3 s)	tested on films
PEA	12 µm	500 µm	-	fast (2 s)	tested on films
FLIMM	1 µm	10 µm	5 µm	slow (>40 min)	tested on films
TPT	0.5 µm	38 µm	30 µm	fast (≈10 s)	tested on films and cables

Publications

Thermal-Pulse Tomography of polarization distributions in a cylindrical geometry
R. Flores Suarez; M. Wegener; W. Wirges; A. Mellinger;
R. Gerhard-Multhaupt and R. Singh
IEEE Transactions on Dielectrics and Electrical Insulation,
Vol. 13, 1030-1035 (2006)

Zerstörungsfreie Tomographie von Raumladungs- und Polarisationsverteilungen mittels Wärmepulsen
A. Mellinger; R. Flores Suarez; R. Singh; M. Wegener;
W. Wirges and R. Gerhard-Multhaupt
tm-Technisches Messen,
Vol. 74, 437-444 (2007)

Thermal-Pulse Tomography of Polarization Distributions in a Cylindrical Geometry

Rosaura Flores Suárez, Axel Mellinger, Michael Wegener, Werner Wirges, Reimund Gerhard-Multhaupt
University of Potsdam
Department of Physics
Am Neuen Palais 10
14469 Potsdam, Germany

Rajeev Singh
University of Allahabad
Department of Electronics & Communication
Allahabad (U.P.)-211002, India

ABSTRACT

Fast, three-dimensional polarization mapping in piezoelectric sensor cables was performed by means of the novel thermal-pulse tomography (TPT) technique with a lateral resolution of 200 µm. The active piezoelectric cable material (a copolymer of polyvinylidene fluoride with trifluoroethylene) was electrically poled with a point-to-cable corona discharge. A focused laser was employed to heat the opaque outer electrode, and the short-circuit current generated by the thermal pulse was used to obtain 3D polarization maps via the scale transformation method. The article describes the TPT technique as a fast non-destructive option for studying cylindrical geometries.

Index Terms — **Thermal-pulse tomography, piezoelectric materials, sensor cables, polarization profile, polyvinylidene fluoride, pyroelectric effect.**

1 INTRODUCTION

THE research of poled or charged electret polymers, whose main applications are focused on sensors and actuators, needs efficient techniques to map their polarization and space-charge distributions [1]. While destructive techniques, such as cross-sectional imaging with a scanning electron microscope [2], have found their place in electret research, non-destructive methods are preferred in most cases. Examples include several acoustic techniques (e.g., laser-induced pressure-pulses (LIPP), the pulsed electroacoustic method (PEA) and piezoelectrically generated pressure steps (PPS) [3]) as well as thermal techniques [4], such as the laser intensity modulation method (LIMM) [5] and the thermal-pulse (TP) method [6] to obtain the depth-profiles of the electric field. The latter methods use a pulsed or periodic heating (usually by means of laser light absorbed by an opaque electrode) of the sample to generate a short-circuit current or change in surface potential which contains information about the spatial distribution of electric dipoles or space charges. The LIMM technique is an implementation in the frequency domain, while the TP method works in the time domain. Using nanosecond laser-pulses, near-surface depth resolutions in the sub-µm range are easily achieved [7]. A recent comparison of LIMM with the TP method showed excellent agreement between the two techniques [8]. The advantage of the latter is a significantly higher data acquisition speed (up to 50 times faster than LIMM). Taking advantage of the higher speed, three-dimensional maps of the polarization distribution in poled polymer films were obtained by focusing the laser to spot sizes down to approx. 40 µm and scanning it across the sample. This approach, known as thermal-pulse tomography (TPT), yielded a lateral and near-surface depth resolution of 38 µm and 0.5 µm, respectively [9]. A similar implementation, known as the focused laser intensity modulation method (FLIMM) [10], was previously performed in the frequency domain. Although the authors reported lateral resolutions down to 5 µm, this method requires a significantly longer data acquisition time which limits the number of beam pointings.

Polymer films investigated with thermal-pulse tomography include ferroelectric polyvinylidene fluoride (PVDF) and its copolymers with trifluoroethylene (P(VDF-TrFE)) [11,12], as well as polytetrafluoroethylene (PTFE) [9] as an example of a non-polar space-charge electret. The current work presents an application of TPT in a cylindrical geometry. Piezoelectric sensor

Manuscript received on 13 April 2006 in final form 3 July 2006.

cables are used as robust sensors for mechanical stress in, e.g., intrusion detection and traffic counting applications [13]. Their manufacturing, electrical poling, and characterization have been described in detail in an earlier publication [14]. In that work, the electromechanical properties and the one-dimensional polarization depth profiles of corona-poled P(VDF-TrFE) coaxial cables were obtained by means of dielectric resonance spectroscopy and the piezoelectrically generated pressure step method (PPS), respectively. However, the resulting polarization profile is an average over the angular coordinate due to the relatively large electrode diameter of 5 mm. The present work is the first three-dimensional study of the polarization in these sensor layers.

2 EXPERIMENTAL DETAILS

The cables investigated in the present study were manufactured by Huber & Suhner AG, Herisau, Switzerland, and consist of a P(VDF-TrFE) dielectric extruded onto a multi-wire core. The thickness of the active P(VDF-TrFE) layer is approx. 210 µm (Figure 1). Two sets of cables were poled in a stationary laboratory setup. The poling was performed by means of a single needle, located at 30 mm from the cable, with voltages of –25 kV and –60 kV in air and SF_6, respectively. The SF_6 atmosphere was necessary to prevent gas breakdown at the higher voltage. After poling, the multi-wire core was removed (cf. Figure 1) and replaced by a stainless steel pin of 0.7 mm diameter. The outer opaque electrode was provided by evaporating 200 nm of Cu onto the P(VDF-TrFE) cylinder in high vacuum. For comparison, several cables of the same type, but poled at voltages around 20 kV in a continuous industrial process with a 4-tip corona discharge, were mounted in the same fashion.

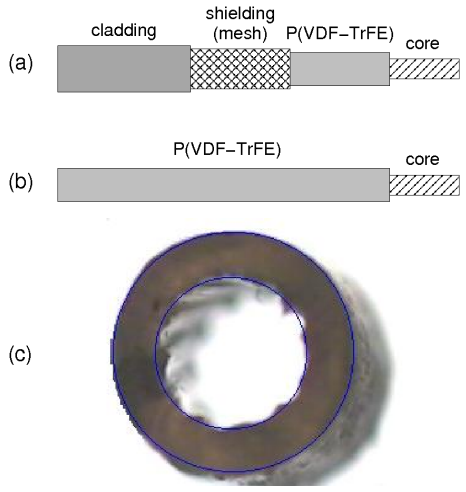

Figure 1. (a): schematic view of a typical piezoelectric sensor cable, (b): cable before corona-poling, (c): optical micrograph (cross-section) of the (VDF-TrFE) insulator. Its outer diameter is approx. 1.1 mm and its thickness approx. 210 µm. For thermal pulse experiments, the outer insulator surface was coated in high vacuum with 200 nm of copper.

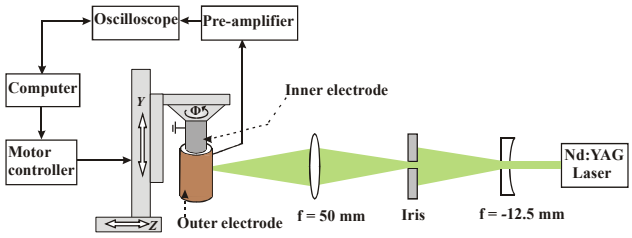

Figure 2. Experimental setup for the focused thermal-pulse technique.

Our thermal-pulse tomography setup is capable of scanning both planar and cylindrical geometries, i.e. films [9, 11] and coaxial cables. The setup for investigating cylindrical geometries is shown in Fig. 2. The cables were mounted on a motorized rotary stage (DMT 40, OWIS GmbH), which permitted to rotate the sample through angles ϕ ranging from nearly 0° to 360° (limited only by the length of the thin contact wire to the outer electrode).

Motion in the *X* and *Y* directions was achieved by means of a motorized *XY* positioning stage (ERLIC 85, OWIS GmbH). The thermal pulses were created by focusing a Nd:YAG laser (New Wave Polaris III) beam onto the Cu electrode. The short-circuit pyroelectric current was amplified by a Stanford Research SR 570 current-to-voltage converter and recorded with a digital storage oscilloscope (Agilent 54833A) at a rate of $(\Delta t)^{-1} = 2\times10^6$ Hz. For each beam pointing, the data from 30 laser pulses were averaged, requiring an acquisition time of less than 10 s (at a pulse repetition rate of 6 Hz). The resulting waveform with N = 360 000 data points was stored for further processing.

The laser beam spot size (defined by the diameter between the points where the intensity drops to $1/e^2$ of the central value [15]) could be adjusted between 400 and 25 µm by varying the *Z* position of the sample holder along the optical axis and was determined with the help of a knife-edge focuser. All scans were carried out with a spot size of 200 µm which represents a good compromise between spatial resolution and signal-to-noise ratio.

3 DATA ANALYSIS

The raw data (i.e., the transient current $I(t_k)$ as a function of time) was transformed into the frequency domain using a fast Fourier transform (FFT) algorithm [16]. While data analysis in the time and frequency domain is equivalent in principal [8], correcting for the frequency-dependent complex gain and phase shift of the pre-amplifier $\tilde{\alpha}(f_n)$ is a simple division in the frequency domain:

$$\tilde{J}_{\exp}(f_n) = \frac{\Delta t}{\tilde{\alpha}(f_n)} \sum_{k=0}^{N-1} I(t_k) e^{-2\pi i k n / N} \qquad (1)$$

with

$$f_n = \frac{n}{N\Delta t}, \qquad n = 1 \ldots \frac{N}{2} \qquad (2)$$

Here, $\tilde{J}_{\exp}(f_n)$ is the (complex) frequency-domain current. It is related to the profile of the pyroelectric coefficient *p(x, y, z)* via the LIMM equation, which in three dimensions can be

written as

$$\tilde{J}_{\text{calc}}(f_n) = \frac{i2\pi f_n}{d} \int_0^d \int_{-\infty}^{\infty} \int_{-\infty}^{\infty} p(x,y,z)\tilde{T}(x,y,z,f_n)\,dx\,dy\,dz \qquad (3)$$

where $\tilde{T}(x,y,z,f_n)$ and d are the frequency-domain temperature amplitude of the thermal wave and the sample thickness, respectively. For a multilayer geometry with a Gaussian-shaped thermal source, $\tilde{T}(x,y,z,f_n)$ can only be calculated numerically, for example by means of the finite element method [9, 11, 16]. However, for pyroelectric distributions that do not strongly vary as a function of the in-plane coordinates x and y, equation (3) may be replaced by its one-dimensional form

$$\tilde{J}_{\text{calc}} = \frac{i2\pi f_n A}{d} \int_0^d p(z)T(z,f_n)\,dz \qquad (4)$$

where A is the electroded area. A solution of the LIMM equation taking into account the dependence of p on the x and y dimensions is currently in progress [11]. Equation (4) is a Fredholm integral equation of the first kind. The solution of this equation with respect to p is an ill-posed problem. However, there exist a number of techniques to obtain a physically meaningful solution $p(z)$ for a given current spectrum. For example, regularized solutions are obtained by minimizing

$$\sum_n \left\| \tilde{J}_{\text{exp}}(f_n) - \tilde{J}_{\text{calc}}(f_n) \right\|^2 + \lambda^2 \int_0^d \left(\frac{d^2 p(z)}{dz^2} \right)^2 dz \qquad (5)$$

with respect to each of the coefficients. In equation (5), λ is the regularization parameter, whose main function is to determine whether minimization of the first or second term (controlling the smoothness of the solution) has the greater priority. This parameter may be calculated using, for example, the L-curve method [17].

For depths $z<d/4$, an approximation of the pyroelectric distribution $p_a(z)$ in sensor cables was calculated by means of the scale-transformation method [18]:

$$p_a(z) = \frac{c\rho d}{\eta j_\sim A} \left[(\Re - \Im)\tilde{J}_{\text{exp}}\left(\omega = 2D/z^2\right) \right] \qquad (6)$$

In this equation, c, ρ, η and D are the heat capacity, the density, the absorption coefficient and the thermal diffusivity of the sample; $j_\sim$ is the laser-light intensity. The scale-transformation method provides an unambiguous solution in a region near the sample surface and preserves the high depth-resolution inherent to thermal techniques. Notice the simplicity of the method, since it only requires subtracting the imaginary part of the complex frequency-domain current $\Im(\tilde{J}_{\text{exp}})$ from its real counterpart $\Re(\tilde{J}_{\text{exp}})$. In the present case, with $d \approx 210$ µm, the polarization distribution for depths up to approx. 54 µm can be extracted via the scale transformation method. This depth is small compared to he curvature radius of the cable (550 µm), thereby justifying the 1-dimensional approximation. In any case, the finite recoding time $t = N\Delta t = 0.18$ s of the transient current limits the maximum probe depth to approx. $z = \sqrt{Dt} = 103$ µm (for a thermal diffusivity of $D = 6\times10^{-8}$ m^2/s). Since the pyroelectric coefficient is related to the polarization P via $p = \partial P/\partial T = \alpha_T P$ (where α_T is the relative temperature coefficient of the polarization), maps of the pyroelectric coefficient indicate the spatial distribution of the polarization.

4 RESULTS AND DISCUSSIONS

The polarization maps calculated from the experimental data with the scale transformation method are presented in Figures 3 and 4, respectively. The scanned area covers approx. 350° around the circumference and ca. 19 mm in length. The maps are the result of 1000 individual thermal-pulse measurements (20 and 50 points on the ϕ and Y axes, respectively). The corona tip positions are marked with a cross.

The cable poled at –25 kV exhibits a non-uniform polarization distribution along the radial (depth) coordinate (Figure 3). In addition to a depolarized layer near the surface (up to depths of approx. 6 µm), there is a noticeable increase of the polarization in the radial direction towards the core. This behavior is expected in a cylindrical geometry, since the electric poling field depends on the depth z as

$$E(z) = \frac{V_p}{\ln(r_o/r_i)} \frac{1}{(r_o - z)} \qquad (7)$$

where V_p is the applied poling voltage, and r_o and r_i are the outer and inner radii of the P(VDF-TrFE) layer, respectively. This depth-dependence of the polarization was also observed in a previous study performed with the acoustic PPS method [14], although the RC time constant led to a significant distortion of the signal. Due to the slower diffusion speed of thermal pulses (compared with the propagation of acoustic waves), the present measurements do not suffer from this effect.

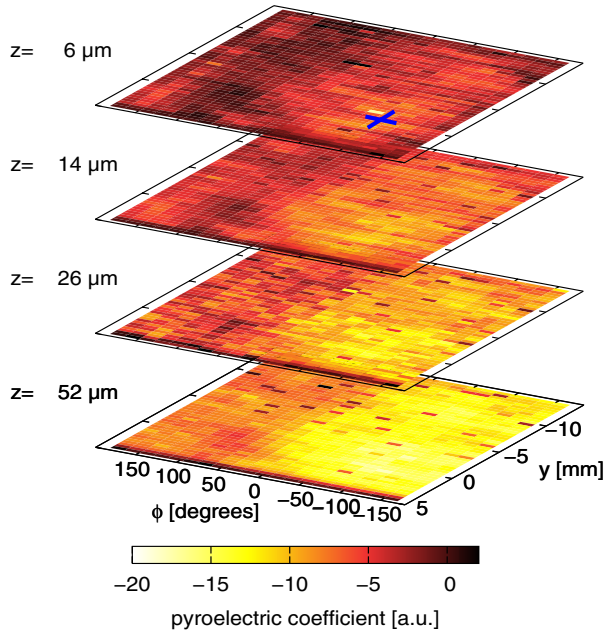

Figure 3. Polarization map of a stationary corona-poled P(VDF-TrFE) sensor cable. The voltage applied to the single needle located at (ϕ = 88°, Y = 0 mm) was 25 kV. The cross marks the ϕ and Y coordinates of the corona tip.

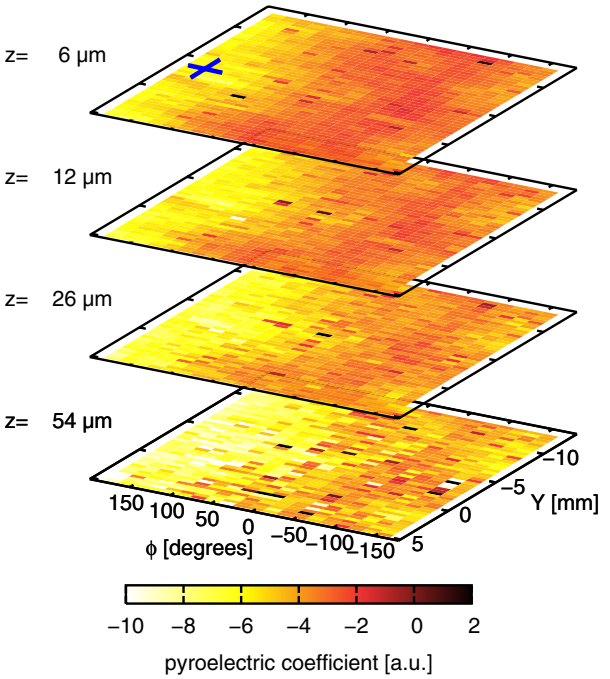

Figure 4. Polarization map of a stationary corona-poled P(VDF-TrFE) sensor cable. The voltage applied to the single needle located at (= 158°, *Y* = 2 mm) was 60 kV. The cross marks the and *Y* coordinates of the corona tip.

The edge depolarization at low depths was also observed in another thermal-pulse experiment where the entire cable insulation was heated by placing the cable into a diffuser [19]. It is thus thought to originate from surface impurities, rather than being caused by the thermal stress induced on the sample. In addition, care was taken to limit the laser fluence to values below 0.1 J/cm² at all times.

In the (ϕ, *Y*) plane, the polarized area is very well defined, extending approx. ± 50° and (+5, −10) mm from the needle position. Beyond this area, the polarization tends to decrease smoothly. Figure 5a shows the polarization as a function of the angular coordinate ϕ at *Y*=0 mm (the needle position along the symmetry axis) for different depths. From these profiles, it is clearly seen that the polarization maximum is reached at the projected position of the corona tip at $\phi = -88°$ for all scanned depths.

The polarization tomogram for the cable poled at −60 kV (Figure 4) shows, as in the previous case, higher polarization values with increasing depth, although with a less pronounced depth-dependence. Due to the higher poling voltage, the poling field reached or exceeded the coercive field at nearly all depths. In the cross sectional view at $Y = -2$ mm (Fig. 5(b)) there is a region of low polarization values from $\phi \approx -150°$ to 50°. Notice that at lower depths up to z = 6 µm, there is already a narrow area of higher polarization values (ranging from 100 to 150 degrees). The maximum of polarization is reached beyond ϕ = 150°, just at the edge of the scanned angular range. According to these results, we have polarized a region approx. 100° wide at −25 kV and approx. 50° wide at −60 kV. Thus, achieving a homogeneous polarization along the circumference of the cable appears to require a setup with a ring of 6 corona needles at 60° intervals.

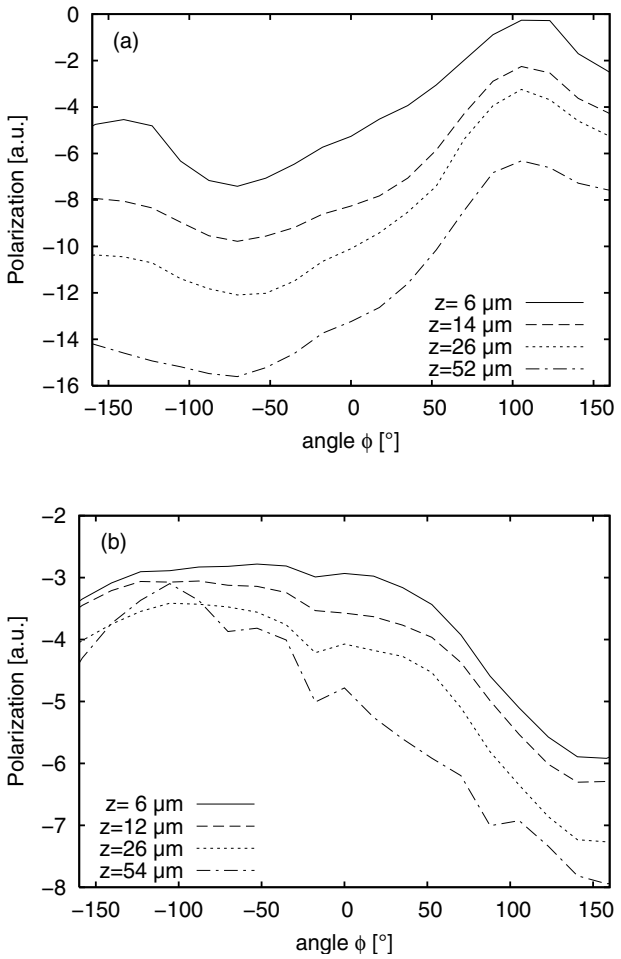

Figure 5. Calculated polarization as a function of the angle at a fixed *Y* position (directly under the corona needle) for different depths *z* in sensor cables poled with a single needle. (a): poling voltage 25 kV, *Y*=0 mm, (b): poling voltage 60 kV, *Y*=2 mm (cf. Figs. 3 and 4).

Cables poled in a continuous process exhibit a significantly different polarization distribution (Figure 6). Due to the corona geometry with four needles evenly distributed around the cable, there is no "hot spot" as in the stationary poled specimens. However, Figure 6 shows noticeable inhomogeneities in the *Y* direction along the length of the cable.

A comparison of the polarization inhomogeneities along the *Y* coordinate at a fixed depth (z = 52 µm) for the cables poled under either stationary or continuous conditions is shown in Figure 7. For the stationary poled samples, the chosen angles ϕ correspond to a location directly under the corona tip. To obtain a quantitative measure for the inhomogeneities, we define a relative root mean square (rms) value of the polarization:

$$\sigma_{rms} = \frac{\sqrt{\sum_{i=i_1}^{i_2} \left(P_i - \overline{P}\right)^2}}{\overline{P}} \qquad (8)$$

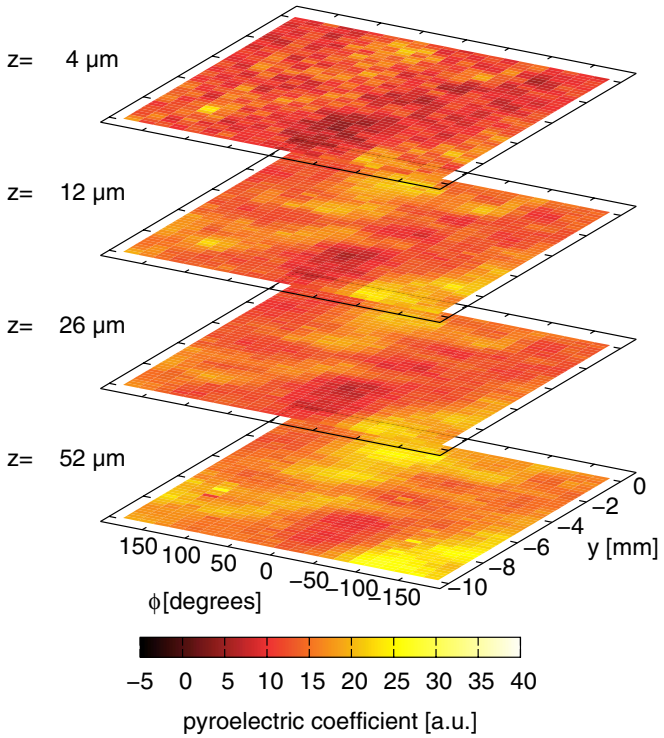

Figure 6. Polarization map of a continuously poled P(VDF-TrFE) sensor cable. Poling was performed by means of a 4-needle corona discharge and tip voltages of 20 kV.

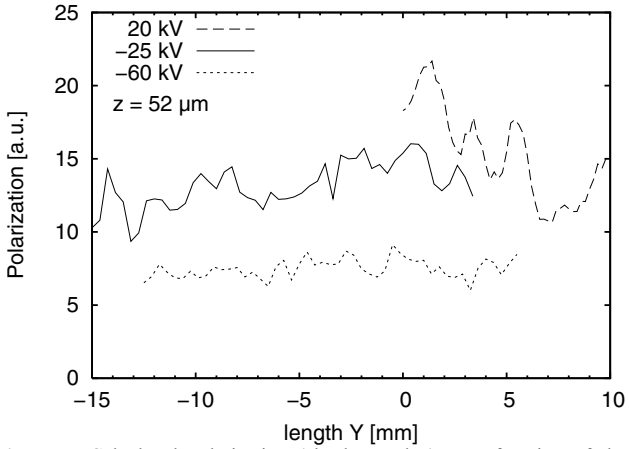

Figure 7. Calculated polarization (absolute value) as a function of the Y position at a fixed angle □ and depth $z = 52$ µm in sensor cables poled either in a continuous process (poling voltage 20 kV,□□°) or in a stationary process (poling voltages: 25 kV,□□–□□°, and 60 kV, □□1□□°). The traces represent cross-sections of Figs. 3, 4 and 6.

where P_i is the i-th value of the polarization along the Y axis and $\overline{P}$ is the mean value of polarization. The summation window (from i_1 to i_2) was chosen to comprise a length of 10 mm in all three samples. This interval is small compared to the extent of the poled region for the stationary poled cables. For the continuously poled cables we obtained an rms value of 0.20, whereas the highest σ_{rms} values for the samples poled at –25 and –60 kV under stationary conditions were 0.10 and 0.087, respectively. Thus, the continuous poling process results in inhomogeneities approx. twice as large as for the stationary process.

A possible explanation lies in the relatively high drawing speed, which limits the effective poling time (for which the electric field exceeded the coercive field of P(VDF-TrFE)) to 300 ms. On the other hand, the surface-potential build-up time in a corona discharge may be of the order of seconds [20]. Therefore, the corona discharge operates far from steady state conditions. Torsional motion (known to occur in the poling process) may account for the variation of the polarization in the angular direction. Thus, a slower extrusion speed (and possibly a higher corona voltage in an SF_6 atmosphere) is required for a more uniform polarization.

5 CONCLUSION

Using focused thermal pulses, the spatial distributions of the polarization in ferroelectric polymers can be measured with high lateral resolution. Due to the high data acquisition speed of this technique it is possible to obtain detailed scans in short periods of time (≈ 10 s per beam pointing). Moreover, the thermal-pulse tomography technique may be employed to investigate different sample geometries, such as planar polymer films and cylindrical polymer layers. An industrial, continuous poling process of P(VDF-TrFE) sensor cables was shown to yield polarization inhomogeneities about twice as high as a stationary one.

ACKNOWLEDGMENT

The work was funded in part by the European Regional Development Fund and the German Science Foundation. R. S. acknowledges financial support from the German Academic Exchange Service (DAAD). The authors also wish to thank Lakshmi Meena Ganesan for her help with the FFT software.

REFERENCES

[1] R. J. Fleming, "Space charge profile measurement techniques: Recent advances and future directions", IEEE Trans. Dielectr. Electr. Insul., Vol. 12, pp. 967-978, 2005.

[2] J. Hillenbrand and G. M. Sessler, "Piezoelectric properties of polypropylene/air and poly(vinylidene fluoride)/air composites," IEEE Conf. Electr. Insul. Dielectr. Phenomena, Piscataway, NJ: IEEE Service Center, 2000, pp. 161–165.

[3] G. M. Sessler, *Distribution and transport of charge in polymers*, in: R. Gerhard-Multhaupt (ed.), Electrets, 3rd ed., Vol. 2, Laplacian Press, 1998, pp. 41-80.

[4] S. Holé, T. Ditchi, and J. Lewiner, "Non-destructive methods for space charge distribution measurements: What are the differences?", IEEE Trans. Dielectr. Electr. Insul., Vol. 10, no. 4, pp. 670–677, 2003.

[5] S. B. Lang and D. K. Das-Gupta, "A technique for determining the polarization distribution in thin polymer electrets using periodic heating," Ferroelectrics, Vol. 39, pp. 1249–1252, 1981.

[6] R. E. Collins, "Analysis of spatial distribution of charges and dipoles in electrets by a transient heating technique," J. Appl. Phys., Vol. 47, no. 11, pp. 4804–4808, 1976.

[7] S. Bauer and S. Bauer-Gogonea, "Current practice in space charge and polarization profile measurements using thermal techniques", IEEE Trans. Dielectr. Electr. Insul., Vol. 10, no. 5, pp. 883–902, 2003.

[8] A. Mellinger, R. Singh, and R. Gerhard-Multhaupt, "Fast thermal-pulse measurements of space charge distributions in electret polymers", Rev. Sci. Instr., Vol. 76, p. 013903, 2005.

[9] A. Mellinger, R. Singh, M. Wegener, W. Wirges, R. Flores Suárez, S. B. Lang, Lucas F. Santos and R. Gerhard-Multhaupt, "High-resolution three-dimensional space-charge and polarization mapping with thermal pulses", IEEE 12th Intern. Sympos. Electrets, IEEE Service Center, Piscataway, NJ, 2005.

[10] D. Marty-Dessus, L. Berquez, A. Petre, and J. L. Franceschi, "Space charge cartography by FLIMM: a three-dimensional approach", J. Phys. D: Appl. Phys., Vol. 35, pp. 3249–3256, 2002.
[11] A. Mellinger, R. Flores Suárez, R. Singh, M. Wegener, W. Wirges, R. Gerhard-Multhaupt and S. B. Lang, "Thermal-pulse tomography of ferroelectric polymers: three-dimensional thermal analysis", to be published.
[12] R. Flores Suárez, *Polarization Profiles in Poled PVDF Sensor Cables*", Master Thesis, University of Potsdam, 2005.
[13] B. Mazurek, T. Janiczek, and J. Chmielowiec, "Assessment of vehicle weight measurement method using PVDF transducers", J. Electrostatics., Vol. 51-52, pp.76-81, 2001.
[14] M. Wegener and R. Gerhard-Multhaupt, "Electric poling and electromechanical characterization of 0.1 mm-thick sensor films and 0.2 mm-thick cable layers from piezoelectric poly(vinylidene fluoride-trifluoroethylene)", IEEE Trans. Ultrason. Ferroelectr. Freq. Control, Vol. 50, pp. 921–931, 2003.
[15] M. Young, *Optics and Lasers. Including fibers and optical Waveguides*, 4th Ed. Springer-Verlag, 1993.
[16] M. Frigo and S. G. Johnson, "The design and implementation of FFTW3", Proc. IEEE Vol. 93 , 216–231, 2005.
[17] P. C. Hansen and D. P. O'Leary, "The use of the L-curve in the regularization of discrete ill-posed problems," SIAM J. Sci. Comput., Vol. 14, no. 6, pp. 1487–1503, 1993.
[18] B. Ploss, R. Emmerich, and S. Bauer, "Thermal wave probing of pyroelectric distributions in the surface region of ferroelectric materials: A new method for the analysis", J. Appl. Phys., Vol. 72, pp. 5363–5370, 1992.
[19] R. Schwödiauer, G. S. Neugschwandtner, K. Schrattbauer, M. Lindner, M. Vieytes, S. Bauer-Gogonea, and S. Bauer, "Preparation and characterization of novel piezoelectric and pyroelectric polymer electrets", IEEE Trans. Dielectr. Electr. Insul., Vol. 7, pp. 578–586, 2000.
[20] José A. Giacometti, P. A. Ribeiro, M. Raposo, J. N. Marat-Mendes, J. S. Cavalho Campos and Aimé S. DeReggi, "Study of poling behavior of biaxially stretched poly(vinylidene fluoride) films using the constant-current corona triode", J. Appl. Phys., Vol. 78, pp. 5597-5603, 1995.

Rosaura Flores Suárez was born in Mexico City, Mexico, on 29 April 1980. She received the Bachelor degree in physics and mathematics from the National Polytechnic Institute of México (IPN) and the M.Sc. degree in polymer science jointly from the University of Potsdam and the Free University, Humboldt University and Technical University in Berlin, with a thesis on polarization profiles in poled PVDF sensor cables. She is currently a Ph.D. Student at the University of Potsdam. Her research interests include the investigation of ferroelectric polymers through thermal techniques such as thermal-pulse tomography and applications of these polymers in sensors and actuators.

Axel Mellinger was born in Munich, Germany, on 25 August 1967. He studied physics at the Technical University in Munich, where he obtained the diploma and Ph.D. degrees in 1992 and 1995, respectively (his Ph.D. work was performed at the Max-Planck-Institute for Extraterrestrial Physics). He held a two year post-doctoral position at UC Berkeley in the Department of Chemistry, where he investigated the reaction dynamics of the ketene molecule. Since December 1997 he is a senior staff member at the University of Potsdam, Germany, where he obtained the highest German university degree, the *habilitation*, in September 2005. His present work focuses on charge storage mechanisms in polymer electrets, optically induced charge-detrapping, multi-dimensional mapping of polarization and space-charge distributions and dielectric resonance studies of novel piezoelectric materials. From 1987 until 1992, he was a fellow of the *Studienstiftung des Deutschen Volkes*. He received the VDE/ITG 2004 award for a publication on dielectric resonance spectroscopy and the 2006 "Best Paper Award" by the German IEEE Instrumentation & Measurements chapter for his work on polarization tomography. In his spare time, he enjoys taking high-resolution mosaic images of astronomical objects for use in planetariums around the world.

Michael Wegener was born on 24 September 1968 in Neuruppin, Germany. He studied physics and mathematics at the University of Potsdam from 1990 to 1995. In February 2000, he received the Ph.D. degree in physics. From 1997 until 2000, as Ph.D. student, he was admitted to the DFG-sponsored joint Research Training Group on "Polymer Materials" of the Berlin and Potsdam universities and received a merit-based scholarship. He also completed an industry internship at Huber & Suhner AG in Herisau, Switzerland during July and August 1998. Since March 2000 he is a senior member of scientific staff and a project manager in the Applied Condensed-Matter Physics group at the University of Potsdam. Main topics of his present research are the investigation of novel voided space-charge electrets (ferroelectrets) as well as of ferroelectric polymers, their electrical and electromechanical properties as well as their applications in piezoelectric sensors and actuators.

Werner Wirges was born on 23 January 1962 in Bonn (Germany). He was trained as a plumber before studying Physical Engineering at the Aachen University of Applied Sciences. He graduated as Dipl.-Ing. in April 1988. Between 1988 and 1992 he worked at the Heinrich Hertz Institute für Nachrichtentechnik, where he was in charge of the production and coating of viscoelastic control layers. From 1992 to 1997 he worked on the technology of thin film polymer systems for non-linear optical applications. This work focused on the production and poling of polymer multilayers. At the same time he started his work on plasma deposition of new fluoropolymers for optical communication. Until April 2000, he was employed in two industrial projects on passive optical components (thermo-optical switches and polymeric waveguide filter elements). His work is being continued in Potsdam since May 2000 in the group of Prof. R. Gerhard-Multhaupt, where he focuses on production and characterization of non-polar fluoropolymers.

Reimund Gerhard-Multhaupt (S'80–M'84–SM'85–F'93) studied mathematics and physics at the Darmstadt University of Technology in Germany from 1972 until 1978. After graduating as Diplom-Physiker, he spent one year as research fellow at the Collège Militaire Royal in St-Jean, Québec, Canada. From 1979 until 1985, he did his Ph.D. thesis with Professor Gerhard M. Sessler in Darmstadt. From 1985 until 1994, he was research scientist and project manager at the Heinrich-Hertz Institute for Communications Technology in Berlin. Since 1994 he has been an associate professor and since 1997 a full professor in the Physics Department of the University of Potsdam in Germany. The main research areas of Prof. Gerhard-Multhaupt are polymer electrets and ferroelectrets, in particular the mechanisms of space-charge storage and dipole polarization in dielectric polymers and polymer composites, their ferro-, pyro- and piezoelectrical properties, and their applications in sensors and actuators, as well as the nonlinear optical properties of polymers, and more recently also the physics of musical instruments. From 1974 until 1979, he was a fellow of the Studienstiftung des Deutschen Volkes. In 1988, he was awarded an ITG-Preis by the Informationstechnische Gesellschaft im VDE. In 1989, he received a Silver medal from the Stiftung Werner-von-Siemens-Ring. In 2001, he was awarded the first Technologietransfer-Preis by the Technologie-Stiftung Brandenburg and the Prof.-Adalbert-Seifriz-Preis by the Verein Technologie-Transfer Handwerk for his technological collaborations with small industrial companies. Reimund Gerhard-Multhaupt is a member of the American, European and German Physical Societies. Since 2002, he serves as Digest Editor of the IEEE Dielectrics and Electrical Insulation.

Rajeev Singh was born in 1968 and received several degrees (B.Sc. in Physics, B.Tech. in electronics & telecommunication, and M.Tech. in electronics engineering) from the University of Allahabad in India. Since 1996 he is a lecturer in the Department of Electronics & Communication at the University of Allahabad. He is currently in the process of obtaining a Ph.D. degree. Part of his doctoral work was performed during a 15-month visit to the University of Potsdam, Germany in 2003/4, funded by the German Academic Exchange Service (DAAD).

Zerstörungsfreie Tomographie von Raumladungs- und Polarisationsverteilungen mittels Wärmepulsen

Axel Mellinger, Rosaura Flores Suárez, Universität Potsdam,
Rajeev Singh, University of Allahabad, Indien
Michael Wegener, Werner Wirges, Reimund Gerhard(-Multhaupt),
Universität Potsdam

Manuskripteingang: 16. Juni 2007; zur Veröffentlichung angenommen: 12. Juli 2007

Mittels laserinduzierter Wärmepulse lassen sich dreidimensionale Raumladungs- und Polarisationsverteilungen in Elektret-Materialien auf zerstörungsfreie Weise abbilden. Bei Testmessungen an pyroelektrischen Poly(vinylidenfluorid)-Folien wurden bis zu 45 × 45 Pixel große Bilder mit einer Tiefenauflösung von weniger als 0,5 μm und einer lateralen Auflösung von 40 μm gewonnen. Der die laterale Auflösung begrenzende Faktor war die rasche Wärmediffusion in der lichtabsorbierenden, metallischen Frontelektrode. Erste Tests an piezoelektrischen Sensorkabeln und strukturiert aufgeladenen Polytetrafluorethylen-Folien zeigen die vielfältigen Anwendungsbereiche dieses Messverfahrens.

Schlagwörter: Wärmepuls-Tomographie, Polarisation, Raumladung

Non-destructive Space-charge and Polarization Tomography with Thermal Pulses

Non-destructive, three-dimensional imaging of space-charge and polarization distributions in electret materials has been implemented by means of laser-induced thermal pulses. In pyroelectric films of poled poly(vinylidene fluoride), images of up to 45 × 45 pixels with a depth resolution of less than 0.5 μm and a lateral resolution of 40 μm were recorded, the latter being limited by fast thermal diffusion in the absorbing metallic front electrode. Initial applications include the analysis of polarization distributions in corona-poled piezoelectric sensor cables and the detection of patterned space-charge distributions in polytetrafluoroethylene films.

Keywords: Thermal-pulse tomography, polarization, space charge

1 Einführung und Messprinzip

Seit der Erfindung des Elektret-Kondensator-Mikrofons [1] durch *G. Sessler* und *J. West* im Jahre 1962 sowie der Entdeckung von Piezo- und Pyroelektrizität in Poly(vinylidenfluorid) [2] sind Elektrete in zahlreiche Anwendungen der Sensorik und Filtertechnik vorgestoßen. Elektrete sind Materialien mit einer permanenten elektrischen Polarisation oder einer Überschussladung. Für Grundlagenuntersuchungen, aber auch zur Qualitätskontrolle ist es notwendig, diese mittels zerstörungsfreier Methoden zu charakterisieren. Solche Verfahren wurden bereits in den 70er- und 80er-Jahren des 20. Jahrhunderts entwickelt und beruhen darauf, dass im Material durch eine externe Anregung (in der Regel mechanisch, thermisch oder elektrisch) eine lokale Veränderung (z. B. der Dichte oder der Dielektrizitätskonstanten) erfolgt. Besitzt der Werkstoff eine elektrische Polarisation P oder eine elektrische Überschussladung ρ, wird er hierauf mit einer (elektrischen oder mechanischen) Antwort reagieren, welche durch ihren Zeitverlauf Informationen über die Verteilung des internen elektrischen Feldes (und damit von P oder ρ) trägt.

Bei den ersten thermischen Tiefenprofil-Messverfahren wurde die lichtundurchlässige Oberflächenelektrode mit Hilfe von Blitzlampen erwärmt. Der so erzeugte Wärmepuls diffundiert in den Werkstoff und erzeugt eine orts- und zeitabhängige Temperaturverteilung (Bild 1), welche wiederum einen pyroelektrischen (bei pyroelektrischen Materialien) oder Verschiebungs-Strom (bei Raumladungs-Elektreten) [3] hervorruft. Wenige Jahre später wurde das Verfahren auch in der Frequenzdomäne implementiert, indem die Wärmeenergie mittels eines intensitätsmodulierten Dauerstrich-Lasers zugeführt wurde [4]. Letzteres ist in der Literatur als Laser-Intensitäts-Modulations-Methode (LIMM) bekannt. Hierbei entsteht in der Probe eine Wärmewelle, deren Amplitude und Eindringtiefe von der Modulationsfrequenz abhängt, welche über einen Frequenzbereich von mehreren Dekaden (typischerweise zwischen 10 Hz und 100 kHz) durchgestimmt wird. In einem 2003 erschienenen Übersichtsartikel wird die weitere Entwicklung ausführlich dargestellt [5].

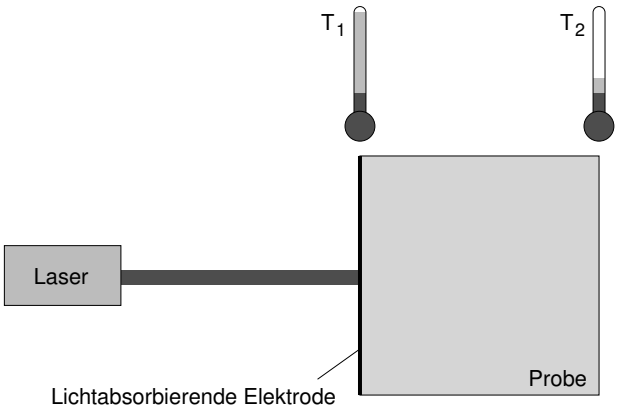

Bild 1: Prinzip des Wärmepuls-Verfahrens. Der absorbierte Laserstrahl erzeugt eine räumliche und zeitliche Temperaturverteilung.
Figure 1: Principle of the thermal-pulse method. The absorbed laser beam gives rise to a spatially and temporally variable temperature distribution.

Ein kürzlicher Vergleich zwischen LIMM und der Wärmepuls-Methode (wobei beide Verfahren mittels moderner Laser- und Messtechnik implementiert wurden) zeigte eine exzellente Übereinstimmung der Ergebnisse [6]. Deutlich unterschied sich allerdings die Messzeit: Das komplette Raumladungs-Tiefenprofil einer 17 µm dicken Polytetrafluorethylen- (PTFE-) Folie konnte mit der Wärmepuls-Methode in nur 40 s aufgenommen werden, während eine LIMM-Messung ca. 30 min dauerte. Hiervon ausgehend wurde eine Apparatur zur dreidimensionalen Messung von Polarisationsprofilen entwickelt, in der die Probe mittels eines fokussierten, gepulsten Laserstrahls abgetastet wird. Ähnliche Ansätze wurden bereits früher mittels des LIMM-Verfahrens in der Frequenzdomäne verfolgt, blieben jedoch aufgrund der wesentlich längeren Messdauer auf eindimensionale Messungen [7], zweidimensionale Abtastungen weniger Messpunkte bei voller Tiefenauflösung [8] oder die Abtastung größerer Flächen mit begrenzter Tiefeninformation [9; 10] beschränkt.

2 Experimenteller Aufbau

Zur Erzeugung der Wärmepulse dient ein gütegeschalteter, frequenzverdoppelter Nd:YAG-Laser (Polaris III, New Wave Research), welcher 5 ns lange Pulse mit einer Wiederholrate zwischen 2 und 6 Hz erzeugt. Die Lichtpulse werden mittels eines Teleskops auf die Metallelektrode der Probe fokussiert (Bild 2), wobei durch Variation der Probenposition Strahldurchmesser zwischen 30 und 400 µm einstellbar sind [11]. Die Proben (in der Regel 10 bis 250 µm dicke Polymerfolien) werden beidseitig mit lichtundurchlässigen Aluminium- oder Kupferelektroden (Dicke 200 nm) bedampft und auf ein Edelstahlsubstrat aufgeklebt, um thermoelastische Resonanzschwingungen zu vermeiden, welche sich dem Messsignal überlagern würden [12]. Die Positionierung im Laserstrahl erfolgt in der Probenebene (X- und Y-Richtung) mit zwei motorisierten Mikro-

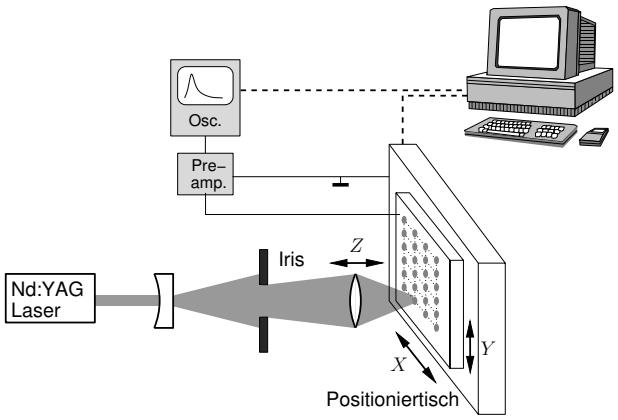

Bild 2: Versuchsaufbau für die Wärmepuls-Tomographie mit fokussierten Laserpulsen.
Figure 2: Experimental setup for focused thermal-pulse tomography.

meterschlitten (ERLIC 85, OWIS GmbH) sowie in Strahl- (Z-) Richtung mittels eines manuell einstellbaren Positioniertisches. Durch Hinzufügen eines zusätzlichen Drehmesstisches (DMT 40, OWIS GmbH) können außerdem zylinderförmige Objekte, wie z. B. koaxiale Sensorkabel (Bild 3), untersucht werden. Diese Kabel (Huber & Suhner, Schweiz) wurden nach Entfernen ihres Innenleiters, der äußeren Schutzschicht sowie der Abschirmung auf einen Edelstahlstift mit 0,7 mm

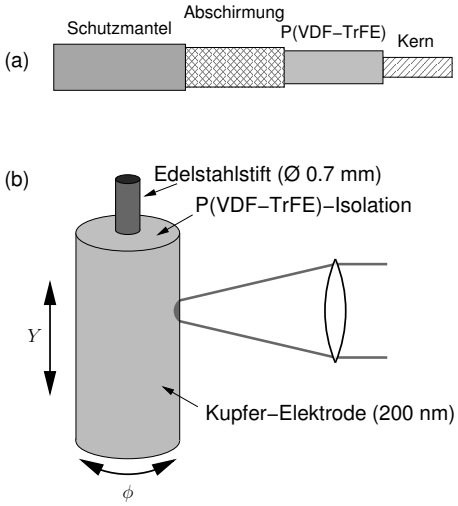

Bild 3: (a): Aufbau eines piezoelektrischen koaxialen Sensorkabels. (b): Untersuchung mittels Wärmepuls-Tomographie.
Figure 3: (a): Schematic view of a piezoelectric coaxial sensor cable. (b): Investigation by means of thermal-pulse tomography.

Durchmesser aufgezogen. Auf die aktive Schicht wird wie bei den planaren Filmen eine 200 nm dicke Kupferschicht aufgedampft, welche als lichtabsorbierende Elektrode dient.

Der Kurzschlussstrom wird mit einem Strom-Spannungs-Wandler variabler Verstärkung und Bandbreite (Stanford Research SR 570) verstärkt und mit einem digitalen Speicheroszilloskop (Agilent 54833A) aufgezeichnet. Man erhält so ein transientes Stromsignal mit ca. $N = 512\,000$ Datenpunkten, wobei zur Verbesserung des Signal/Rausch-Verhältnisses ca. 30 bis 50 Pulse gemittelt werden. Die Abtastung einer Probe mit 45×45 Messpunkten (also einem Bild mit ca. 2000 Bildpunkten) liefert insgesamt etwa 4 GB an Rohdaten.

3 Auswertung

Der transiente Kurzschlussstrom $I(t_k)$, $k = 1 \ldots N$ wird mittels Fourier-Transformation in die Frequenzdomäne konvertiert:

$$\tilde{J}_{\mathrm{exp}}(f_n) = \frac{\Delta t}{\tilde{\alpha}(f_n)} \sum_{k=0}^{N-1} I(t_k) e^{-2\pi i k n/N}\,, \tag{1}$$

wobei

$$f_n = \frac{n}{N\Delta t}\,, \quad n = 1 \ldots \frac{N}{2} \tag{2}$$

und Δt das Zeitintervall ist, mit dem das transiente Signal aufgezeichnet wird. Gegenüber einer Auswertung in der Zeitdomäne hat man hier den Vorteil, dass die frequenzabhängige Verstärkung und Phasenverschiebung des Strom-Spannungs-Wandlers (ausgedrückt durch die komplexe Größe $\tilde{\alpha}(f_n)$) mittels einer einfachen Division kompensiert werden kann [6], wie in Gl. (1) geschehen.

Der Zusammenhang zwischen der Verteilung des pyroelektrischen Koeffizienten $p(x, y, z)$ und dem pyroelektrischen Strom wird durch die sog. LIMM-Gleichung

$$\tilde{J}(f_n) = \frac{i2\pi f_n}{d} \int_0^d \int_{-\infty}^{\infty} \int_{-\infty}^{\infty} p(x, y, z) \times \tilde{T}(x, y, z, f_n)\,\mathrm{d}x\,\mathrm{d}y\,\mathrm{d}z \tag{3}$$

gegeben, wobei d die Probendicke und $\tilde{T}(x, y, z, f_n)$ die frequenzabhängige Temperaturamplitude der Wärmewelle ist. Die Koordinaten x und y geben die Position auf der Probe in lateraler Richtung an; z ist die Tiefenkoordinate. Im eindimensionalen Fall (näherungsweise erfüllt, wenn sich p in lateraler Richtung nur langsam verändert) reduziert sich Gl. (3) auf (vgl. [13]):

$$\tilde{J}(f_n) = \frac{i2\pi f_n A}{d} \int_0^d p(z)\tilde{T}(z, f_n)\,\mathrm{d}z\,. \tag{4}$$

Für homogene Polymerschichten existiert eine analytische Lösung $\tilde{T}(z, f_n)$ der eindimensionalen Wärmeleitungsgleichung [12], während die Temperaturverteilung im allgemeinen Fall nur numerisch berechnet werden kann.

Gleichung (4) ist eine Fredholm'sche Integralgleichung erster Art, deren Lösung $p(z)$ bei bekannter linker Seite $\tilde{J}(f_n)$ ein schlecht gestelltes Problem ist. Grob gesagt existieren unendlich viele Lösungen, die – innerhalb der experimentellen Unsicherheit – die Messdaten korrekt wiedergeben. Es gibt jedoch eine Reihe von Verfahren, um aus dieser Lösungsschar die physikalisch sinnvollste Lösung zu isolieren, wie z. B. iterative Ansätze [14], Tikhonov-Regularisierung [15] oder ein sehr einfach anzuwendendes Näherungsverfahren [16], welches in Oberflächennähe sehr zuverlässige Resultate liefert. Letztere Verfahren wurden auch in der vorliegenden Arbeit angewandt. Eine allgemeine Lösung für die dreidimensionale LIMM-Gleichung (3) ist noch Gegenstand aktueller Forschungsarbeiten.

4 Ergebnisse

4.1 Ebene Poly(vinylidenfluorid)-Folien

Erste Tests des Wärmepuls-Tomographieverfahrens wurden an 11 µm dicken, uniaxial verstreckten Folien aus β-Poly(vinylidenfluorid) (PVDF) durchgeführt. Diese erhielten eine strukturierte Polung, in dem auf die Oberseite eine „T"-förmige Aluminiumelektrode aufgedampft wurde, über die ein elektrisches Feld oberhalb der Koerzitivfeldstärke angelegt wurde. Nach erfolgter Polung wurde diese Elektrode durch eine vollflächige 200 nm dünne Kupferelektrode ersetzt. Anschließend wurde eine Fläche von $7 \times 7\,\mathrm{mm}^2$ mit einer Schrittweite von 200 µm abgetastet. Das Messergebnis ist in Bild 4 dargestellt. Deutlich ist die strukturierte Polarisation erkennbar, wobei trotz des hohen Polungsfeldes von $100\,\mathrm{V/\mu m}$ (doppelt so groß wie die Koerzitivfeldstärke) für $z < 1$ µm eine deutliche Randdepolarisation auftritt. Die Tiefenauflösung ist nach [16] durch die Beziehung zwischen der Eindringtiefe z_a einer thermischen Welle und der Frequenz gegeben:

$$z_a = \sqrt{\frac{D}{\pi f}}\,, \tag{5}$$

wobei D die Wärmediffusivität der Probe ist, welche aus der Wärmeleitfähigkeit κ, der Dichte ρ und der Wärmekapazität c mittels $D = \kappa/(c\rho)$ berechnet werden kann und z. B. für PVDF ca. $6 \times 10^{-8}\,\mathrm{m}^2/\mathrm{s}$ beträgt. Hieraus ist ersichtlich, dass die Tiefenauflösung in Oberflächennähe im Wesentlichen durch die Bandbreite

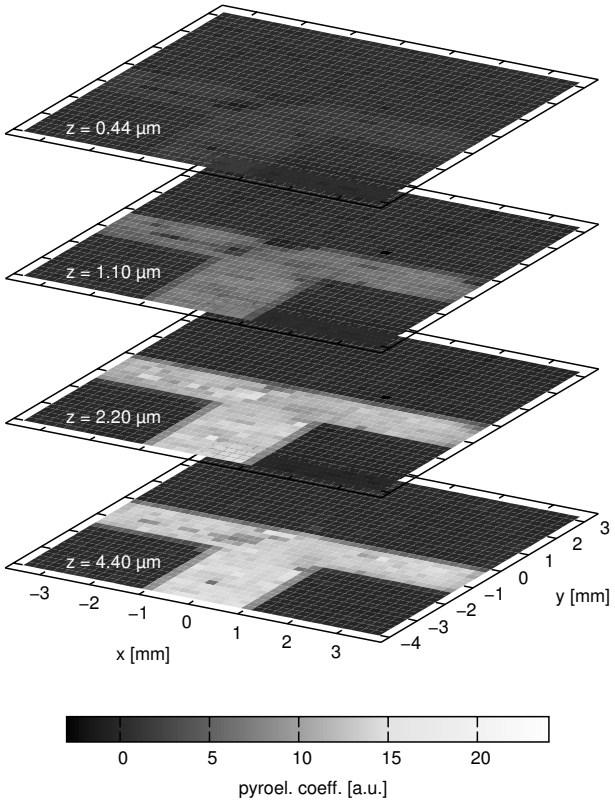

Bild 4: Karte der Polarisationsverteilung in einer 11 µm dicken PVDF-Folie, welche mit einer strukturierten Elektrode gepolt wurde.
Figure 4: Polarization map of an 11 µm PVDF film poled with a patterned electrode.

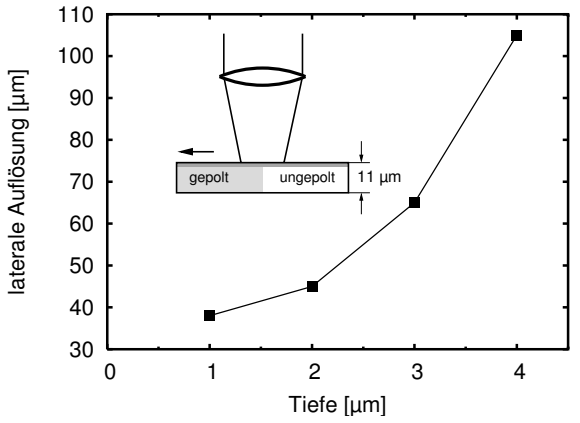

Bild 5: Tiefenabhängigkeit der lateralen Auflösung in PVDF bei einem Strahldurchmesser von 30 µm.
Figure 5: Depth-dependence of the lateral resolution in PVDF at a beam spot size of 30 µm.

der Verstärkerelektronik gegeben ist; bei einer Bandbreite von 100 kHz erreicht man beispielsweise Werte von ca. 0,4 µm.

Um die laterale Auflösung zu ermitteln, wurde eine Reihe von Scans über die Kante der „T"-Elektrode durchgeführt, also einen abrupten Übergang zwischen gepoltem und ungepoltem Material. Der Laserstrahl wurde hierbei auf eine Größe von 30 µm fokussiert. Wie aus Bild 5 ersichtlich, verschlechtert sich die laterale Auflösung von 38 µm in einer Tiefe von 1 µm auf mehr als 100 µm in einer Tiefe von 4 µm. Trotzdem ist dies eine deutliche Verbesserung gegenüber vergleichbaren, mit akustischen Verfahren gewonnenen Resultaten [17]. Die Tiefenabhängigkeit der lateralen Auflösung wird durch die sehr unterschiedlichen Wärmediffusivitäten des Polymers und der Metallelektrode verursacht, die sich um ca. einen Faktor 1000 unterscheiden. Da die Diffusionslänge ℓ zu einer gegebenen Zeit t durch $\ell = \sqrt{Dt}$ gegeben ist, breitet sich der Wärmepuls in der Metallelektrode ca. $\sqrt{1000} \approx 30$ mal schneller aus als im Polymer, wodurch der Wärmepuls in lateraler Richtung „zerfließt". Eine interessante Folge ist, dass die ursprünglich geheizte Frontelektrode dadurch schneller abkühlt als das benachbarte Polymer und sich daher von einer Wärmequelle in eine Wärmesenke verwandelt. Diese qualitative Betrachtung wird durch Finite-Elemente-Rechnungen bestätigt [11]. Eine Verbesserung der lateralen Auflösung erfordert daher ein Elektrodenmaterial mit guter elektrischer, aber geringer thermischer Leitfähigkeit.

4.2 Koaxiale Sensorkabel aus PVDF-TrFE

Koaxiale Sensorkabel (bei denen die aktive Schicht aus einem piezoelektrischen Material wie z. B. P(VDF-TrFE), dem Kopolymer aus Vinylidenfluorid und Trifluorethylen, besteht) werden z. B. bei der Verkehrsüberwachung oder in Einbruchsmeldeanlagen eingesetzt. Die Polarisation der aktiven Schicht wird üblicherweise dadurch erzeugt, dass das extrudierte Kabel durch eine Korona-Entladung läuft, welche durch einen Kranz aus Nadeln erzeugt wird, an denen Hochspannung anliegt. Während die gemittelten piezoelektrischen Eigenschaften bereits untersucht wurden [18], gab es bisher keine Studien zur räumlichen Verteilung der Polarisation. Dies konnte nun erstmals mit Hilfe der

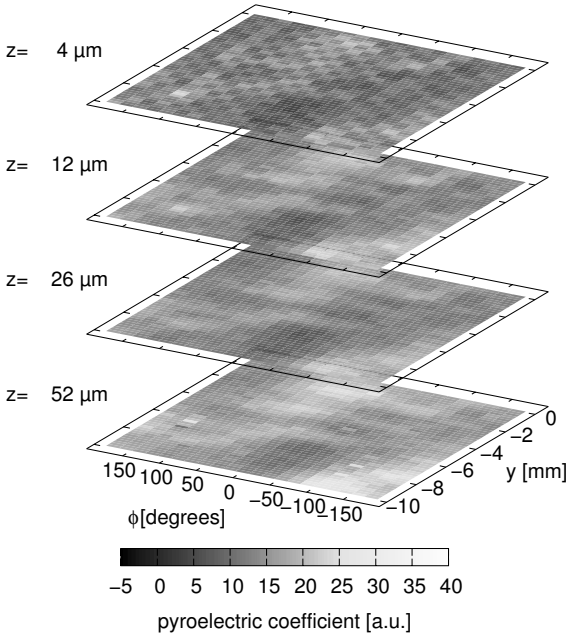

Bild 6: Polarisationsverteilung eines piezoelektrischen Sensorkabels, welches in einem kontinuierlichen Prozess mit vier ringförmig angeordneten Korona-Nadeln bei +20 kV gepolt wurde.
Figure 6: Polarization map of a piezoelectric sensor cable poled in a continuous process with four corona needles at +20 kV.

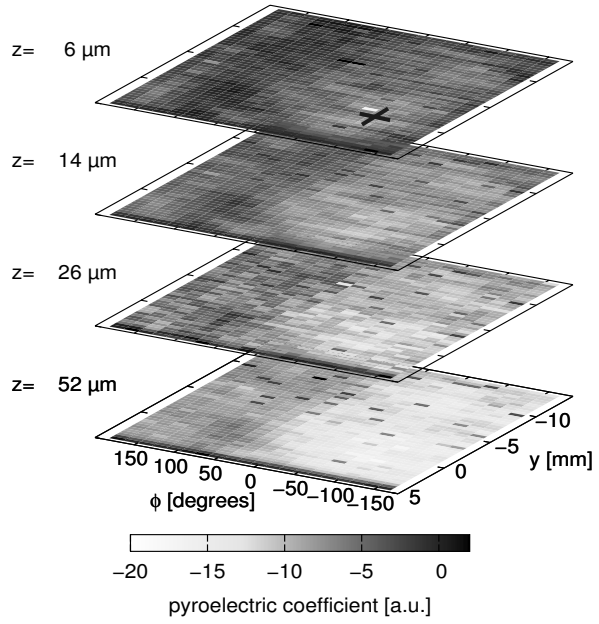

Bild 7: Polarisationsverteilung eines piezoelektrischen Sensorkabels, welches stationär mit einer Koronaspannung von −25 kV gepolt wurde. Das Kreuz markiert die projizierte Position der Nadel.
Figure 7: Polarization map of a piezoelectric sensor cable poled for 30 s with a single fixed needle at −25 kV. The cross marks the projected needle position.

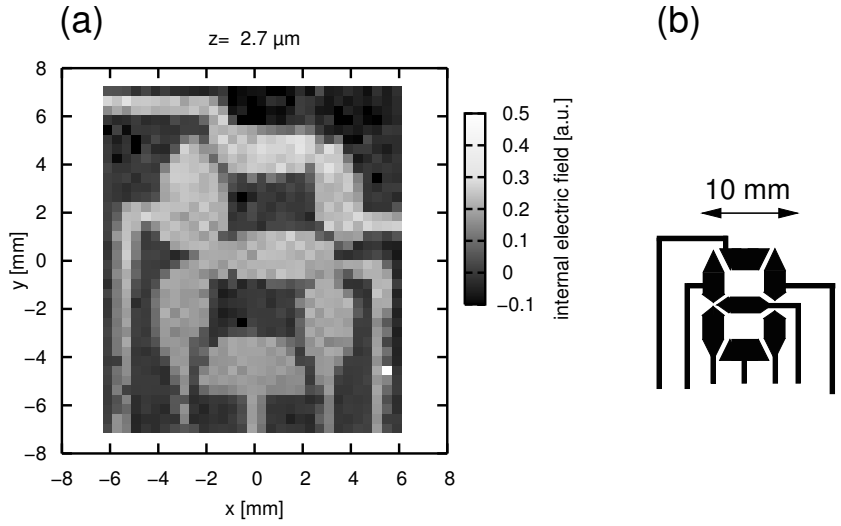

Bild 8: Internes elektrisches Feld in einer mittels Elektronenstrahl aufgeladenen, 17 µm dicken PTFE-Folie. (a): Feldverteilung in einer Tiefe von $z = 2{,}7$ µm, (b): für die Aufladung verwendete Maske. (Aus [11]. Die Probe wurde freundlicherweise von Dr. Lucas F. Santos, Instituto de Física de São Carlos, Brasilien, zur Verfügung gestellt.)
Figure 8: Internal electric field in electron-beam irradiated PTFE film ($d = 17$ µm). (a): field distribution at a depth of $z = 2.7$ µm, (b): shadow mask used for charging. (From [11]. Sample courtesy of Dr. Lucas F. Santos, Instituto de Física de São Carlos, Brazil.)

Wärmepuls-Tomographie erreicht werden. In der vorliegenden Arbeit wurden sowohl Kabel untersucht, die in dem oben beschriebenen kontinuierlichen Prozess gepolt wurden, als auch Proben, die mittels einer einzelnen, stationären Koronaentladung behandelt wurden. Wie aus Bild 6 ersichtlich, zeigen erstere eine relativ ungleichmäßige Polarisationsverteilung, sowohl in Längs- (Y-) Richtung als auch entlang ihres Umfangs. Dies dürfte darauf zurückzuführen sein, dass die effektive Zeit, während der ein bestimmtes Kabelteilstück der Koronaentladung ausgesetzt war, aufgrund der relativ hohen Durchzugsgeschwindigkeit lediglich 300 ms betrug. In dieser kurzen Zeit kann sich noch kein hinreichend konstantes Oberflächenpotenzial aufbauen [19]. Die stationär gepolten Kabel, bei denen die Polungsdauer mindestens 30 s betrug, zeigen hingegen eine wesentlich gleichmäßigere Verteilung mit einem breiten Maximum unterhalb der Korona-Nadel (Bild 7).

4.3 Raumladungs-Elektrete

Mittels Wärmepuls-Tomographie können neben Polarisationsverteilungen auch Dichteverteilungen von Raumladungen gemessen werden. Als Beispiel ist in Bild 8a die Verteilung des durch die Raumladungen erzeugten internen elektrischen Feldes in einer 17 µm dicken PTFE-Probe dargestellt, welche mittels eines monoenergetischen Elektronenstrahls (15 keV) durch eine Maske (Bild 8b) hindurch strukturiert aufgeladen wurde. Alle Details der Maske werden detailgetreu abgebildet.

5 Zusammenfassung

Wärmepuls-Tomographie ist eine vielseitige, zerstörungsfreie Methode, um dreidimensionale Polarisations- und Raumladungsverteilungen mit einer lateralen Auflösung von bis zu 40 µm zu untersuchen. Es können sowohl planare als auch zylindrische Geometrien, wie sie z. B. in piezoelektrischen Sensorkabeln vorkommen, vermessen werden. Durch Optimierung des Elektrodenmaterials und eine verbesserte Datenauswertung, welche die Wärmeausbreitung in der Fläche berücksichtigt, sollte die Auflösung – vor allem in größeren Tiefen – in Zukunft noch verbessert werden können.

Literatur

[1] *G. M. Sessler und J. E. West*: Self-biased condenser microphone with high capacitance. J. Acoust. Soc. Am. 34 (1962), S. 1787.
[2] *H. Kawai*: The piezoelectricity of poly(vinylidene fluoride). Jpn. J. Appl. Phys. 8 (1969), S. 975–977.

[3] *R. E. Collins*: Analysis of spatial distribution of charges and dipoles in electrets by a transient heating technique. J. Appl. Phys. 47 (1976), S. 4804–4808.
[4] *S. B. Lang und D. K. Das-Gupta*: A technique for determining the polarization distribution in thin polymer electrets using periodic heating. Ferroelectrics 39 (1981), S. 1249–1252.
[5] *S. Bauer und S. Bauer-Gogonea*: Current practice in space charge and polarization profile measurements using thermal techniques. IEEE Trans. Dielectr. Electr. Insul. 10 (2003), S. 883–902.
[6] *A. Mellinger, R. Singh und R. Gerhard-Multhaupt*: Fast thermal-pulse measurements of space charge distributions in electret polymers. Rev. Sci. Instrum. 76 (2005), S. 013903.
[7] *Ş. Yilmaz, S. Bauer, W. Wirges und R. Gerhard-Multhaupt*: Scanning electro-optical and pyroelectrical microscopy for the investigation of polarization patterns in poled polymers. Appl. Phys. Lett. 63 (1993), S. 1724–1726.
[8] *D. Marty-Dessus, L. Berquez, A. Petre und J. L. Franceschi*: Space charge cartography by FLIMM: a three-dimensional approach. J. Phys. D: Appl. Phys. 35 (2002), S. 3249–3256.
[9] *B. Ploss, W. Hassler, H. Hulz und G. Kobernik*: Investigation of the polarization depth distribution of PZT thick films by LIMM. In: *Proceedings, 11th IEEE Symp. on Applications of Ferroelectrics*, S. 207–210. IEEE Service Center, Piscataway, NJ (1998).
[10] *A. Quintel, J. Hulliger und M. Wübbenhorst*: Analysis of the polarization distribution in a polar perhydrotriphenylene inclusion compound by scanning pyroelectric microscopy. J. Phys. Chem. B 102 (1998), S. 4277–4283.
[11] *A. Mellinger, R. Singh, M. Wegener, W. Wirges, R. Flores Suárez, S. B. Lang, L. F. Santos und R. Gerhard-Multhaupt*: High-resolution three-dimensional space-charge and polarization mapping with thermal pulses. In: *Proceedings, 12th International Symposium on Electrets*, S. 212–215. IEEE Service Center, Piscataway, NJ (2005).
[12] *P. Bloß und H. Schäfer*: Investigations of polarization profiles in multilayer systems by using the laser intensity modulation method. Rev. Sci. Instrum. 65 (1994), S. 1541–1550.
[13] *S. B. Lang*: Laser intensity modulation method (LIMM): Review of the fundamentals and a new method for data analysis. IEEE Trans. Dielectr. Electr. Insul. 11 (2004), S. 3–12.
[14] *A. Mellinger*: Unbiased iterative reconstruction of polarization and space-charge profiles from thermal-wave experiments. Meas. Sci. Technol. 15 (2004), S. 1347–1353.
[15] *A. N. Tikhonov, A. V. Goncharskii, V. V. Stepanov und I. V. Kochikov*: Ill-posed image processing problems. Sov. Phys.-Doklady 32 (1987), S. 456–458.
[16] *B. Ploss, R. Emmerich und S. Bauer*: Thermal wave probing of pyroelectric distributions in the surface region of ferroelectric materials: A new method for the analysis. J. Appl. Phys. 72 (1992), S. 5363–5370.
[17] *T. Maeno*: Three-dimensional PEA charge measurement system. IEEE Trans. Diel. Electr. Insul. 8 (2001), S. 845–848.
[18] *M. Wegener und R. Gerhard-Multhaupt*: Electric poling and electromechanical characterization of 0.1 mm-thick sensor films and 0,2 mm-thick cable layers from piezoelectric poly(vinylidene fluoride-trifluoroethylene). IEEE Trans. Ultrason. Ferroelectr. Freq. Control 50 (2003), S. 921–931.
[19] *R. Flores Suárez, A. Mellinger, M. Wegener, W. Wirges, R. Gerhard-Multhaupt und R. Singh*: Thermal-pulse tomography of polarization distributions in a cylindrical geometry. IEEE Trans. Dielectr. Electr. Insul. 13 (2006), S. 1030–1035.

Priv.-Doz. Dr. Axel Mellinger ist wissenschaftlicher Mitarbeiter und Dozent am Institut für Physik der Universität Potsdam. Sein Hauptarbeitsgebiet ist die Physik polymerer Elektrete, insbesondere deren Charakterisierung mittels einer Reihe von optischen, elektrischen und mechanischen Methoden, sowie die Untersuchung mikroskopischer Mechanismen der Ladungsspeicherung.
Adresse: Universität Potsdam, Institut für Physik, Am Neuen Palais 10, 14469 Potsdam, E-Mail: axm@uni-potsdam.de

Rosaura Flores Suárez, M.Sc. absolvierte 2005 ihr Studium der Polymerwissenschaft als *Master of Science* und ist seither als Doktorandin am Institut für Physik der Universität Potsdam tätig, wo sie an der Weiterentwicklung thermischer Messverfahren sowie deren Anwendung auf ferroelektrische Polymere arbeitet.
Adresse: Universität Potsdam, Institut für Physik, Am Neuen Palais 10, 14469 Potsdam, E-Mail: floressu@uni-potsdam.de

Rajeev Singh, M.Tech. ist Dozent am Department of Electronics & Communication an der University of Allahabad, Indien, und arbeitet gegenwärtig an der Fertigstellung seiner Dissertation. Teile seiner Doktorarbeit entstanden während eines 15-monatigen, vom DAAD finanzierten Gastaufenthalts an der Universität Potsdam.
Adresse: University of Allahabad, Department of Electronics & Communication, (U. P.)-211002 Allahabad, INDIA, E-Mail: r_singhjkiapt@rediffmail.com

Dr. Michael Wegener ist seit Januar 2007 wissenschaftlicher Mitarbeiter am Fraunhofer Institut für Angewandte Polymerforschung in Potsdam-Golm und war zuvor Projektleiter am Institut für Physik der Universität Potsdam. Seine Hauptarbeitsgebiete sind die Untersuchung neuer zellulärer Raumladungselektrete (sog. Ferroelektrete) und ferroelektrischer Polymere, deren elektrische und elektromechanische Eigenschaften sowie deren Anwendungen für Sensoren und Aktoren.
Adresse: Fraunhofer Institut für Angewandte Polymerforschung (IAP), FB Funktionale Polymersysteme, Geiselbergstraße 69, 14476 Potsdam-Golm,
E-Mail: michael.wegener@iap.fraunhofer.de

Dipl.-Ing. Werner Wirges ist Forschungs-Ingenieur am Institut für Physik der Universität Potsdam. Seine Arbeitsschwerpunkte liegen in der Herstellung und Charakterisierung neuer polymerer Sensorwerkstoffe.
Adresse: Universität Potsdam, Institut für Physik, Am Neuen Palais 10, 14469 Potsdam,
E-Mail: wwirges@uni-potsdam.de

Prof. Dr. Reimund Gerhard-Multhaupt ist Inhaber des Lehrstuhls für Angewandte Physik kondensierter Materie an der Universität Potsdam.
Adresse: Universität Potsdam, Institut für Physik, Am Neuen Palais 10, 14469 Potsdam,
E-Mail: rgm@uni-potsdam.de

Der Artikel ist eine Überarbeitung eines Beitrags zur Tagung „Sensoren und Messsysteme“, Freiburg, 13.–14.03.2006.

3.4 Theoretical framework

3.4.1 Signal generation

Let us consider the electrical signal generated from a sample metallized on both sides. Since the electroded area of the sample commonly has larger dimensions than the thickness, the transient temperature distribution inside the sample can be considered in one dimension, i.e. in the depth z [69, 29]. The generated short-circuit pyroelectric current is [19]:

$$I(t) = \frac{A}{d} \int_0^d r(z) \frac{\partial T(z,t)}{\partial t} dz, \tag{3.1}$$

where A is the electroded area and $r(z)$ a function which contains contributions from the spatially dependent spontaneous polarization and space charge density,

$$r(z) = \alpha_p P(z) - (\alpha_z - \alpha_\epsilon)\epsilon_0 \epsilon E(z). \tag{3.2}$$

α_p , α_z, α_ϵ, ϵ and $E(z)$ are the relative temperature dependence of the polarization, relative thermal expansion coefficient, relative temperature dependence of the permittivity, the relative permittivity of the material, and the thickness-dependent electric field, respectively.

It should be stressed that the thermal techniques provide a distribution function $r(z)$ without distinguishing specific contributions from polarization or space charge. In order to obtain unique information, prior knowledge of the investigated dielectric is necessary. Bauer and Bauer-Gogonea [19] mentioned two types of materials which generate an electrical signal that can be discriminated.

- Nonpolar dielectrics such as PTFE (known as Teflon) and its copolymers, since only the contribution of $E(z)$ in equation 3.2 is observed.
- Polar polymers such as PVDF, its copolymers and other ferroelectric materials, since there is a local compensation of the polarization distribution $\rho(z) = dP/dx$ by charges. Thus, only $P(z)$ contributes in equation 3.2.

Likewise, acoustic techniques have the same difficulty of distinguishing contributions from $E(z)$ and $P(z)$ on the measured electrical signal. In this case, the pyroelectric coefficient has to be replaced by the piezoelectric coefficient.

3.4.2 Temperature distribution

If the heated area is larger than the thickness d of the sample, then the one-dimensional heat-conduction equation gives the temperature distribution inside the sample [69].

$$D\frac{\partial^2\widetilde{T}(z,t)}{\partial z^2} = \frac{\partial\widetilde{T}(z,t)}{\partial t} \tag{3.3}$$

D is the thermal diffusivity, also expressed as $D = \kappa/c\rho$, κ is the thermal conductivity, the product $c\rho$ is the heat capacity per volume and $\widetilde{T}$ is the complex temperature amplitude as a function of z and time t.

The boundary conditions to solve the previous equation are

$$\kappa\frac{\partial\widetilde{T}(z,t)}{\partial z}_{z=0} = \eta\widetilde{j}e^{i\omega t} \tag{3.4}$$

$$\kappa\frac{\partial\widetilde{T}(z,t)}{\partial z}_{z=d} = 0 \tag{3.5}$$

η is the absorption coefficient of the deposited electrode and $\widetilde{j}e^{i\omega t}$ the light intensity. Solving equation 3.3, the complex amplitude of the transient temperature can be expressed as [78]:

$$\widetilde{T}(z,t) = \frac{\eta j\cosh[k(d-z)]}{k\kappa\sinh(kd)}e^{i\omega t} \tag{3.6}$$

with

$$k = (i+1)k_r \tag{3.7}$$

and

$$k_r = \sqrt{\omega/2D}. \tag{3.8}$$

In equation 3.6 the sample thickness is denoted as d. From the thermal excitation, the short-circuit pyroelectric current $I(t) = \widetilde{I}e^{i\omega t}$ is given by equation 3.1.

Now considering a compensation of the polarization $P(z)$ by a charge density $\rho(z)$, as in the case for a polar ceramic or polymer, equation 3.2 is simplified as:

$$r(z) = \alpha_p P(z) = p(z) \tag{3.9}$$

Otherwise, in case of a non-polar sample ($P(z) = 0$), only the electric field is calculated. If equations 3.6 and 3.9 are inserted into 3.1 also known as the LIMM equation,

$$\widetilde{I} = \frac{A}{d}\frac{\eta j}{c\rho}\frac{k}{\sinh(kd)}\int_0^d p(z)\cosh[k(d-z)]dz, \tag{3.10}$$

the problem of determining the pyroelectric coefficient from the measured pyroelectric spectrum is a deconvolution problem. The resultant equation (3.10) belongs to the so-called

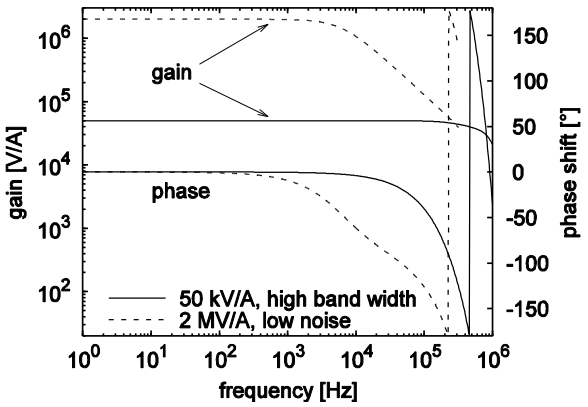

Figure 3.8: The strong dependence of the thermal-pulse signal on the gain and bandwidth settings of the pre-amplifier [65].

Fredholm integral equations of the first kind. The inversion of these equations is an ill-posed problem. Thus, a large number of polarization distributions $p(z)$ will satisfy the equation within the experimental uncertainties [30]. In order to find the most suitable function it is necessary to know the dielectric under investigation, i.e. its thermal parameters (thermal diffusivity), thickness, poling method and the origin of the measured electrical signal, which can be generated by oriented-dipoles and/or trapped-charges in the bulk [19].

In the present work, the same experimental implementations used by Mellinger et al. [25] were followed. The pyroelectric current is divided by the gain spectrum. The objective is to compensate the distortion caused by the strong current dependence on the gain and bandwidth setting of the preamplifier (see Fig. 3.8). Afterwards, the current is transformed into the frequency domain using a Fast Fourier transform (FFT) algorithm [79]. Thus, a similar analysis as used for LIMM data is possible.

$\widetilde{J}(f_n)$ is the pyroelectric current in the frequency domain

$$\tilde{J}(f_n) = \frac{\Delta t}{\widetilde{\alpha}(f_n)} \sum_{k=0}^{N-1} I(t_k) e^{-2\pi i k n/N} \,, \tag{3.11}$$

where $I(t_k)$ is the short circuit current in the time domain and $\tilde{\alpha}(f_n)$ is the gain spectrum. The frequency points f_n are defined by

$$f_n = \frac{n}{N\Delta t} \,, \qquad n = 1 \ldots \frac{N}{2} \,. \tag{3.12}$$

where Δt is the sampling interval and N is the number of recorded data points.

3.5 Methods for data analysis

As mentioned before, the deconvolution may be achieved by finding the Fourier coefficients from the distribution function. The number of coefficients (approx. 10) is limited to the accuracy of the electrical response if the sample has been measured from both sides. The information yielded is more accurate near the sample surface. There are other methods such as the Scale Transformation technique [80], Regularization [77, 81, 30] and more recently Monte Carlo method [31, 82, 83]. Some of them are described briefly in the next section.

3.5.1 Regularization techniques and L-curve method

There is a well-known method for deconvolution called regularization that requires a smooth polarization distribution which may contain hills and valleys but no sharp transitions. Lang [30] introduced the Polynomial Regularization Method (PRM) where the polarization distribution is represented as an eighth-degree polynomial

$$p(z) = \lambda_0 + \lambda_1\gamma(z) + \lambda_2\gamma(z)^2 + ... \tag{3.13}$$

where

$$\gamma(z) = \frac{\log(z) - \log(z_1)}{\log(z_2) - \log(z_1)}. \tag{3.14}$$

z_1 and z_2 are the spatial coordinates of upper (irradiated) and lower surfaces of the sample, respectively. The coefficients λ_i must be determined. Equation 3.13 should be inserted into equation 3.1 and the integral is evaluated numerically. Then the real and imaginary parts of the pyroelectric current $\widetilde{J}_{\text{calc}}$ as a function of the λs are calculated. In the Regularization technique, the equation below is minimized with respect to the λs.

$$\sum_n \left\| \widetilde{J}_{\text{exp}}(f_n) - \widetilde{J}_{\text{calc}}(f_n) \right\|^2 + r \int_0^d \left(\frac{d^2 p(z)}{dz^2} \right) dz \tag{3.15}$$

r is known as the weight factor or regularization parameter. It determines the weight of the first or second term of the equation. If r is too small then artifacts such as maxima and minima will be introduced. If r is too large, the computed distribution will be overestimated and no details will be found. The L-curve method (LCM) presented by Hansen and O'Leary [77] is the most appropriate graphical tool for finding the optimal value of r. By selecting a range of values of r, two parameters are calculated for each r_i:

The data fit residual:

$$\phi(r) = \sum_n \left\| \widetilde{J}_{\text{exp}}(f_n) - \widetilde{J}_{\text{calc}}(f_n) \right\|^2 \tag{3.16}$$

and the roughness residual:

$$\eta(r) = \int_0^d \left(\frac{d^2 p(z)}{dz^2} \right) dz. \tag{3.17}$$

This last one represents the lack of smoothness in the calculated polarization distribution. The resulting graph of $log(\rho)$ versus $log(\eta)$ shows a characteristic L-shape. The best regularization parameter, r, will be the value of the maximum curvature.

The accuracy of the method is shown in Fig.3.9. Lang et al. [82] took two arbitrarily simulated data, denominated *true*, from a PZT plate (20 µm thick) and report how the discontinuity of the *true* polarization distribution may reduce the accuracy of the L-curve method.

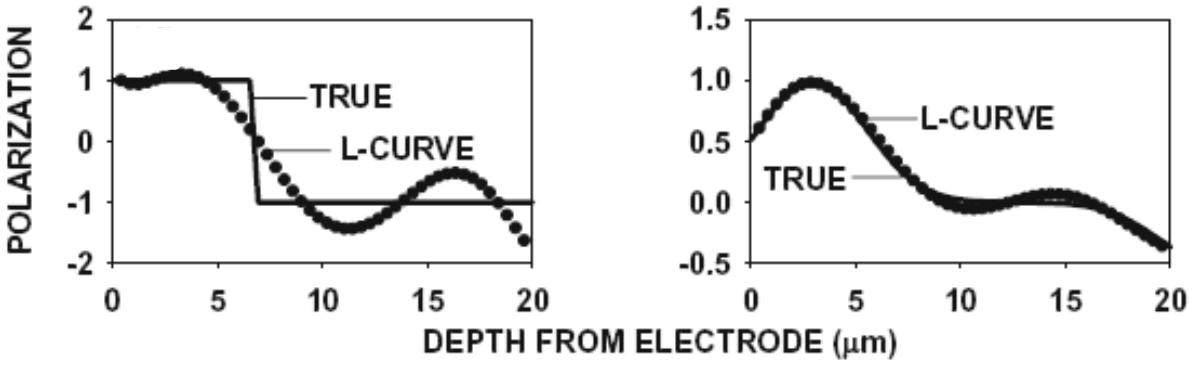

Figure 3.9: Weak side of the L-curve method (circles). The *true* data are a simulated polarization distribution from a PZT plate (solid line) [82, 83]

.

3.5.2 Scale Transformation method (ST)

This technique was reported by Ploss et al. [80]. This is one of the most widely used methods to obtain the pyroelectric distribution in a region near the sample surface. The main equations are summarized in this section.

The transient temperature that gives an approximate solution to the LIMM equation equation is,

$$\Delta\widetilde{T}(z,t) = \frac{\eta\widetilde{j}}{\kappa}\frac{e^{-kz}}{k}e^{i\omega t}. \tag{3.18}$$

This expression of the temperature amplitude differs by less than 1% from the original values in the range $0 \leq z \leq d/4$, and the precision reduces beyond this range (around 25% when $z = d/2$). Consequently, the pyroelectric current $\widetilde{I}$ is expressed as

$$\widetilde{I} = \frac{\eta\widetilde{j}A}{c\rho d}\int_0^\infty p(z)ke^{-kz}dz \tag{3.19}$$

Then separating the real $\Re$ and imaginary $\Im$ parts of the pyroelectric current $\widetilde{I}$, the component which has a phase shift of $\pi/4$ compared to the incoming light $\tilde{j}$ is called the "Thermal-Window Function" (TWF) by Lang [30],

$$(\Re - \Im)\,\widetilde{I} = \frac{\eta\widetilde{j}A}{c\rho d}\int_0^\infty p(z)2k_r\sin(k_r z)e^{-k_r z}dz \tag{3.20}$$

Considering now a position

$$z_r = 1/k_r = \sqrt{2D/\omega} \tag{3.21}$$

Then a function $p_a(z_r)$ is obtained

$$p_a(z) = \frac{c\rho d}{\eta\tilde{j}A}\left[(\Re - \Im)\widetilde{I}(\omega = 2D/{z_r}^2)\right]. \tag{3.22}$$

From the pyroelectric current spectrum $I(\omega)$, the function $p_a(z_r)$ can be calculated. Moreover it represents an approximation for the distribution of the pyroelectric coefficient.

$$p_a(z_r) = \int_0^\infty p(z)\frac{2}{z_r}\sin\left(\frac{z}{z_r}\right)e^{-z/z_r}dz. \tag{3.23}$$

The kernel of the integral is a product of the pyroelectric coefficient $p(z)$ with a normalized scanning function,

$$f_a(z,z_r) = \frac{2}{z_r}\sin\left(\frac{z}{z_r}\right)e^{-z/z_r} \tag{3.24}$$

whose expectation value is z_r. The functions $f_a(z,z_r)$ overcome the ill-conditioned equation 3.19. The method, as it is shown, is very simple and provides a straight-forward analysis of the data. The only drawback of this technique is the limited spatial resolution.

3.5.3 Monte Carlo (MC) method

Since the true space-charge or polarization distribution in a sample is not known, the accuracy of the methods for solving the LIMM equation can only be tested by using simulated data. In 2005 Tuncer and Lang [31] suggested a numerical approximation based on the Monte Carlo method. The numerical procedure is implemented as follows:

1. Write the LIMM equation as a summation over a random number n of z values, which should be around 90% of the number of frequency data points.
2. The complex transient temperature $\partial T(z,\omega)/\partial t$ is evaluated (real and imaginary parts) for each of the z and w values.
3. A matrix $\mathbf{T}$ is generated using the simulated frequencies as rows and the real and imaginary parts of the $\partial T(z,\omega)/\partial t$ as the columns. The result is a $2m \times n$ matrix.
4. The current is then represented as a column vector $\mathbf{j}$ whose length is m and the unknown distribution is also represented by a column vector with length $2m$.
5. The least-squares problem $T \bullet g = j$ is solved for $\mathbf{g}$. The minimization is run many times with different newly selected values and the resulting g values are averaged. A histogram is then plotted with the z_n and g_n values from each step.
6. The histograms, the result of dividing the z axis into 128, 64, 32 or 16 bins (channels) and the above-mentioned averaged values of g give the most probable polarization distribution.

In order to show and compare the accuracy of the Monte Carlo and the Scale Transformation method, Lang et al. [83] used simulated data of space-charge distribution in a PTFE film, 30 µm thickness (see Fig. 3.10).

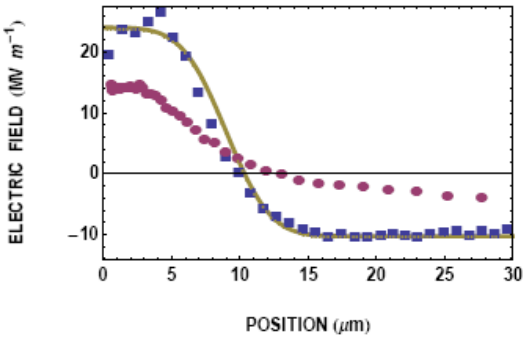

Figure 3.10: Methods to solve the LIMM equation: (a)Monte Carlo (squares) and Scale Transformation (circles) using an electric field distribution on a PTFE film (solid line) [83].

Partial conclusions

Ferroelectric polymers such as PVDF and its copolymers are promising materials for sensors. Despite the smaller pyroelectric-coeffcient values than those reported for ceramics, PVDF films exhibit a high flexibility. Research on processing and improvement of its properties is being actively performed. It was mentioned that there are two main groups of techniques to determine the space-charge and polarization profiles on ferroelectric materials: thermal- and acoustic methods. Both of these groups complement each other. The former methods show higher resolution near the sample surface. In our studies, samples with thicknesses ranging between 15 and 200 µm are investigated, therefore implementing a thermal method is preferable.

TP and LIMM (the most known thermal techniques) have been adapted in order to determine a three-dimensional map of polarization and space charge in relatively short times. These methods, known as TPT and FLIMM respectively, are candidates for future mapping of more complex systems such as polymer dispersed liquid crystals and multilayer ferroelectrets. The TPT method is also suitable for scanning planar and cylindical geometries.

There are several ways to perform the deconvolution process of the LIMM equation, which relates the short-circuit current with the polarization- and electric-field distribution. The most used methods since the 1990s are Regularization and the Scale Transformation method. In 2005, the Monte Carlo method was proposed as one possibility to determine a polarization or space-charge distribution with higher accuracy than by means of ST and other regularizations. Monte Carlo requires highly complex computation skills, relatively high computer requirements even for one-dimensional data, and is a new method that requires discussion. The Scale Transformation method is a straightforward analysis of the TPT data that offers physically meaningful solutions of the LIMM equation. Also, ST is a simple method and offers continuous results without introducing any artifacts (unlike regularization methods) since it is directly related to the raw data. Therefore, the results presented in Chapter 4 were obtained after analysis with the ST method.

Chapter 4

TPT on Polymer Ferroelectrics

In this chapter the experiments performed on P(VDF-TrFE) samples by means of conventional Thermal-Pulse Tomography and the achieved publications are included. First, ferroelectric switching studies on ferroelectric copolymer films are discussed. Later, some possibilities to test and increase the lateral resolution of the TPT are described. Several samples metallized with narrower electrodes were used to test the resolution of thermal techniques. The characteristics and advantages of different patterned electrodes are discussed. The comparison of the three-dimensional mapping using TPT and FLIMM is also presented, and advantages and disadvantages of both techniques are highlighted. Finally, an improved (free-of-aberrations) TPT setup is presented.

4.1 Ferroelectric switching

Polarization reversal in copolymer of VDF with TrFE has been already observed with acoustical probing techniques (PPS) [84]. It was revealed that a drift of injected charges to the boundaries of the crystallites and a dipole alignment are required to stabilize the remanent polarization. The PPS method was also used by Bauer et al. to study the inhomogeneous polarization distribution in PVDF films and its influence in second-harmonic generation experiments [85]. The authors reported a local depolarization near the sample electrodes. The occurrence of depolarized surface layers has been explained as typical in the homopolymer and has been also observed with thermal methods [80]. The main objective of this section is to observe for the first time a depth resolved polarization reversal in P(VDF-TrFE) films and complement the studies that are being performed elsewhere [5,6,40,41,86].

4.1.1 Sample preparation

The samples used were prepared from a 15 mol% solution of P(VDF-TrFE) (65/35) (Solvay, Advanced Polymers, France) dissolved in acetone/dimethyl sulfoxide (20/80) wt%. This concentration solution assured sample thicknesses ranging from 10 to 20 µm. Spin-coating

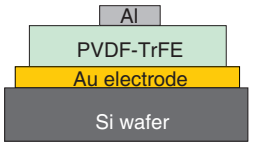

Figure 4.1: Electrode deposition on Si substrate films.

was performed at room temperature in air. The angular velocity was 1500 rpm for 50 s and the angular acceleration 50 rpm/s. The samples were deposited onto 50 nm gold-deposited silicon wafers (0.3 mm thickness and 50 mm diameter). In order to increase the crystallinity, the annealing treatment was carried out at 145 °C for 60 min in a clean atmosphere [6]. The final thickness of our samples was 15 µm. The circular back electrode consisted of 50 nm thick gold and the circular front electrode of 50 nm thick aluminum. The effective electrode area was determined by the 12 mm-diameter circular front electrode (Fig. 4.1).

4.1.2 Poling Conditions

All samples under investigation were poled by applying an unipolar/bipolar electric field (Fig. 4.2 left) at 10 mHz [34]. A sinusoidally varying field in a bipolar loop was applied with the polarization flips from positive to negative values of the coercive field. The last unipolar loops consist of a reversal of the remanent polarization from its previous orientation (Fig. 4.2 right). For our samples, once the coercive field around 55 MV/m was reached, the frequency was reduced to 3 mHz and three more cycles were applied. Switching studies on the ferroelectric films were performed on very well poled samples. Later the samples were scanned with the TPT method while they were subjected to different electric field values from zero until the remanent polarization was reached.

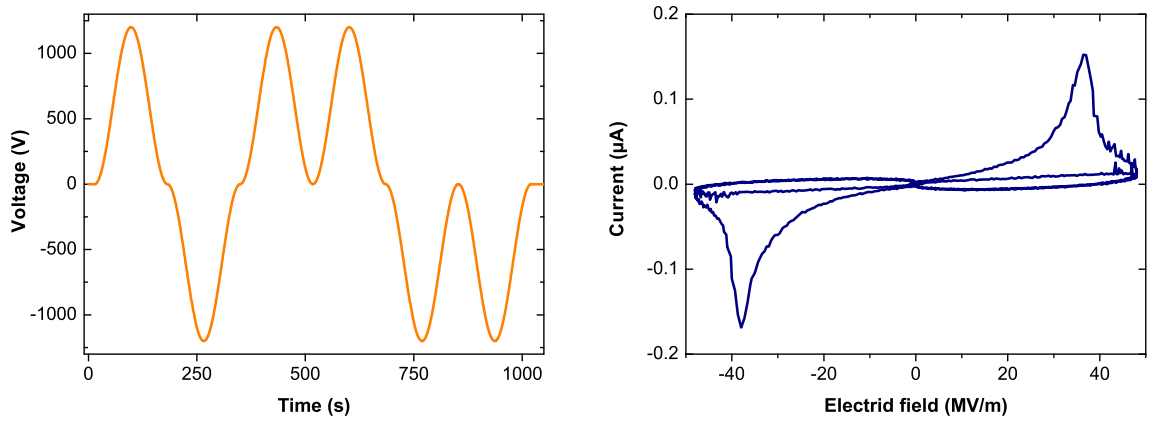

Figure 4.2: Poling P(VDF-TrFE) films applying a unipolar/bipolar electric field (left) and its corresponding current/voltage loop (right).

4.1.3 Thermal Pulse Tomography settings

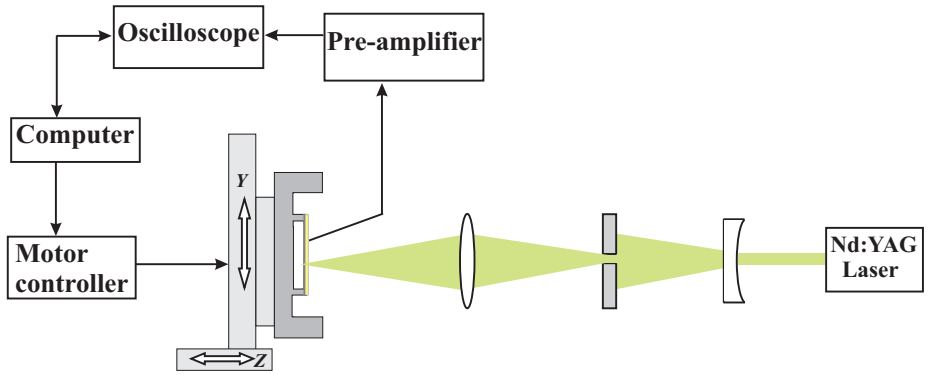

Figure 4.3: Thermal-Pulse Tomography setup for a planar geometry.

The thermal-pulse tomography setup has been already described for planar [25] and cylindrical geometry (see page 23). The setup is composed of a DC-Motor Controller (ERLIC 85, OWIS GmbH) which allows displacements in the $x-y$ plane. The thermal stimulation, provided by a Nd:YAG laser, is focused through a simple lens arrangement (Fig. 4.3). That produces spot sizes ranging from 400 µm down to 35 µm (Fig. 4.4). The spot sizes of the laser beam [87] were determined by means of a photodiode behind a knife-edge profiler, the latter placed at the sample holder. Another photodiode was placed as a reference before all optical elements. As the laser beam is incident on both photodiodes, electric current is generated and this is proportional to the incident power. The signal from the photodiode at the sample holder is later amplified, converted to voltage and stored in the oscilloscope. The intensity is then normalized with respect to the signal coming from the reference photodiode. The experiments were performed taking into account the threshold laser fluence at which strong evaporation may occur i.e. $\Phi_{th} = \rho\Omega\sqrt{D\tau_L}$ [88]. Ω is the specific enthalpy of evaporation, ρ is the density of aluminum and $\sqrt{D\tau_L}$ is the heat-diffusion length. This expression is valid when the duration of the laser pulse τ_L is of greater order than the lattice heating time τ_i of the metal electrode. Then, the energy deposited inside the metal electrode at a certain moment becomes larger than its specific enthalpy of evaporation. Considering the diffusivity of aluminum is $D = 9.8 \cdot 10^{-5}$ m^2/s and the laser-pulse duration is τ_L= 5 ns the resulting ablation threshold is 0.9 J/cm^2. This value was experimentally confirmed (see Appendix A).

Once the laser energy and the spot sizes were set, the short-circuit displacement current produced by the pyroelectric material was sent to a FEMTO LCA-200K-20M current-to-voltage converter (20 MV/A). The voltage was recorded by an Agilent 54833A oscilloscope with a sampling rate of 10 MSamples/s. For each beam pointing, the data from 30 laser pulses were averaged. The data obtained were analyzed using the Scale Transformation method (equation 3.22), where the thermal diffusivity of the P(VDF-TrFE) is $D = 7.9 \cdot 10^{-8}$ m^2/s.

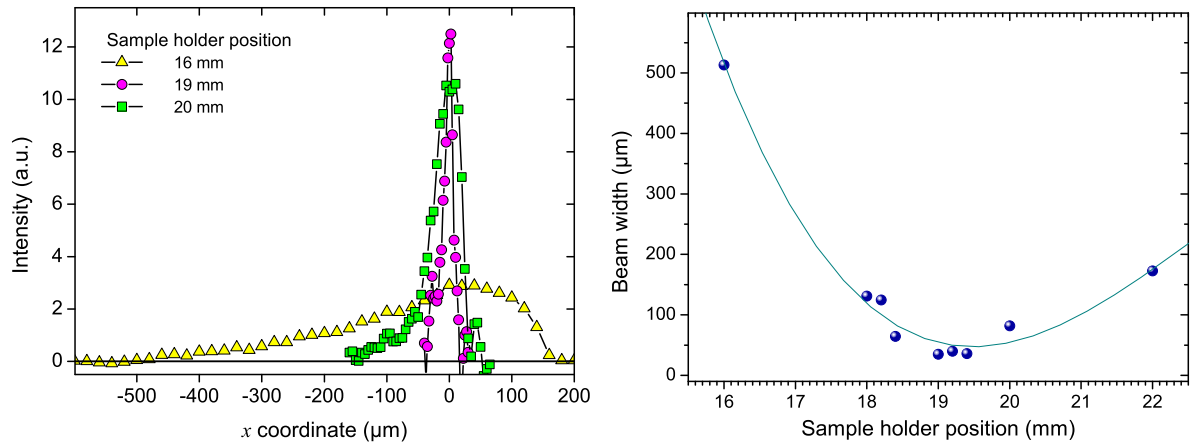

Figure 4.4: The laser beam intensity behind the knife edge as a function of the y position (left) and the dependence of the laser beam width on the sample position (right).

4.1.4 Results and discussion

The negatively poled spin-coated samples (15 µm thickness) were measured with the TPT method along the hysteresis loop after applying periodic electric fields (Fig. 4.5a) The experimental data were analyzed by means of regularization method in combination with the L-curve method. Starting from $E = 0$ MV/m (Fig. 4.5b), the map shows the expected negative polarization along different depths z. Even though the films were prepared in a clean atmosphere, the inhomogeneities can be associated with some impurities. As we increased the electric field ($E < E_c$), a significant change in the polarization maps can be observed at $E = 49$ MV/m (Fig. 4.5c). The polarization values beyond $z = 1$ µm start to reach zero, however the layer near to the rear electrode remained negatively poled. The same pinning is observed when values above the coercive field i.e. $E = 55$ MV/m were applied. In the last case, the polarization is mostly reversed beyond $z = 1$ µm. Likewise, the 3D mapping at the saturated polarization ($E = 93$ MV/m) already presents positive polarization (Fig. 4.5d). Our results were compared several times and are reproducible.
This inhomogeneous reversal was already discussed by Furukawa [5,39]. In his publication he describes the mechanism of the polarization reversal. First the reversal occurs at a molecular level, i.e. single chains suffer reversal of their dipoles. Later there is an intermolecular expansion of chain rotations, in other words a reversal in a lamella. Finally the effect is propagated in the bulk producing aggregates of a crystalline lamella (domain wall motion). Nakajima et al. [86] also support the idea that the polarization reversal occurs at grain level via nucleation and growth. Sakai et al. [40] and Nakajima et al. associated the inhomogeneous reversal and the pinning of the layers near the electrode surface to a fatigue effect. They subjected their films to up to 10^4 cycles of a sinusoidal electric field, but in our case we only applied at most 4 cycles above the coercive field. Nevertheless they associate fatigue with space charges and interface properties. Thus if space charges

are present and the crystalline domains near the electrode surface do interact with them, the distribution of the polarization is expected to be nonuniform.

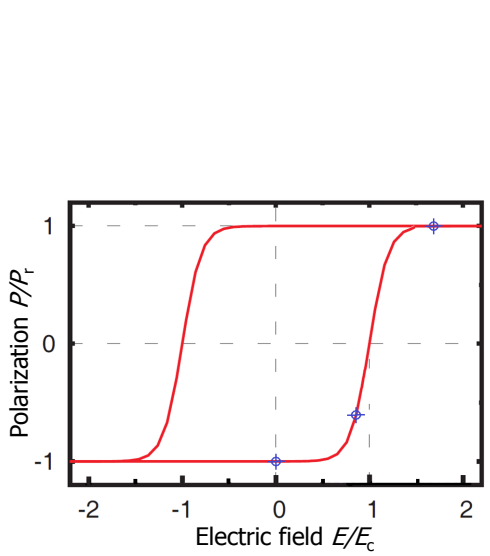

(a) Hysteresis curve. $E_c = 55$ MV/m and P_r are the coercive field and the remanent polarization, respectively.

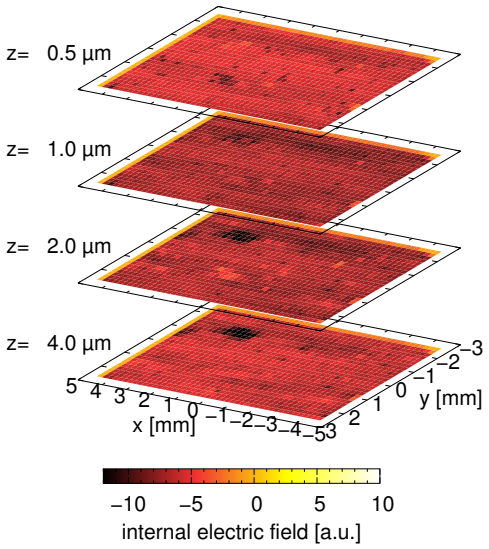

(b) $E = 0$ MV/m.

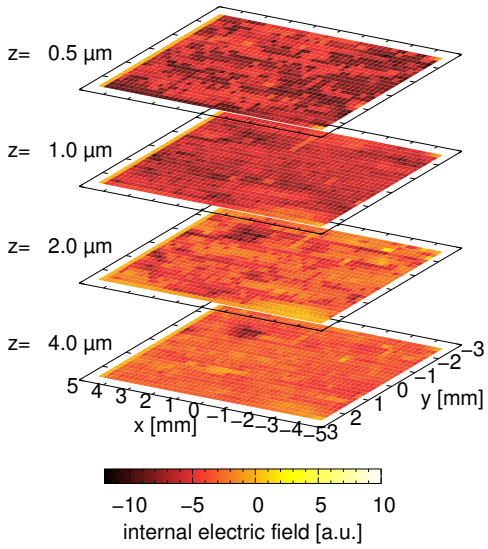

(c) $E = 49$ MV/m.

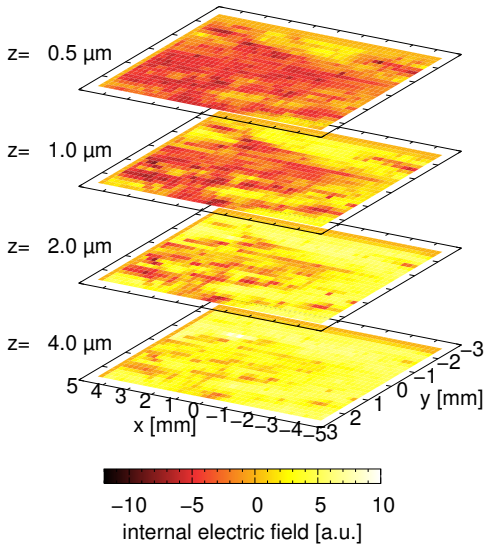

(d) $E = 93$ MV/m.

Figure 4.5: Polarization maps in P(VDF-TrFE) films measured along the hysteresis curve.

Publication

Thermal-Pulse Tomography of space-charge and polarization distributions in electret polymers

A. Mellinger; R. Flores Suarez; R. Singh, M. Wegener; W. Wirges;
R. Gerhard and S. B. Lang
International Journal of Thermophysics,
Vol. 29, 2046-2054 (2008)

Int J Thermophys (2008) 29:2046–2054
DOI 10.1007/s10765-008-0532-8

Thermal-Pulse Tomography of Space-charge and Polarization Distributions in Electret Polymers

Axel Mellinger · Rosaura Flores-Suárez · Rajeev Singh · Michael Wegener · Werner Wirges · Reimund Gerhard · Sidney B. Lang

Published online: 15 November 2008

Abstract A new, non-destructive technique for the analysis of electret materials is presented. Thermal-pulse tomography produces three-dimensional images of space-charge and polarization distributions with a lateral resolution of better than 50 μm and a depth resolution of less than 0.5 μm. A focused-pulsed laser heats a circular spot on the opaque upper electrode. While diffusing through the sample, the thermal pulse causes local changes in the sample geometry or dielectric properties, resulting in a short-circuit current in the presence of space charge or electric dipoles. From the transient current, the distribution of the internal electric field can be reconstructed by means of scale transformation or regularization methods.

Keywords Electret · LIMM · Polarization · Polyvinylidene fluoride · Space charge · Thermal-pulse tomography

A. Mellinger · R. Flores-Suárez · R. Singh · M. Wegener · W. Wirges · R. Gerhard
Institute of Physics and Astronomy, University of Potsdam, 14476 Potsdam-Golm, Germany

A. Mellinger (✉)
Department of Physics, Central Michigan University, Mount Pleasant, MI 48859, USA
e-mail: axel.mellinger@cmich.edu

R. Singh
Department of Electronics and Communication, University of Allahabad, Allahabad 211002, UP, India

Present Address:
M. Wegener
Fraunhofer Institute for Applied Polymer Research, 14476 Potsdam-Golm, Germany

S. B. Lang
Department of Chemical Engineering, Ben-Gurion University of the Negev, P.O.B. 653,
Beer Sheva 84105, Israel

1 Introduction

Electret materials are the key to many sensor and actuator applications, such as pressure-sensitive devices, motion sensors, flat loudspeakers, etc. [1]. Research and development in this field requires a non-destructive technique to measure the distribution of the internal electric field caused by embedded space charges or electric dipoles. Since the 1970s, a number of techniques for probing charge and polarization depth profiles have been developed (see the reviews [2–4] and the references therein). Among these, thermal methods are attractive because they provide sub-μm depth resolution at moderate cost and can often be applied in situ for, e.g., experiments in a vacuum environment. The basic concept is to provide an external stimulus in the form of a thermal step, pulse, or wave which propagates through the dielectric medium, thus causing local changes in the geometry or the dielectric properties of the material under study. These changes in turn give rise to a short-circuit current between the metal electrodes at the front and rear surfaces which contain information on the depth-profile of the internal electric field. Thermal profiling has been implemented both in the frequency domain (commonly referred to as the laser intensity modulation method (LIMM) [5]), and in the time domain (thermal pulse (TP) [6] and thermal step [7] methods). It is related to photopyroelectric measurements with pulsed lasers [8,9].

In most published thermal profiling techniques, the lateral extension of the heated zone was large compared to the sample thickness, thus yielding one-dimensional information only. Nevertheless, several attempts were made or suggested [10–12], where the thermal excitation was confined to a small region on the sample surface. Scanning the thermal excitation spot across the sample then yields three-dimensional images of the polarization or space-charge distribution. As laser beams can be brought to a tight focus by suitable optics, the focused LIMM method has the potential for high lateral resolution. However, its relatively slow data acquisition speed often required a compromise between full depth-resolution with a limited number of in-plane data points [13], or larger, high-resolution area maps at selected modulation frequencies [12,14]. Thermal-pulse measurements, however, can be carried out up to 50 times faster than a comparable LIMM scan, as was recently demonstrated in a direct comparison [15] of LIMM and TP which showed excellent agreement between the two techniques (Fig. 1). This triggered the implementation of thermal-pulse tomography (TPT) [16], as described in the following sections.

2 Experimental Setup

The TPs are generated via the absorption of short light pulses by an opaque metal (Cu or Al) electrode. Typically, pulses with an energy of 10 μJ to 500 μJ [generated with a Q-switched, frequency-doubled Nd:YAG laser (Polaris III, New Wave Research)] are focused to spot sizes between 40 μm and 400 μm in diameter. The pulse duration of 5 ns is much shorter than the inverse preamplifier bandwidth (see below) and hence has no effect on the depth resolution. The samples are positioned in the laser beam with a computer-controlled X–Y translation stage (ERLIC 85, OWIS GmbH) and a manual Z translation stage. Optionally, adding a rotary stage allows the investigation

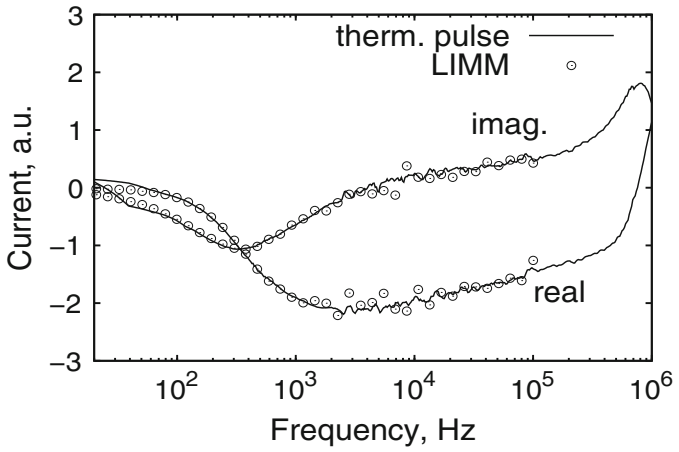

Fig. 1 Comparison of the Fourier-transformed thermal-pulse signal (*solid line*) and the LIMM spectrum (*open circles*) of a volume-charged PTFE film of 17 µm thickness. Data acquisition time was 40 s for the TP signal vs. 30 min for the LIMM curve (*source*: from [15])

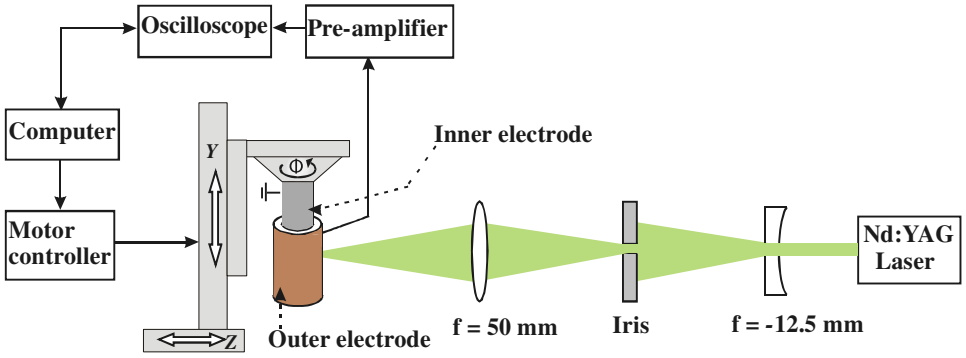

Fig. 2 Experimental setup for focused TPT. The depicted configuration was used for the study of cylindrical geometries (i.e., piezoelectric coaxial cables) (*source*: from [26])

of piezoelectric polymer cables (cf. Fig. 2). The short-circuit current is amplified by a low-noise Stanford Research SR570 current-to-voltage converter and sampled at a typical rate of 10 Msamples/s with a digital storage oscilloscope (Agilent 54833A). Operating in short-circuit mode keeps the RC time constant small, resulting in a high bandwidth, and hence a good depth resolution. With a typical preamplifier bandwidth of 100 kHz, a depth resolution of less than 0.5 µm is achieved. In order to improve the signal-to-noise ratio, up to 50 pulses may be averaged for each beam pointing. As each transient has approximately $N = 512{,}000$ data points, the total amount of raw data for a 2 kpixel pyroelectric image is of the order of 4 GB.

3 Theory and Data Processing

The propagation of the thermal wave in the sample is described by the heat-conduction equation,

$$\nabla^2 T(x, y, z, t) = \frac{1}{D}\frac{\partial T(z, t)}{\partial t}, \tag{1}$$

where $T(x, y, z, t)$ is the temperature and D is the thermal diffusivity of the material. When the size of the heated spot is much larger than the sample thickness d, a one-dimensional solution $T(z, t)$ is usually sufficient [17]. The validity of this assumption

in the present case will be discussed in Sect. 4.1. In the presence of a polarization or space-charge, the TP in a sample with an electrode area A gives rise to the current [2]

$$I_{\sim}(t) = \frac{A}{d} \int_0^d g(z) \frac{\partial T_{\sim}(z,t)}{\partial t} \, \mathrm{d}z \tag{2}$$

with the distribution function

$$g(z) = (\alpha_\varepsilon - \alpha_z) \int_0^z \rho(\xi) \, d\xi + p(z), \tag{3}$$

where α_ε is the temperature coefficient of the permittivity, α_x the thermal expansion coefficient, $\rho(z)$ the space-charge density, and $p(z)$ is the pyroelectric coefficient.

The framework of Eqs. 1–3 can be solved for $g(z)$, $\rho(z)$, or $p(z)$, either in the time or in the frequency domain. For a thermal-pulse experiment, the time domain appears to be the obvious choice. However, to preserve the phase information in the signal, it is crucial to remove any phase shift introduced by the amplifier electronics [15], which is most easily done in the frequency domain. Thus, the transient thermal-pulse current $I(t_k)$, $k = 1 \ldots N$, is converted to the frequency domain using the discrete fast Fourier transform [18] and divided by the (complex) preamplifier gain $\tilde{\alpha}$:

$$\tilde{J}(f_n) = \frac{\Delta t}{\tilde{\alpha}(f_n)} \sum_{k=0}^{N-1} I(t_k) \mathrm{e}^{-2\pi i k n/N}, \tag{4}$$

with the discrete frequency points defined by

$$f_n = \frac{n}{N \Delta t}, \qquad n = 1 \ldots \frac{N}{2}, \tag{5}$$

where Δt is the sampling interval.

Solving Eq. 2 (a Fredholm integral equation of the first kind) is known to be an ill-posed problem. Several techniques have been developed in order to extract physically meaningful solutions $g(z)$ from the experimental data, such as Tikhonov regularization [19] (sometimes combined with polynomial approximations [20,21]), a scale-transformation method [22], iterative approaches [23], and *Monte Carlo* techniques [24]. In the present study, regularization in combination with the L-curve method [25] was used for thinner samples ($d < 25\,\mu\mathrm{m}$) [16], whereas the simpler scale-transformation approach was used when the near-surface polarization in thicker samples was of interest [26]. A general solution for the three-dimensional equivalent of Eq. 2 is currently under development. By taking into account lateral thermal diffusion, an effective increase in lateral resolution is expected.

4 Results and Discussion

4.1 Polyvinylidene Fluoride Films

Initial tests of the new tomographic technique were carried out on films of polyvinylidene fluoride (PVDF), which had received a structured polarization by applying an electric field of approximately $100\,\mathrm{MV}\cdot\mathrm{m}^{-1}$ to a patterned, 'T'-shaped electrode (Fig. 3a), which was later overcoated with a light-absorbing 200 nm Cu electrode (Fig. 3b). From the thermal-pulse data, the polarization map was calculated by means of Tikhonov regularization, with the regularization parameter being obtained via the L-curve method [25]. The lateral resolution of 200 µm (limited here by the chosen laser spot size) is clearly superior compared to recent acoustic approaches [27].

Detailed studies of the lateral resolution were carried out by performing a series of one-dimensional scans across the edge of the 'T' electrode (parallel to the Y-axis in Fig. 3c). The width of the poled/unpoled transition region in the PVDF sample is determined by electrical stray fields, and is expected to be less or equal to the sample thickness of 11 µm. For a laser beam waist of 40 µm, one would therefore expect a lateral resolution equal to this spot size. However, Fig. 4a shows a strong dependence of the lateral resolution on depth, caused by the very different thermal diffusivities $D = \kappa/(c\rho)$ of the metal electrode and the polymer material (where κ denotes the thermal conductivity and $c\rho$ the heat capacity per unit volume). As the diffusion length at a given time t is $\ell = \sqrt{Dt}$, the lateral diffusion speed of the TP in the electrode (with a diffusivity of approximately $10^{-4}\,\mathrm{m}^2\cdot\mathrm{s}^{-1}$) is some 30× faster than the vertical diffusion speed into the polymer (where $D \approx 10^{-7}\,\mathrm{m}^2\cdot\mathrm{s}^{-1}$). As a consequence, the

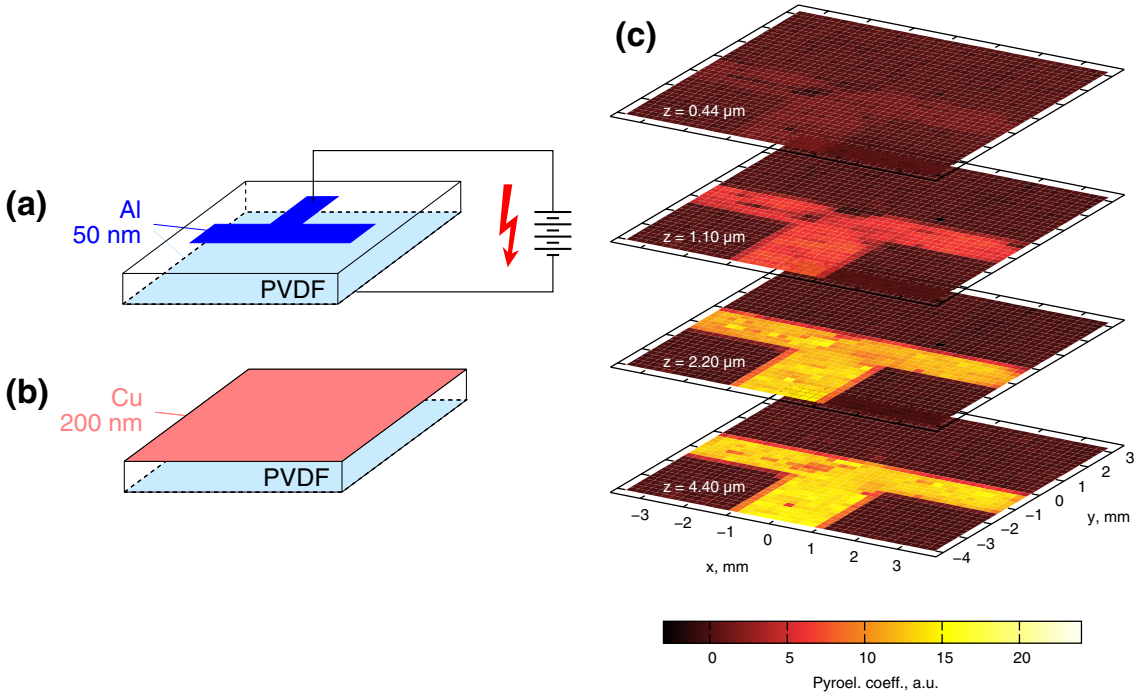

Fig. 3 Preparation of PVDF test samples with (**a**) a patterned Al electrode used for poling, (**b**) the final Cu electrode used for the TP experiments, and (**c**) polarization map at different depths

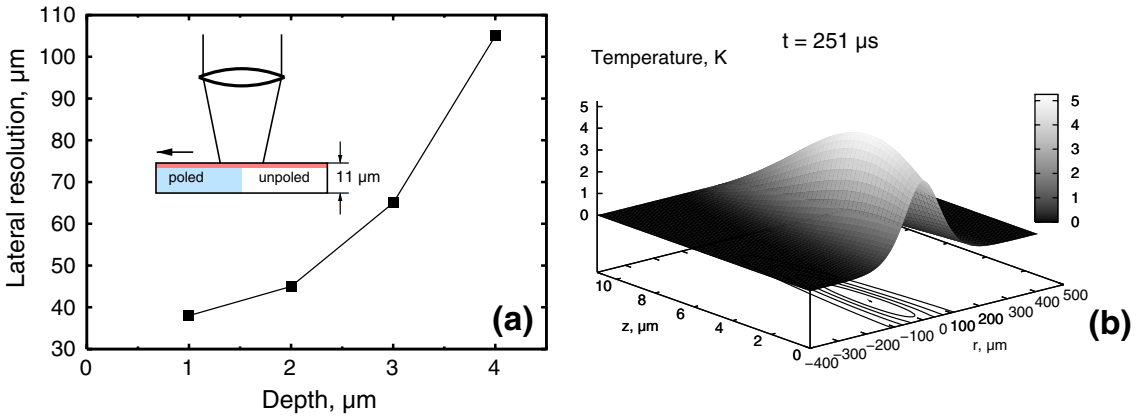

Fig. 4 (**a**) Depth-dependence of the lateral resolution in PVDF at a beam spot size of approximately 40 µm. The data were obtained by scanning the poled/unpoled transition region, as shown in the inset. (**b**) Temperature distribution in the electrode and polymer 251 µs after the laser pulse, calculated by means of the finite-element method [28]. Note the different diffusion lengths in the radial (r) and depth (z) directions

heated front electrode cools more rapidly than the polymer, thus turning from a heat source in to a heat sink, so that the point of maximum temperature starts moving into the polymer (Fig. 4b). Recent finite-element calculations of the temporal and spatial evolution of the heat pulse confirmed this qualitative discussion [28]. Enhancing the lateral resolution thus depends on the ability to find a surface electrode with good electrical conductivity to maintain the short-circuit condition, but low thermal diffusivity. In addition, a solution of the LIMM Eq. 2 taking into account the three-dimensional heat diffusion needs to be found. In regions with a strong in-plane variation of the polarization, a 3-D analysis could enhance the lateral resolution.

Besides providing a test case for the lateral spatial resolution, PVDF films showed unexpected inhomogeneities in the polarization when subjected to bipolar electric fields. In order to investigate the polarization switching behavior, the poling cycle was interrupted at various levels of the electric field. Figure 5 shows an incomplete switching in the bulk, and a polarization pinning at depths up to 1 µm. Polarization pinning

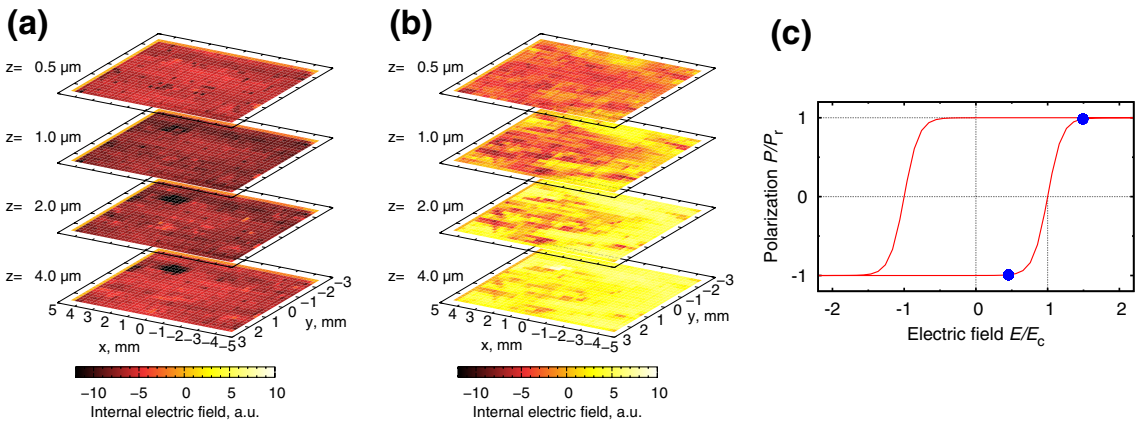

Fig. 5 Polarization maps in PVDF poled at fields of (**a**) $25\,\mathrm{MV\cdot m^{-1}}$ and (**b**) $82\,\mathrm{MV\cdot m^{-1}}$. The poling fields were applied by cycling the electric field through one or more full hysteresis loops (**c**) and stopping at the respective field, indicated by *solid circles* on the hysteresis curve. P_r and E_c denote the remanent polarization and the coercive field, respectively

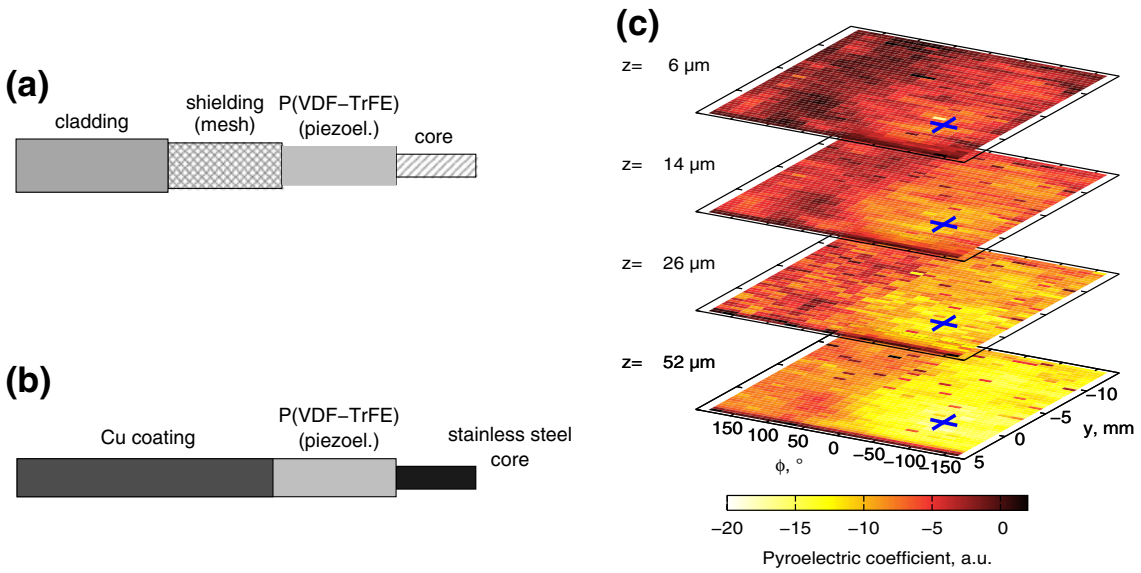

Fig. 6 Schematic view of a piezoelectric sensor cable: (**a**) as received, (**b**) after preparation for TPT. The stainless steel pin serves both as inner electrode and as mounting point. (**c**) Polarization map of a sensor cable poled with a single stationary needle at −25 kV (right). The *crosses* mark the needle position (*source*: from [26])

has been observed in PVDF by other authors, but has been attributed to material fatigue after more than 10^4 poling cycles [29]. Further studies are needed to determine the cause of the incomplete switching.

4.2 PVDF–TrFE Coaxial Sensor Cables

Coaxial sensor cables with an active layer made of piezoelectric PVDF–TrFE copolymer (cf. Fig. 6a) have found important applications in traffic monitoring and intrusion detection. Typically, they are poled (and thus given their piezoelectric properties) by subjecting the extruded cables to a corona discharge formed by a series of high-voltage points around the cable [30]. Recently, polarization maps were obtained with the new tomographic technique from cables poled either in the above-described continuous process or in the laboratory with a single stationary needle [26]. The cables were prepared for TPT measurements by replacing their soft wire core with a stainless steel pin, removing their protective cladding and shielding, and coating the active PVDF–TrFE layer with a Cu electrode (Fig. 6b). Samples poled in the continuous process show a rather uneven distribution that can be attributed to the fact that any point on the cable was exposed to the corona discharge for no more than 300 ms at the given drawing speed. The laboratory-poled cables, on the other hand, show a smooth polarization centered on the needle position in a region approximately 50–100° wide (cf. Fig. 6c), depending on the poling voltage [26]. It was thus shown that optimum poling can be achieved with a set of four to six corona needles at slow drawing speeds.

4.3 Space-charge Electrets

TPT is also suitable for mapping the charge distribution in space-charge electrets. For example, films of polytetrafluoroethylene (PTFE, thickness 17 µm) were irradiated

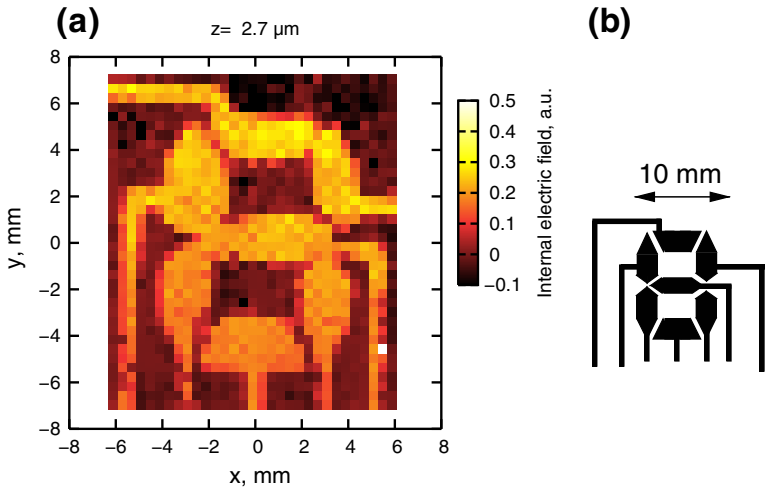

Fig. 7 Internal electric field in electron-beam irradiated PTFE film: (**a**) field distribution at a depth of $z = 2.7$ µm and (**b**) shadow mask used for charging (*source*: from [28])

with a monoenergetic electron beam (15 keV) through a shadow mask (cf. Fig. 7b). The resulting patterned space-charge distribution is shown in Fig. 7a. All the details of the mask are very well reproduced by the space-charge pattern. For the maximum signal-to-noise ratio, the samples had to be glued to a substrate in order to avoid thermo-elastic resonances [31].

5 Conclusions

TPT is a versatile, non-destructive method for obtaining tomographic images of space-charge and polarization distributions in electret materials. A depth-dependent lateral resolution of 38 µm to 105 µm has been achieved in ferroelectric PVDF films. Non-planar geometries can be studied as well, as was demonstrated on piezoelectric PVDF-TrFE sensor cables. Work is in progress to improve the lateral resolution by optimizing the electrode material with respect to thermal conductivity and thermal diffusivity, as well as through a numerical data-analysis procedure taking into account the in-plane thermal diffusion.

Acknowledgments The authors would like to thank Lucas F. Santos (Instituto de Física de São Carlos, Brazil) for providing the electron-beam charged PTFE samples. The equipment was funded in part by the European Regional Development Fund. R.S. acknowledges financial support from the German Academic Exchange Service (DAAD).

References

1. G.M. Sessler, R. Gerhard-Multhaupt (eds.), *Electrets*, 3rd edn., vol. 1–2. (Laplacian Press, Morgan Hill, CA, 1999)
2. S. Bauer, S. Bauer-Gogonea, IEEE Trans. Dielect. Elect. Insul. **10**, 883 (2003)
3. J. Lewiner, S. Holé, T. Ditchi, IEEE Trans. Dielect. Elect. Insul. **12**, 114 (2005)
4. R.J. Fleming, IEEE Trans. Dielect. Elect. Insul. **12**, 967 (2005)
5. S.B. Lang, D.K. Das-Gupta, Ferroelectrics **39**, 1249 (1981)
6. R.E. Collins, J. Appl. Phys. **47**, 4804 (1976)

7. A. Toureille, P. Notingher Jr., N. Vella, S. Malrieu, J. Castellon, S. Agnel, Polym. Int. **46**, 81 (1998)
8. H. Coufal, Thin Solid Films **193**, 905 (1990)
9. H. Coufal, A. Mandelis, Ferroelectrics **118**, 379 (1991)
10. Ş. Yilmaz, S. Bauer, W. Wirges, R. Gerhard-Multhaupt, Appl. Phys. Lett. **63**, 1724 (1993)
11. S. Bauer, J. Appl. Phys. **80**, 5531 (1996)
12. B. Ploss, W. Hassler, H. Hulz, G. Kobernik, Proceedings of the 11th IEEE Symposium on Applications of Ferroelectrics (IEEE Service Center, Piscataway, NJ, 1998), pp. 207–210
13. D. Marty-Dessus, L. Berquez, A. Petre, J.L. Franceschi, J. Phys. D: Appl. Phys. **35**, 3249 (2002)
14. A. Quintel, J. Hulliger, M. Wübbenhorst, J. Phys. Chem. B **102**, 4277 (1998)
15. A. Mellinger, R. Singh, R. Gerhard-Multhaupt, Rev. Sci. Instrum. **76**, 013903 (2005)
16. A. Mellinger, R. Singh, M. Wegener, W. Wirges, R. Gerhard-Multhaupt, S.B. Lang, Appl. Phys. Lett. **86**, 082903 (2005)
17. R. Emmerich, S. Bauer, B. Ploss, Appl. Phys. A **54**, 334 (1992)
18. M. Frigo, S.G. Johnson, Proc. IEEE **93**, 216231 (2005)
19. A.N. Tikhonov, A.V. Goncharskii, V.V. Stepanov, I.V. Kochikov, Sov. Phys. Doklady **32**, 456 (1987)
20. S.B. Lang, IEEE Trans. Dielect. Elect. Insul. **11**, 3 (2004)
21. S.B. Lang, J. Mater. Sci. **41**, 147 (2006)
22. B. Ploss, R. Emmerich, S. Bauer, J. Appl. Phys. **72**, 5363 (1992)
23. A. Mellinger, Meas. Sci. Technol. **15**, 1347 (2004)
24. E. Tuncer, S.B. Lang, Appl. Phys. Lett. **86**, 071107 (2005)
25. P.C. Hansen, D.P. O'Leary, SIAM J. Sci. Comput. **14**, 1487 (1993)
26. R. Flores Suárez, A. Mellinger, M. Wegener, W. Wirges, R. Gerhard-Multhaupt, R. Singh, IEEE Trans. Dielect. Electr. Insul. **13**, 1030 (2006)
27. T. Maeno, IEEE Trans. Dielect. Elect. Insul. **8**, 845 (2001)
28. A. Mellinger, R. Singh, M. Wegener, W. Wirges, R. Flores Suárez, S.B. Lang, L.F. Santos, R. Gerhard-Multhaupt, Proceedings of 12th International Symposium on Electrets (IEEE Service Center, Piscataway, NJ, 2005), pp. 212–215
29. S. Sakai, M. Date, T. Furukawa, Jpn. J. Appl. Phys. **41**, 3822 (2002)
30. M. Wegener, R. Gerhard-Multhaupt, IEEE Trans. Ultrason. Ferroelect. Freq. Control **50**, 921 (2003)
31. P. Bloß, H. Schäfer, Rev. Sci. Instrum. **65**, 1541 (1994)

4.2 Lateral resolution: how to increase it?

Many factors affect the lateral resolution. On one side, there is a faster propagation of the thermal pulses in the metal electrodes than in the polymer film (Table 4.1). This is due to the different magnitudes of the thermal diffusivity of metals ($D \approx 10^{-4}$ m^2/s) and the PVDF material ($D \approx 10^{-7}$ m^2/s). The first solution would be to use conductive polymers as electrodes, such as Poly(3, 4−ethylenedioxythiophene) poly(styrenesulfonate) (PEDOT-PPS) [89]; however, the deposition technique needs equipment that is not available at the moment. Nevertheless, an optimization of the thermal techniques, TPT and FLIMM, can be achieved by characterizing the actual resolution using standard test samples such as uniformly poled PVDF films with narrow and well-defined patterned metal electrodes. In this way, the thermal stress on the polymer films will be minimized. Several attempts to obtain narrow patterned electrodes will be discused on the next subsections.

τ_L	l_{Al} (µm)	l_{PVDF}(µm)
5 ns	0.7	0.02
5 µs	22	0.7
5 ms	700	22

Table 4.1: Values of the heat-diffusion length l in the relevant materials.

On the other side, there are spherical aberrations in the optics in the TPT setup. These limit the adjustment of the laser-beam spot size below 30 µm. The problem can be eliminated after replacing the simple lenses by higher quality optical elements.

4.2.1 Use of patterned electrodes

Test samples with narrow well-defined electrodes are needed in order to determine the lateral resolution of a thermal technique while reducing the thermal stress on the films. In the following section, different possibilities for depositing these electrodes are presented. The corresponding depth polarization profiles for each possibility are discussed. The samples for these studies were part of a joint project with the Paul Sabatier University in Toulouse, France. The scientific research group in France uses the Focused LIMM setup, which needs free-standing films.
A 3 wt% solution of P(VDF-TrFE) (65/35) (Solvay, Advanced Polymers, France) dissolved in acetone/dimethyl sulfoxide (20/80 wt%) was drop cast on glass substrates. Approximately 8 ml of the filtered polymer solution was used to prepare films. In order to evaporate the solvent, the films were annealed for 35 min at 100 °C in a clean atmosphere. Afterwards they were cooled at room temperature and then removed from the glass substrates. From this procedure, samples of 25 mm × 25 mm with 12 µm thickness were obtained.

The poling process was performed as described in section 4.1.2 and well above the coercive field.

4.2.1.1 Interdigital electrodes

Using commercial stainless steel interdigital masks on drop-cast, free standing and spin-coated samples, narrow electrodes were achieved. The width of the metal fingers and the distance between them was quite similar, 100 and 105 µm, respectively. First, a square aluminum electrode (6 mm long and 50 nm thick) was deposited on one side of the film. Next, the interdigital mask was attached to the other side of the film with adhesive tape and 150 nm of aluminum was evaporated. Due to the flexibility of the narrow mask fingers, aluminum shadows may be deposited causing a smaller distance between finger electrodes (Fig. 4.6). The poling process was performed above the coercive field as described in section 4.1.2. In the next step, the interdigital electrodes should be removed. A small sponge dipped in 3 wt% sodium hydroxide (NaOH) solution was used to remove the deposited electrodes from the film. Immediately after this, the same side was rinsed with distilled water and dried with nitrogen gas. The back electrode was not effected during the treatment. In order to perform the TPT measurements, an aluminium electrode (50 nm thickness) was evaporated on the front side of the film.

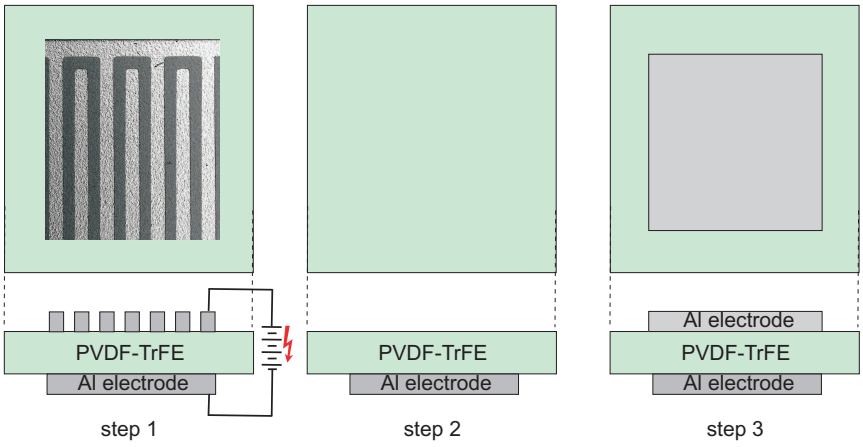

Figure 4.6: Interdigital electrode deposition: evaporation of the fingers and poling process (step 1); removal of finger electrodes (step 2) and final electrode deposition (step 3).

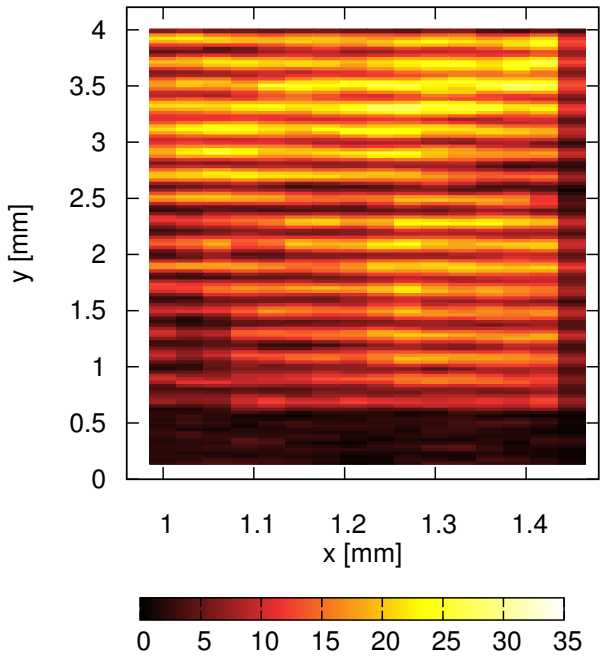

Figure 4.7: Polarization map in P(VDF-TrFE) films with interdigital electrodes 100 µm wide (30 µm spot size).

The tomography data was acquired using a 30 µm wide spot size and similar step size. As can be seen, the distribution of the polarization is not homogeneous and the fingers can be partially distinguished (Fig. 4.7). The reason the tomography does not show a sharp transition between the fingers might be related to interfacial effects. The distance between the metal fingers could be too small to avoid side effects, for example, during the poling process. Moreover, any shadow or defect of the electrode is not taken into account when the sample is scanned. The samples were scanned with the FLIMM and the results (not shown here) were the same. A mesh with greater distance between the finger electrodes is required to overcome this problem.

4.2.1.2 Laser-cut masks (4 fingers)

Mesh with a larger distance between fingers were prepared by ablation of aluminum foil with the maximum power of the Nd:YAG laser (Fig. 4.8a). Three masks with finger patterns, labeled I, II, and III were obtained. The mask parameters are given in table 4.2. The electrode deposition was performed in several steps as described for an interdigital mask. Since shadows may occur during the deposition of the electrodes, the width of the fingers and the distances between them were compared and it was found that the width of the deposited electrodes is slightly larger (around 10%) than that of the mask. This may occur because the profile of the mask is rough and the aluminum foil is very soft (Fig. 4.8b). All samples under investigation were poled by applying a unipolar/bipolar electric field at 10 mHz [34].

Table 4.2: Laser-cut mask parameters

Parameters	I	II	III
Finger width(µm)	195	203	163
Separation (mm)	1.1	1.1	1.1

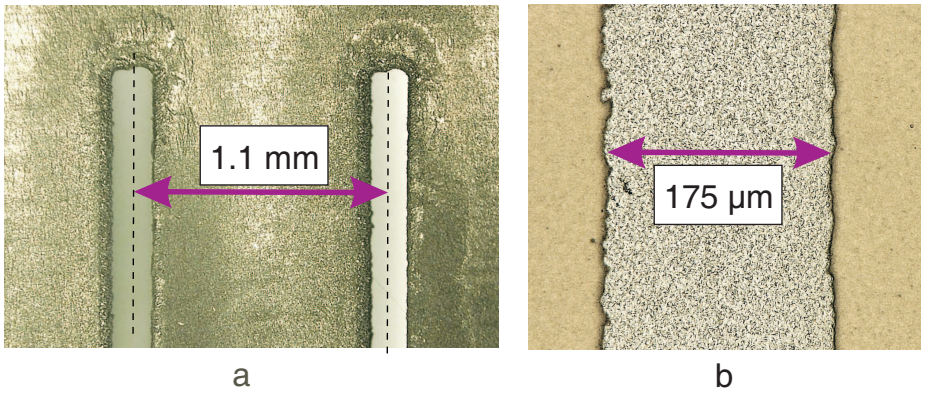

Figure 4.8: Laser-cut mask: (a) Fingers are separated from each other by 1.1 mm, (b) rough edges of the evaporated electrode due to the respective edges of the laser-cut mask.

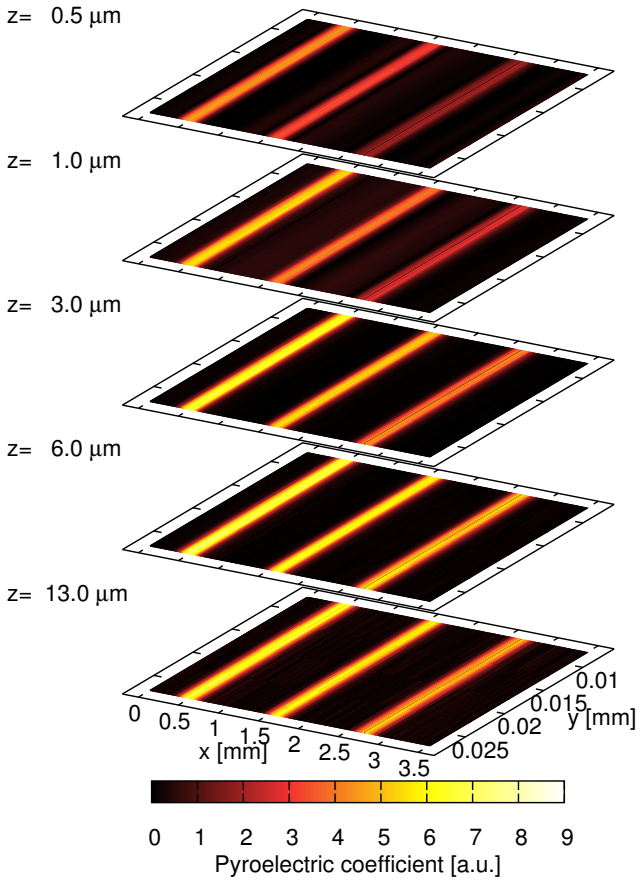

Figure 4.9: Polarization maps in P(VDF-TrFE) films with evaporated laser-cut finger electrodes (35 µm spot size).

The samples with finger electrodes were scanned using a spot-size of 35 µm and a similar step size. The polarization maps reproduce the pattern electrodes (Fig. 4.9). The inhomogeneities characteristic of the polymer are evident along the fingers. The build-up of the polarization in the depth direction is also seen. The area separating the fingers remains unpolarized, as expected. In order to quantify the results, a cut of the polarization along the x coordinate at a fixed y position and several depths z is shown in (Fig. 4.10). The distance between the polarization peaks is the same as on the mask (1.1 mm), though the width of each finger is sligthly larger than expected. This might be related to the evaporation process yielding an uneven electrode thickness. As stated, the edges of the evaporated electrode fingers are not sharp. Moreover, interfacial effects should be considered. Another critical factor is the method employed for the data analysis. As it was discussed in section 3.5, the resolution is higher near the surface electrode.

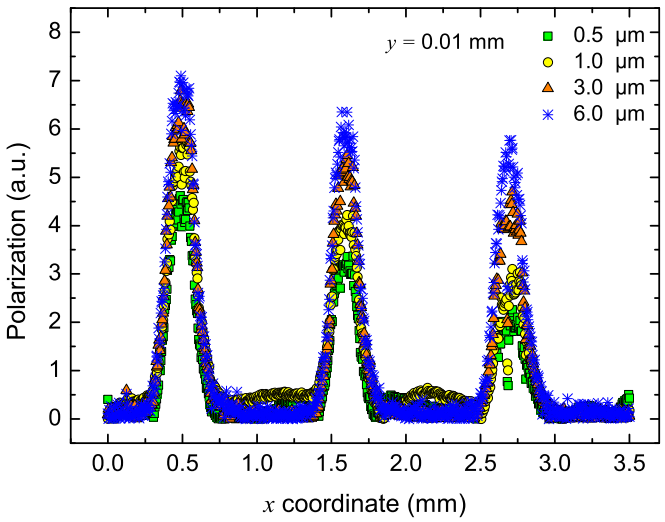

(a) 1D profile

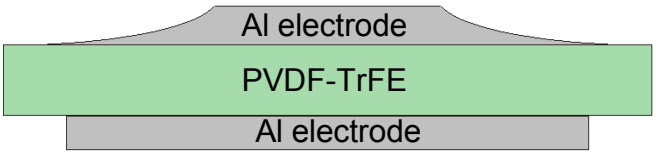

(b) possible electrode profile

Figure 4.10: (a) Polarization profile for different depths at $y = 0.02$ mm; the distance between the peaks corresponds to the distance between the fingers in the mask. (b) Possible electrode profile after deposition using the laser-cut mask.

4.2.1.3 Photolithography

Another possibility to print well-defined patterned metal electrodes on the polymer films was inspected by means of optical lithography. The photolithography is the most used process to pattern nearly all integrated circuits [90]. The basic steps for this process are [91]:

(I) Adhesion promotion. The substrate is dried either thermally or chemically. Heating the substrate eliminates moisture. Chemicals are usually applied to promote the formation of a layer that prevents a lift-off of small photoresist structures from the substrate.

(II) Resist coat. Deposition of photoresists (normally organic polymers that undergo photochemical reactions when exposed to light) is performed by means of spin-coating. The final thickness of the solid resist film is up to 2 µm. This value varies with the dimensions of the desired metal pattern.

(III) Softbake. Afterwards, the substrate may undergo a softbake process, in other words the substrate is heated at low temperatures.

(IV) Alignment. This step consists in placing a mask on certain coordinates of the sample in order to pattern or align features in the substrate.

(V) Exposure. The photoresist materials belong to a positive or negative category. The first type refers to those that become soluble by exposure to light. The last ones are soluble in the presence of chemicals known as resist developers (applied on step I) instead of light. In this step, the photoresist is exposed to a pattern of intense light using a mask. The transmitted light defines the shape of the final structure. Additionally, a post-exposure bake can be applied. Normally, it is used to produce additional chemical reactions.

(VI) Development. The final step is related to the removal of the photoresist. The chemicals used, usually containing NaOH or ammonium hydroxides, are spin-coated on the substrate. This step is often followed by a hard-bake, carried out at higher temperatures (ca. 120 celsius). The objective of this last treatment is to evaporate possible water and/or organic materials, while solidification of the photoresist occurs.

In the present work, the lithography process on 15 µm drop-cast PVDF films was performed at the Paul Sabatier University in Toulouse, France. The films were prepared at Potsdam University. Since the films were annealed after drop casting, there was no need of performing an adhesion promotion. The deposition of organic photoresist was a complicated step since most are polymers and chemical reaction with the PVDF films may occur (4.11 step 1). By means of a patterned mask, the PVDF films were exposed to

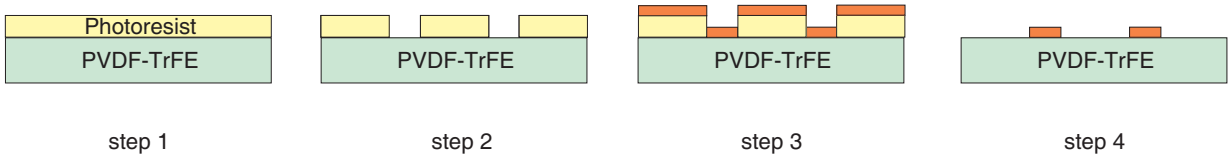

Figure 4.11: Lithography on PVDF films: Spin-coating of the photoresist (step 1), exposure and development process (step 2), metal-electrode deposition (step 3) and lift-off (step 4).

light yielding a well-defined photoresist pattern (4.11 step 2). Afterwards, 50 nm of metal electrode was deposited onto the film (4.11 step 3). The next step is the so called lift-off process, where the photoresist and the metal electrode were removed with solvents. The only metal layer left is the one directly deposited onto the PVDF film (4.11 step 4).

The challenge during photolithography is basically the removal of the photoresists. Normally, acetone is used; however, this is a good solvent for PVDF. For that reason, other organic solvents were chosen. Other difficulties appeared during the lift-off process; thick and rigid samples can be handled better than thin elastic films, but thick samples with deposited fine electrodes are difficult for the poling process. Under these conditions, the lift-off process was hard to achieve and after many trials on the free-standing PVDF films, all the solvents reacted with the polymer samples.

One alternative solution for future deposition of electrodes includes inkjet printing. This technique is an anisotropic process that deposites liquid phase materials or inks over a substrate [92]. Most of the inks include polymers e.g. PEDOT/PSS [93] and other suspensions like organoamine-stabilized silver nanoparticles [94] among others. Thus, several aspects of the liquid phase material such as solvents, viscosity, concentration, etc and of the process e.g. pulse-voltage, nozzle diameter, etc. should be inspected for an optimal electrode printing [95]. The viability of this technique on polymer ferroelectrics and polymer ferroelectrets either films or cables is beyond the scope of this work.

4.2.2 Comparison with the Focused LIMM

In order to compare and complement the measurements obtained with the TPT technique and its counterpart in the frequency domain (the Focused Laser-Intensity Modulation Method), samples with a patterned grid electrode were prepared (Fig. 4.12). The laser-cut finger masks were employed horizontally and vertically to obtain a grid: each finger is 175 µm in width and 1.1 mm is the distance between them. First a squared aluminum electrode (6 mm long and 50 nm thick) was deposited on one side of the film. On the opposite side, the first finger electrodes (50 nm of Al) were deposited (step 1). In order to have a grid, the mask was rotated 90 degrees to the original position and another 50 nm of Al were evaporated (step 2). After poling the sample above the coercive field, the grid-electrode was chemically removed using a 3 wt% NaOH solution and distilled water (step 3). Finally, a full-area Al electrode (50 nm) was evaporated (step 4).

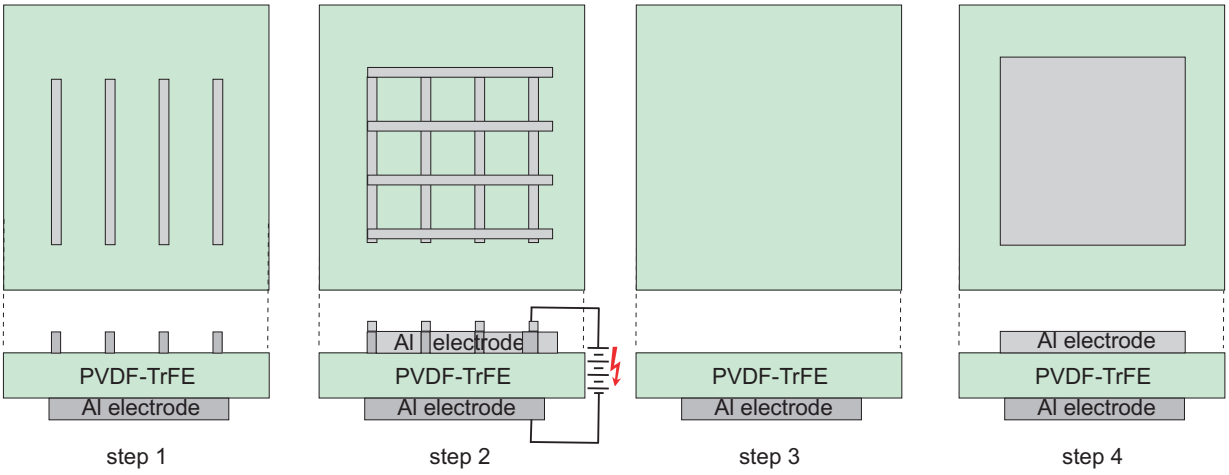

Figure 4.12: Pattern electrode deposition: finger deposition (step 1), a grid is achieved through a second finger evaporation (step 2); after poling, the electrode grid is chemically removed (step 3) and a final top electrode is deposited (step 4).

In order to inspect the success of the home-made mask, a low-resolution scan with a spot size of 500 µm and a step size of 100 µm was performed. Likewise, use of the smallest available laser-beam spot size (35 µm) allows the inspection of inhomogeneities and of the possible interfacial effects. All three-dimensional maps of polarization performed via TPT and FLIMM are included in the publication that follows.

Publication

3D High-resolution mapping of polarization profiles in thin poly(vinylidenefluoride-trifluoroethylene) (PVDF-TrFE) films using two thermal techniques

C.-D. Pham; A. Petre; L. Berquez; R. Flores Suarez; A. Mellinger; W. Wirges and R. Gerhard

IEEE Transactions on Dielectrics and Electrical Insulation, Vol. 16, 676-681 (2009)

3D High-resolution Mapping of Polarization Profiles in Thin Poly(vinylidenefluoride-trifluoroethylene) (PVDF-TrFE) Films Using Two Thermal Techniques

Cong-Duc Pham[1,2], **Anca Petre**[1,2], **Laurent Berquez**[1,2]
[1]Université de Toulouse ; UPS, INP ; LAPLACE (Laboratoire Plasma et Conversion d'Energie)
118 route de Narbonne, F-31062 Toulouse cedex 9, France.
[2] CNRS ; LAPLACE ; F-31062 Toulouse, France

Rosaura Flores-Suárez[3], **Axel Mellinger**[3,4], **Werner Wirges**[3] and **Reimund Gerhard**[3]
[3]Department of Physics and Astronomy, University of Potsdam
Karl-Liebknecht-Strasse 24-25, 14476 Potsdam-Golm, Germany
[4] Department of Physics, Central Michigan University
Mt. Pleasant, MI 48859, USA

ABSTRACT

In this paper, two non-destructive thermal methods are used in order to determine, with a high degree of accuracy, three-dimensional polarization distributions in thin films (12 µm) of poly(vinylidenefluoride-trifluoroethylene) (PVDF-TrFE). The techniques are the frequency-domain Focused Laser Intensity Modulation Method (FLIMM) and time-domain Thermal-Pulse Tomography (TPT). Samples were first metalized with grid-shaped electrode and poled. 3D polarization mapping yielded profiles which reproduce the electrode-grid shape. The polarization is not uniform across the sample thickness. Significant polarization values are found only at depths beyond 0.5 µm from the sample surface. Both methods provide similar results, TPT method being faster, whereas the FLIMM technique has a better lateral resolution.

Index Terms — **Focused laser intensity modulation method**, **FLIMM, thermal pulse tomography, TPT, space charges, polarization, dielectrics, polymers.**

1 INTRODUCTION

DURING the three last decades, many nondestructive thermal techniques [1-3] were developed in order to measure space charges density and polarization in dielectric samples. These techniques have a wide applications field, such as the study of piezoelectric materials ageing processes, the development and optimization of piezoelectric sensors, the ferroelectric memories degradation or the cables breakdown phenomena. The polarization or space charges distribution in dielectric materials is generally known in a global manner, measurements being carried out along only one direction, i.e. the sample thickness. Several attempts were made to obtaining two-dimensional, or three-dimensional mapping by using PEA (Pulsed Electro Acoustic) [4], PWP (Pression Wave Propagation) [5], FLIMM [6, 7], TPT [8, 9] techniques.

In this study, two nondestructive thermal methods called FLIMM (Focused Laser Intensity Modulation Method) and TPT (Thermal-Pulse Tomography) are presented and compared. FLIMM is a frequency-domain technique while TPT is a time-domain technique. In both cases, laser light absorbed by an opaque front electrode creates a thermal gradient, which, in the presence of a polarization or space charges results in a change in the surface charge. By focusing the laser beam to a tight spot size, both methods allow the determination of high resolution 3D distributions.

2 EXPERIMENTAL IMPLEMENTATION

2.1 FLIMM

Based on the LIMM technique [10-14], FLIMM uses a modulated intensity laser diode (45 mW, λ=658 nm) which can be focused on the sample through a Nachet lens leading to a spot size smaller than 10µm. The working frequencies range between 105 Hz to 10 kHz. The FLIMM set-up is shown in Figure 1.

As a consequence of the created thermal gradient, the induced periodical and local expansions cause a relative charge displacement within the irradiated volume: the lower the frequency, the deeper the irradiated zone. Varying the laser

Manuscript received on 31 October 2008, in final form 13 February 2009.

beam modulation frequency, one can control thermal wave's diffusion length and then emphasize the contribution of the corresponding depth into the sample to the total current signal $I(f)$. Under short-circuit conditions, its expression is given by:

$$I(f) = \frac{A}{L} j2\pi f \int_0^L r(z)T(z)dz \qquad (1)$$

with $r(z) = p(z) - (\alpha_x - \alpha_\varepsilon)\varepsilon\varepsilon_0 E(z)$

where $A, L, p(z), E(z), \alpha_x, \alpha_\varepsilon$ are respectively the surface of metal electrodes, the sample thickness, the pyroelectric coefficient in direction of the sample thickness, the internal electric field, the thermal dilatation coefficient of material and the temperature dependence coefficient of the material permittivity respectively. *T(z,f)* describes thermal gradient variations with respect to frequency. Because of its low magnitude (several pA typically), this current must be electronically conditioned by a low-noise wide-bandwidth current-to-voltage converter (FEMTO LCA-200K-20M). The signal is extracted from the noise by a lock-in amplifier (EGG 5302) and recorded by a computer. Finally, a mathematical treatment allows polarization or charge profiles reconstruction within the sample thickness direction [11].

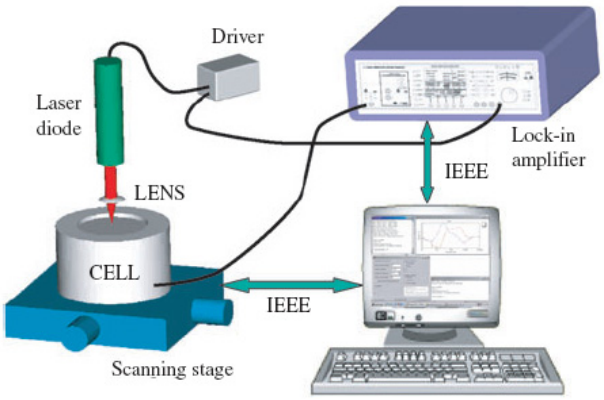

Figure 1. FLIMM set-up.

2.2 TPT

The thermal-pulse technique was first proposed in the early 1970s [12], and is implemented in the time domain. It was recently extended into three dimensions [8] with the new name Thermal-Pulse Tomography. Due to its high acquisition speed, up to 50 times faster than FLIMM, 3D maps of space charge and polarization on cylindrical and planar geometries can be measured [9, 13]. The experimental setup is shown in Figure 2. The thermal pulses are generated using a Nd:YAG laser (New m Wave Polaris III) at a rate of 6 Hz. The positioning of the sample (*X-Y* coordinates) in the laser beam is possible with a motorized translation stage (ERLIC 85, OWIS GmbH). The *Z* position is coordinated annually and the variation of it along the optical axis permits to adjust laser beam spots (defined by the diameter between the points where the intensity drops to $1/e^2$ of the central value) from 30 to 400 µm [14, 15]. The short circuit current was amplified using a FEMTO LCA-200K-20M current to voltage converter (20 MV/A) and recorded on an Agilent 54833A oscilloscope. For each beam pointing, 30 pulses were averaged.

The data analysis was performed as described in [13]. The measured short circuit current $I(t_k)$ was Fourier-transformed and divided by the complex gain spectrum $\tilde{\alpha}(f_n)$ of the FEMTO:

$$\tilde{J}_{\exp}(f_n) = \frac{\Delta t}{\tilde{\alpha}(f_n)} \sum_{k=0}^{N-1} I(t_k) e^{-2\pi i k n / N} \qquad (2)$$

with $f_n = \frac{n}{N\Delta t}, \quad n = 1 \ldots N/2, \qquad (3)$

where Δt is the sampling interval. The complex pyroelectric current in the frequency domain was analyzed using the well-established scale-transformation method [3].

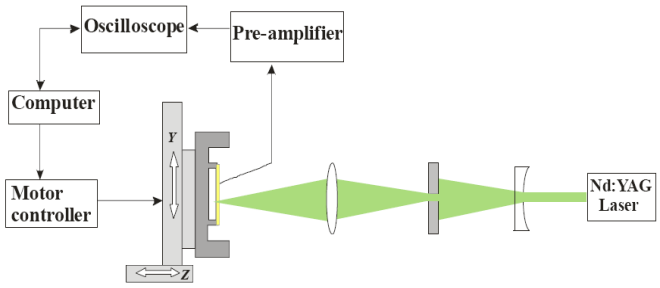

Figure 2. TPT set-up.

3 POLARIZATION MAPPING IN PVDF-TrFE

3.1 SAMPLE PREPARATION

The studied samples were thin films (12 µm) of poly (vinylidene fluoride - trifluoroethylene)) (PVDF-TrFE (65% - 35%))(Figure 3.). Being a PVDF copolymer, PVDF-TrFE has excellent mechanical properties and a good resistance to chemicals. It also shows a greater thermal stability than the homopolymer, and a higher dielectric rigidity. Since the thermal diffusivity on the metal electrode is three orders of magnitude higher than the one in the polymer film, the samples need a very well defined metal electrode pattern in order to minimize the thermal stress.

A finger-mask was cut from an Al foil with the same Nd:YAG laser used for the TPT studies, but operating at its maximum pulse energy. A grid-electrode on the film was achieved as a two-step process: first evaporating 50 nm of Al with the finger mask and then another 50 nm in a perpendicular direction (Figure 4). In order to pole the sample well above the coercive field (>70 MV/m), a back electrode (50 nm Al) was provided. To avoid the resistivity effects on the pyroelectric current, the grid-electrode was chemically removed and then a full-area Al electrode (50 nm) was evaporated.

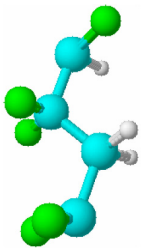

$(-CF_2-CH_2-)_n(-CHF-CF_2-)_m$
65% 35%

Figure 3. PVDF-TrFE molecule.

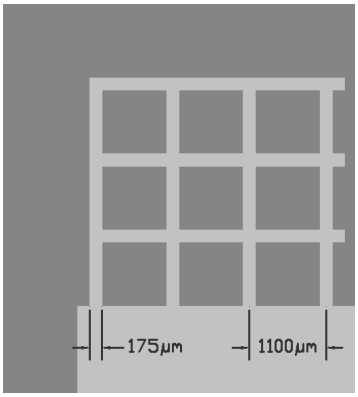

Figure 4. Electrode geometry.

3.2 FLIMM RESULTS

In order to identify the poled sample areas, mapping at a selected depth was carried out in a short time, with a low lateral resolution, by scanning the sample surface at fixed frequencies with a lateral step of 150 µm. As a result, a quick, complete polarization map was obtained, at 4.4 µm depth (f = 1 kHz) as shown in Figure 5. It is significant to notice that grid electrode details are very well reproduced and that the spatial distribution of polarization is not uniform along the grid length. From these first measurements, a specific grid cross was selected to study more precisely the in-depth PVDF-TrFE polarization.

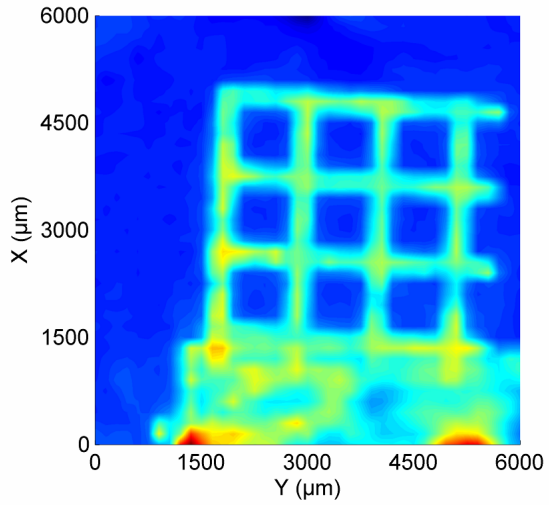

Figure 5. Low resolution polarization map.

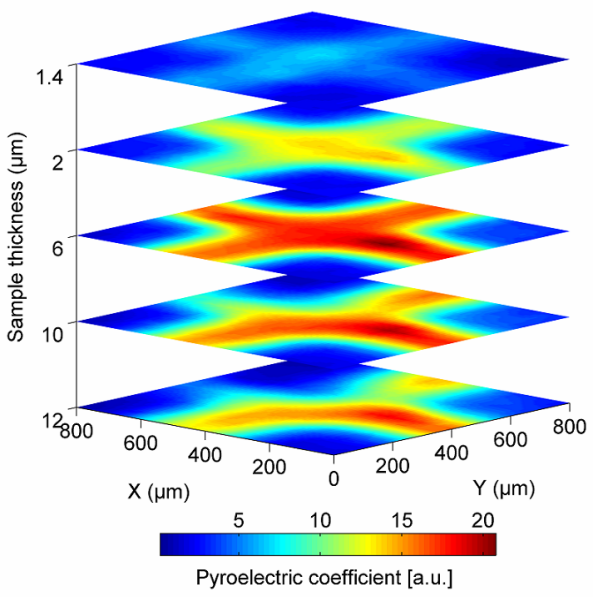

Figure 6. 3D high resolution polarization mapping with FLIMM.

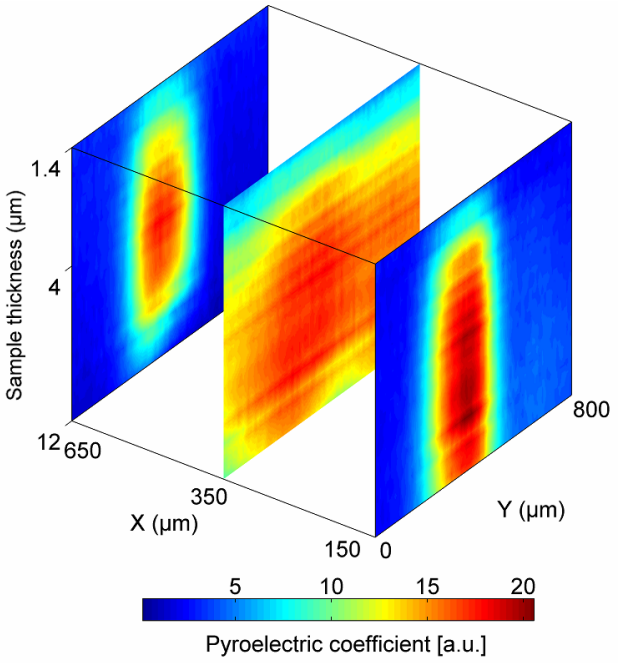

Figure 7. Polarization map in the Y direction.

The pyroelectric current was recorded with a 50 µm lateral measurement step, for frequencies ranging between 105 Hz and 10 kHz and with 10 µm laser beam spot size.

3D polarization mapping (Figure 6) shows that polarization begins at 2 µm depth. Into the sample bulk, non-uniformities of the polarization are well distinguished. For a better understanding of this phenomenon, scanning along the X axis (Y = 150, 400 and 700 µm) and along the Y axis (X = 150, 350 and 650 µm) were carried out, with a 10 µm measurement step as presented in Figures 7 and 8.

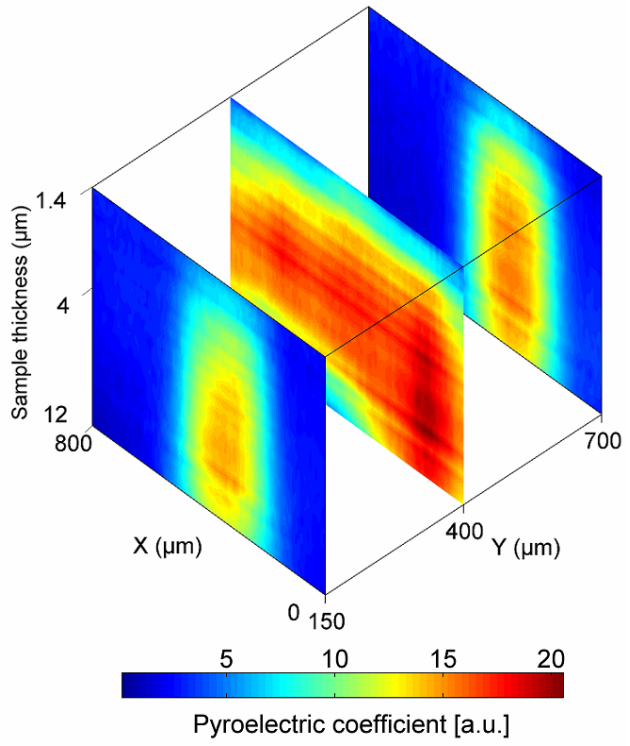

Figure 8. Polarization map in the X direction.

3.3 TPT RESULTS

First, polarization mapping was carried out with a big measurement step (100 µm) and a laser beam spot size of 500 µm (Figure 9). The obtained result allows to finding the electrode-grid shape polarization, starting from 1 µm. As described for FLIMM measurements, high-resolution 3D mapping on and around one cross of the electrode grid was carried out with a 10 µm measurement step and a 35 µm laser beam spot size. The polarization inhomogeneities can be also noticed (Figure 10). Depolarization near the surface and inhomogeneities on PVDF and P(VDF-TrFE) films were already observed on films and sensor cables. [3, 13, 16, 17].

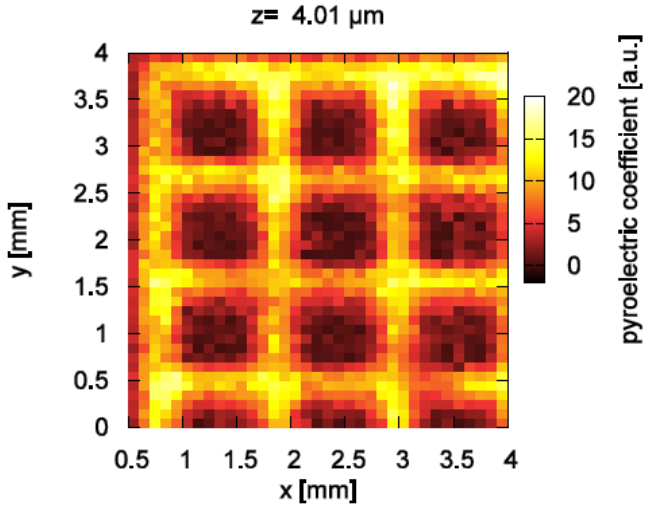

Figure 9. Low resolution polarization mapping with TPT.

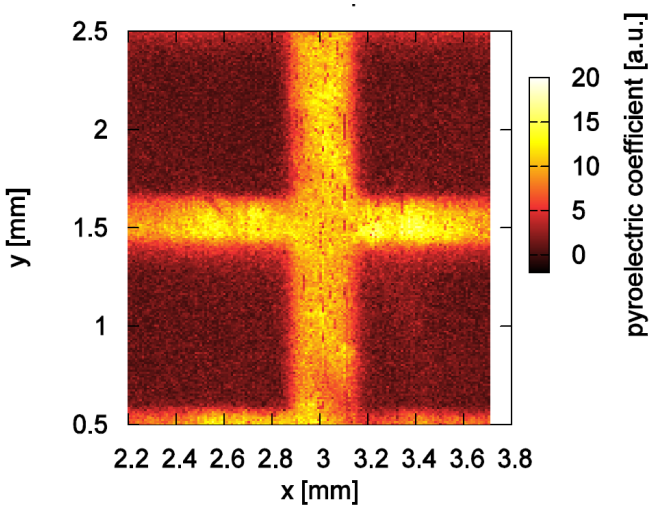

Figure 10. High-resolution polarization mapping with TPT at 4 µm depth.

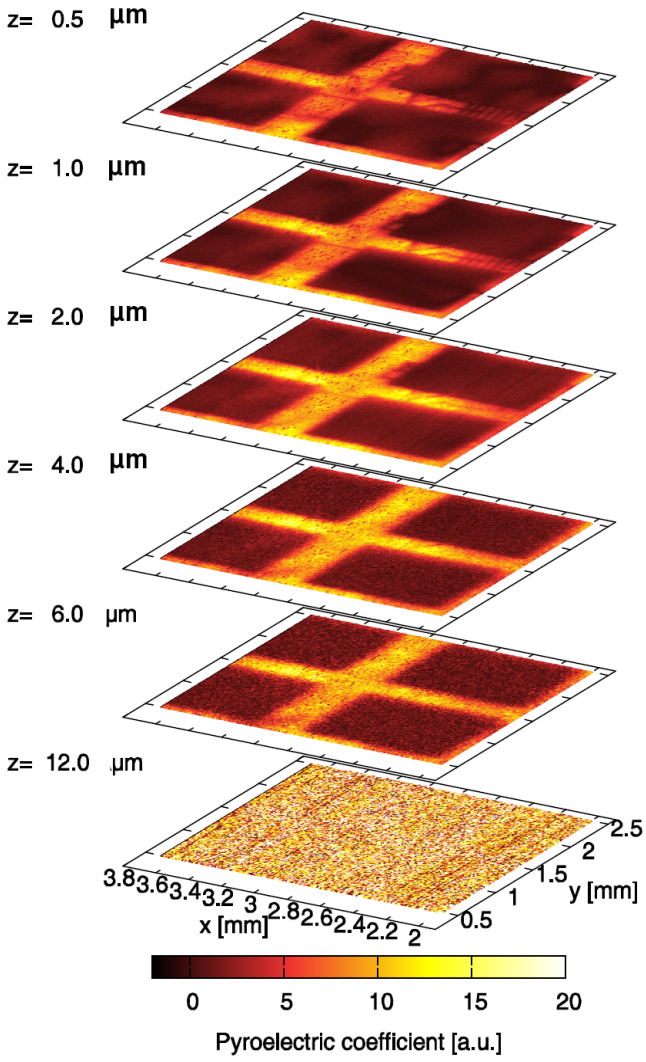

Figure 11. High resolution polarization map by TPT.

As we can see, the TPT technique has a better spatial resolution near the sample surface, polarization maps being obtained from 0.5 µm depth. On the other hand, at z = 12 µm, the FLIMM method can rebuild the cross shape (Figure 6) whereas TPT method doesn't provide a significant signal (Figure 11). The resolution decreases into the bulk, this phenomenon being due to the strong thermal diffusion in the electrode [9].

In order to compare the performances of these two methods, polarization measurements along the axis Y were executed. The obtained data were normalized and the width at middle height H was calculated after Gauss fitting; its value reproduced the electrode grid width. The results are represented in Figures 12 and 13. The full-width values at half maximum (FWHM) are shown in Table 1. They are nearly identical for the two methods and close to the electrode grid width, which proves that these two methods are completely suitable to obtain polarization profiles in thin polymer films.

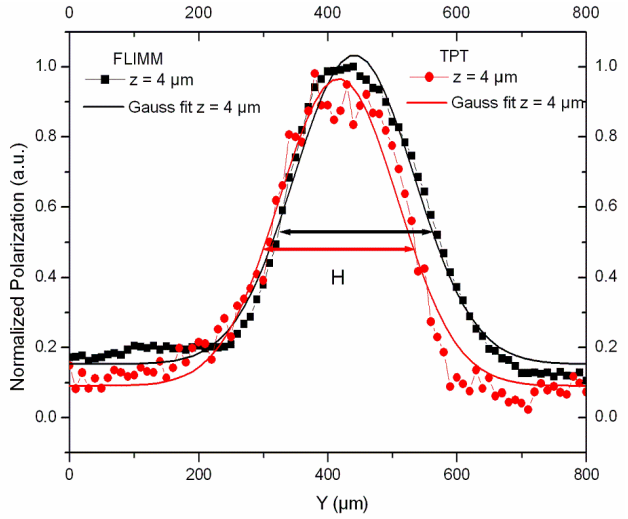

Figure 12. Polarization distributions standardized and interpolated by a Gauss function for z = 4 µm. FLIMM : X = 150 µm, H = 186 µm; TPT : X = 2700 µm, H = 183 µm

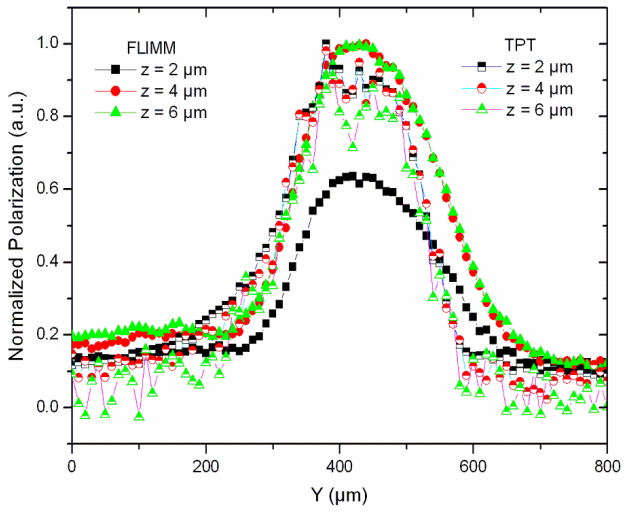

Figure 13. Standardized polarization for different depths: FLIMM : X = 150 µm ; TPT : X = 2700 µm.

Table 1. Full-width values at half maximum.

z (µm) \ H (µm)	FLIMM	TPT
2	183	185
4	186	183
6	186	186

4 CONCLUSION

In this study, two non-destructive thermal methods (FLIMM and TPT) are presented and compared. High-resolution mapping of three-dimensional polarization profiles in a thin film (12 µm) of poly(vinylidenefluoride - trifluoroethylene) (PVDF-TrFE) was carried out. The samples were poled by means of a grid-shaped electrode. 3D mapping with the two methods shows that the polarization inside the sample has the same geometry as the electrode grid. A non-uniform polarization in particular near the electroded surface can be noticed. TPT gives very good, fast results, while FLIMM has a very good lateral resolution. The two methods seem to be complementary for polarization studies on thin dielectric films.

REFERENCES

[1] S. Bauer and S. Bauer-Gogonea, "Current practice in space charge and polarization profile measurements using thermal techniques", IEEE Trans. Dielectr. Electr. Insul. Vol. 10, pp. 883–902, 2003.

[2] R. J. Fleming, "Space charge profile measurement techniques: Recent advances and future directions", IEEE Trans. Dielectr. Electr. Insul., Vol. 12, pp. 967-978, 2005.

[3] B. Ploss, R. Emmerich, and S. Bauer, "Thermal Wave Probing of Pyroelectric Distributions in the Surface Regions of Ferroelectric Materials_A New Method for the Analysis", J. Appl. Phys., Vol. 72, pp. 5363-5370, 1992.

[4] T. Maeno, "Three-dimensional PEA charge measurement system", IEEE Trans. Dielectr. Electr. Insul., Vol. 8, pp. 845-848, 2001.

[5] X. Qin, K. Suzuki, Y. Tanaka and T. Tanaka, "Three-dimensional Space-charge Measurement in a Dielectric using the Acoustic Lens and PWP Method", J. Phys. D: Appl. Phys., Vol. 32, pp. 157-160, 1999.

[6] D. Marty-Dessus, L. Berquez, A. Petre and J.L. Franceschi, "Space charge cartography by FLIMM: a three-dimensional approach", J. Phys. D: Appl. Phys., Vol. 35, pp. 3249-3256, 2002.

[7] A. Petre, D. Marty-Dessus, L. Berquez and J.L. Franceschi, "Space charge cartographies by FLIMM on thin PTFE films irradiated by Scanning Electron Microscope", J. Electrostatics, Vol. 64, pp. 492-497, 2006.

[8] A. Mellinger, R. Singh and R. Gerhard-Multhaupt, "Fast thermal pulse measurements of space-charge distributions in electret polymers", Rev. Sci. Instrum., Vol.76, pp.013903, 2005.

[9] A. Mellinger, R. Singh, M. Wegener, W. Wirges, R. Gerhard-Multhaupt and S. B. Lang, "Three-dimensional mapping of polarization profiles with thermal pulses", Appl. Phys. Lett., Vol. 86, p. 082903, 2005.

[10] S. B. Lang and D. K. Das-Gupta, "Laser-intensity modulation method : A technique for determination of spatial distributions of polarization and space charge in polymer electrets", J. Appl. Phys., Vol. 59, pp. 2151-2160, 1986.

[11] A. Petre, D. Marty-Dessus, L. Berquez, J.L. Franceschi, "A comparison of different mathematical treatments for solving the inverse problem in focused laser intensity modulation method", Jap. J. Appl. Phys., Vol. 43, pp. 2572-2579, 2004.

[12] R. E. Collins, "Analysis of spatial distribution of charges and dipoles in electrets by a transient heating technique", J. Appl. Phys., Vol. 47, pp. 4804–4808, 1976.

[13] R. Flores Suárez, A. Mellinger, M. Wegener, W. Wirges, R. Gerhard-Multhaupt, R. Singh, "Thermal-Pulse Tomography of Polarization Distributions in a Cylindrical Geometry", IEEE Trans. Dielectr. Electr. Insul., Vol. 13, pp. 1030-1035 , 2006.
[14] A. Mellinger, R. Singh, M. Wegener, W. Wirges, R. Flores Suárez, S. B. Lang, Lucas F. Santos and R. Gerhard-Multhaupt, "High-resolution three-dimensional space-charge and polarization mapping with thermal pulses", IEEE 12th Intern. Sympos. Electrets, pp. 212-215, 2005.
[15] M. Young, *Optics and Lasers. Including fibers and optical Waveguides*, 4th Ed. Springer-Verlag, 1993.
[16] B. Ploss and O. Bianzano, "Polarization profiling of the surface region of PVDF and P(VDF-TrFE)", IEEE 8th Intern. Sympos. Electrets, Paris, France, pp. 206-211, 1994.
[17] A. Mellinger, R. Flores-Suarez, R. Singh, M. Wegener, W. Wirges, R. Gerhard, S. B. Lang, "Thermal-Pulse Tomography of Space-charge and Polarization Distributions in Electret Polymers", Int. J. Thermophys. Vol. 29, pp. 2046–2054, 2008.

Cong-Duc Pham was born in Thai Nguyen, Vietnam, in 1981. He received the M.Sc. degree in electrical engineering from Toulouse University in 2006. He is currently a Ph.D. student at the Laboratory of Plasma and Energy Conversion -LAPLACE- Toulouse University. His main research interests concern the multi-dimensional mapping of polarization and space-charge distributions in dielectric polymers.

Anca Petre was born in Romania, on 26 January 1978. She studied mechanics at the Polytechnic University of Bucharest where she obtained the engineer degree in 2001. She received the M.Sc. degree in materials for electrical engineering in 2001 and the Ph.D. degree in 2004 from the University of Toulouse. From 2005 until 2008 she was assistant professor at the University of Toulouse, Laboratory of Plasma and Energy Conversion – LAPLACE and worked on space charge and polarization cartography in thin polymer films. She is currently an assistant professor at the University of Pau, at the Electrical Engineering Laboratory – LGE. Her research activities are focused on the study of the electrical properties of composite materials. In 2005 she received the scientific award from the Académie des Sciences, Inscriptions et belles lettres of Toulouse.

Laurent Berquez was born in Abbeville, France in 1970. He received the M.Sc. degree in acoustic in 1994, and the Ph.D. degree in 1998 from Toulouse University. He is actually an assistant professor at Toulouse University and works on multi-dimensional mapping of polarization and space-charge distributions in thin dielectric polymers at the Laboratory of Plasma and Energy Conversion - LAPLACE

Rosaura Flores-Suárez was born in Mexico City, Mexico, on 29 April 1980. She received the Bachelor degree in physics and mathematics from the National Polytechnic Institute of México (IPN) and the M.Sc. degree in polymer science jointly from the University of Potsdam and the Free University, Humboldt University and Technical University in Berlin, with a thesis on polarization profiles in poled PVDF sensor cables. She is currently a Ph.D. Student at the University of Potsdam. Her research interests include the investigation of ferroelectric polymers through thermal techniques such as thermal-pulse tomography and applications of these polymers in sensors and actuators.

Axel Mellinger was born in Munich, Germany, on 25 August 1967. He studied physics at the Technical University in Munich, where he obtained his Diploma and Ph.D. degrees in 1992 and 1995, respectively (his Ph.D. work was performed at the Max-Planck-Institute for Extraterrestrial Physics). In 1996/7, he held a two years postdoctoral position at UC Berkeley in the Department of Chemistry. From 1997 to 2008 he was a senior scientist at the University of Potsdam, Germany, where he obtained the highest German university degree, the *Habilitation*, in 2005. Since 2008, he is an Assistant Professor at Central Michigan University. His present work focuses on charge storage mechanisms in polymer electrets, optically induced charge-detrapping, and multi-dimensional mapping of polarization and space-charge distributions. From 1987 until 1992 he was a scholar of the German National Academic Foundation. He received the VDE/ITG 2004 award for a publication on dielectric resonance spectroscopy and the 2006 "Best Paper Award" by the German IEEE Instrumentation & Measurements chapter for his work on polarization tomography. In his spare time, he enjoys taking high-resolution mosaic images of astronomical objects for use in planetariums around the world.

Werner Wirges was born on 23 January 1962 in Bonn (Germany). He was trained as a plumber before studying Physical Engineering at the Aachen University of Applied Sciences. He graduated as Dipl.-Ing. in 1988. Between 1988 and 1992 he worked at the Heinrich Hertz Institute für Nachrichtentechnik, where he was in charge of the production and coating of viscoelastic control layers. From 1992 to 1997 he worked on the technology of thin film polymer systems for non-linear optical applications. This work focused on the production and poling of polymer multilayers. At the same time he started his work on plasma deposition of new fluoropolymers for optical communication. Until April 2000, he was employed in two industrial projects on passive optical components (thermo-optical switches and polymeric waveguide filter elements). His work is being continued in Potsdam since May 2000 in the group of Prof. R. Gerhard, where he focuses on production and characterization of non-polar fluoropolymers.

Reimund Gerhard (S'80–M'84–SM'85–F'93) studied mathematics and physics at the Darmstadt University of Technology in Germany from 1972 until 1978. After graduating as Diplom-Physiker, he spent one year as research fellow at the Collège Militaire Royal in St-Jean, Québec, Canada. From 1979 until 1985, he did his Ph.D. thesis with Professor Gerhard M. Sessler in Darmstadt. From 1985 until 1994, he was research scientist and project manager at the Heinrich-Hertz Institute for Communications Technology in Berlin. Since 1994 he has been an associate professor and since 1997 a full professor in the Department of Physics and Astronomy of the University of Potsdam in Germany. Presently, he is Dean of the Science Faculty at his university. The main research areas of Prof. Gerhard are polymer electrets and ferroelectrets, in particular the mechanisms of space-charge storage and dipole polarization in dielectric polymers and polymer composites, their ferro-, pyro- and piezoelectrical properties, and their applications in sensors and actuators, as well as the nonlinear optical properties of polymers, and more recently also the physics of musical instruments. From 1974 until 1979, he was a fellow of the Studienstiftung des Deutschen Volkes. In 1988, he was awarded an ITG-Preis by the Informationstechnische Gesellschaft im VDE. In 1989, he received a Silver medal from the Stiftung Werner-von-Siemens-Ring. In 2001, he was awarded the first Technologietransfer-Preis by the Technologie-Stiftung Brandenburg and the Prof.-Adalbert-Seifriz-Preis by the Verein Technologie-Transfer Handwerk for his technological collaborations with small industrial companies. Reimund Gerhard is a member of the American, European and German Physical Societies. Since 2002, he serves as Digest Editor of the IEEE Dielectrics and Electrical Insulation.

4.2.3 Further discussion: FLIMM vs TPT

The signal measured by the group working on the Focused LIMM was analyzed by implementing a Tikhonov regularization. This type of regularization belongs to the regularization methods described in section 3.5. In the 3D polarization mapping, a depolarization is observed at the edges of the finger electrodes, a stronger polarization of the nodes of the grid, as well as a smooth transition between poled and unpoled areas. In order to quantify this modulated behavior observed in FLIMM and TPT measurements, polarization profiles at selected depths z and the same y position were plotted as a function of the x coordinate (Fig. 4.13). The polarization values were normalized to allow an easy comparison between the FLIMM and TPT data. In both cases, the profiles show a modulated transition between a length showing polarization and another unpolarized length. Theoretically, the distance along the x coordinate showing polarization should correspond to the finger electrode width (175 µm).

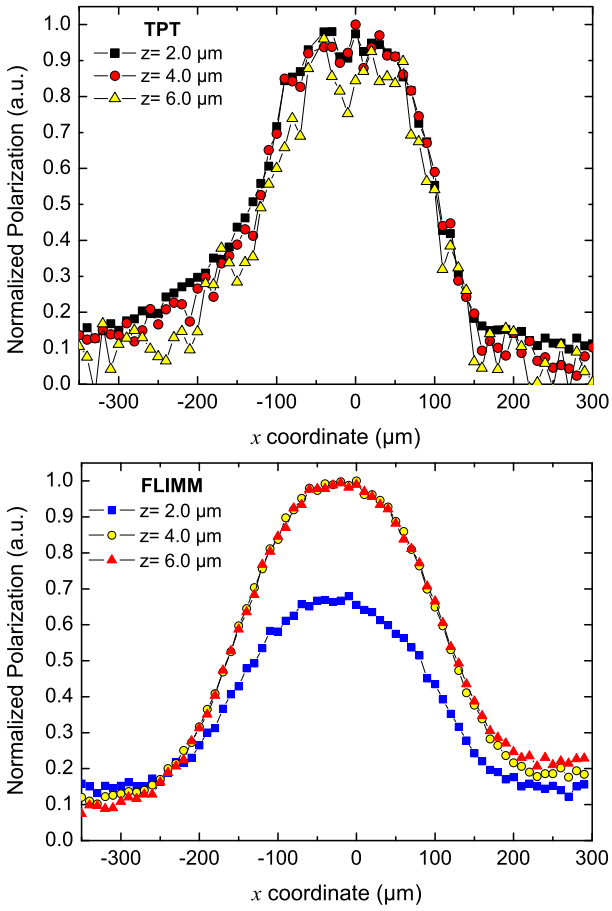

Figure 4.13: One-dimension profiles in P(VDF-TrFE) films coated with grid electrodes obtained through TPT (top) and FLIMM (bottom).

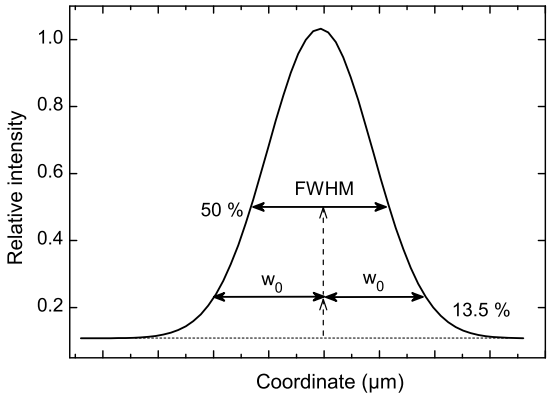

Figure 4.14: A smooth polarization transition showing the $2w_0$: width of the peak and the full width at half maximum (FWHM).

Two parameters of the curve can be inspected. The first is known as the full width at half maximum (FWHM) corresponding to the distance between points on the curve at which the polarization reaches half its maximum value. The second is the distance between points on the curve at which the polarization reaches $(1/e^2) = 13.5\%$ of its maximum value, known as the waist of the curve, $2w_0$ (Fig. 4.14). In the present work, both parameters were inspected at a depth $z = 2$ µm. Table 3.2 summarizes the results. On one side, the calculated FWHM and w_0 values from the TPT data deviate less than those obtained with the FLIMM technique (electrode width = 175 µm).

Taking into account that FLIMM measurements were performed with a better lateral resolution than TPT, the data from both methods are in good qualitative agreement. The time-domain technique complements its counterpart in the frequency domain at low depth values $z \leq 6$ µm. At the same time, missing information beyond this depth ($z \geq 6$ µm) is provided by FLIMM. Therefore, both techniques provide a complete tomography of polarization in thin dielectric films. The hypothesis relating the method of data analysis and the overestimation of the electrode parameters can be discarded since FLIMM and TPT uses regularization and Scale Transformation, respectively.

Table 3.2: Parameters at a depth z =2 µm.

Parameter	FWHM (µm)	error	w_0 (µm)	error
FLIMM	290	66%	210	20%
TPT	228	30%	177	1%

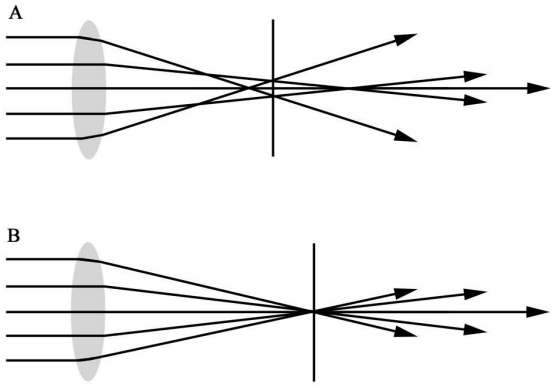

Figure 4.15: If spherical aberration is present, the laser beam spot size is enlarged (A). If spherical aberration is absent, the laser beam spot size is sharp (B).

4.2.4 Improved optics

The TPT setup is arranged with several optical elements; most of them are simple lenses. This yields spherical aberrations, which limits the lateral resolution. Several aberrations are optical effects commonly seen in devices such as mirrors, lenses, etc. Specifically, the spherical aberration originates near the lens rim, where the laser beam irradiates the lens at sharp angles. Consequently, the refraction is greater and the beam is focused nearer to the lens than the light passing through its center (Fig. 4.15). Chromatic aberration is negligible since we are using a monochromatic light source (Nd:YAG laser). Likewise, coma is remedied by using an iris diaphragm (6 mm aperture) and therefore only the Gaussian beam-profile is selected. Image distortions are also negligible since the data obtained with our optical array was reproduced with FLIMM technique as well (see section 4.2.2). Since spherical aberration limits the lateral resolution, the replacement of some optical elements is a viable solution.

In Fig. 4.16, we show the insertion of a microscope objective to focus the laser beam, instead of a positive lens. The previous elements were therefore rearranged so the incoming laser beam could be focused. At this point the beam is still affected by spherical aberration and coma. An iris diaphragm is then used to avoid coma and select the Gaussian beam. The output is then expanded by a negative lens and redirected to the microscope objective. The last element, the microscope objective will focus the laser beam without spherical aberration. The spot sizes of the laser beam were determined by means of a photodiode behind a knife-edge profiler, as described in section 4.1.3. The calculated spot sizes range from 10 µm to 430 µm (Fig. 4.17).

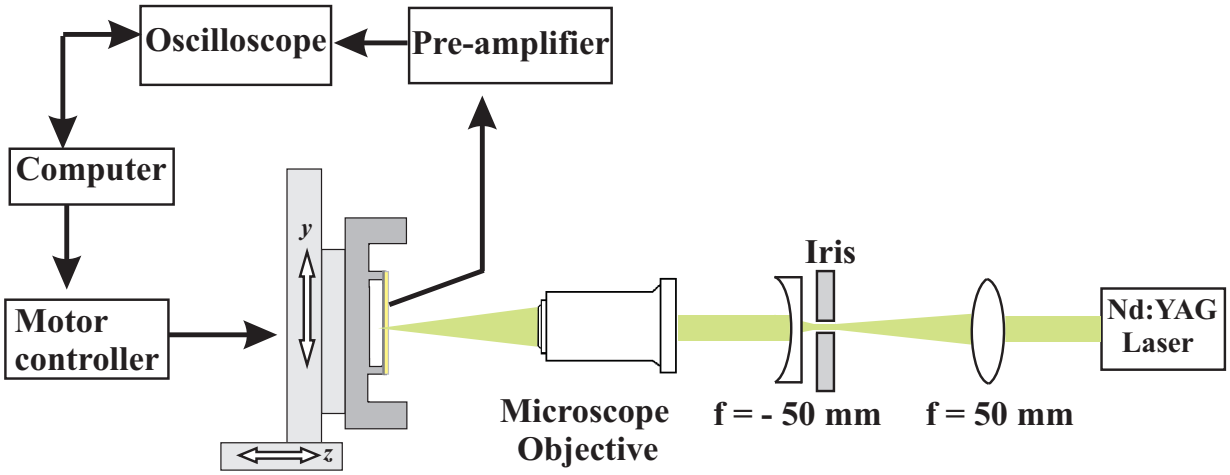

Figure 4.16: New array of optical elements in the TPT setup in order to avoid the spherical aberration.

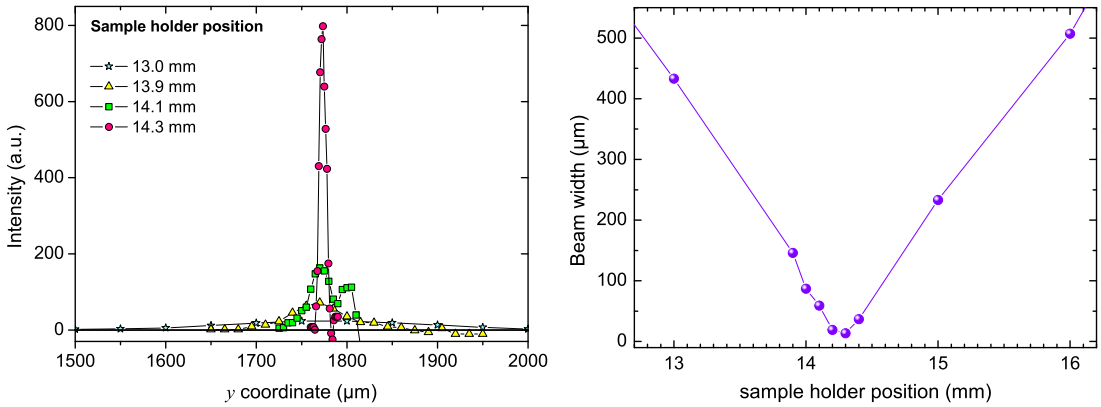

Figure 4.17: (Left) The laser beam intensity behind the knife edge as a function of the y position. (Right) The dependence of the beam width on the sample position.

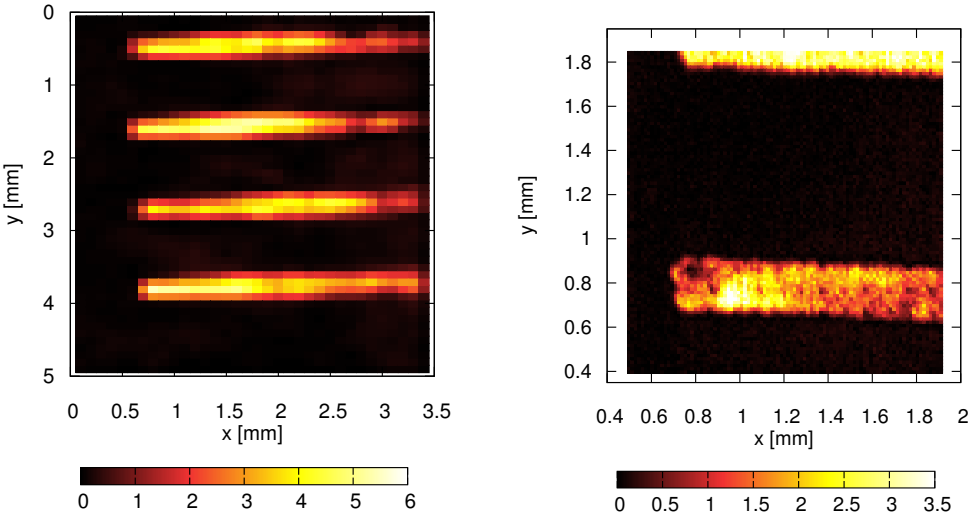

Figure 4.18: Maps of polarization in a P(VDF-TrFE) film with deposited finger electrodes using the new optics of the TPT setup. Spot sizes of 100 µm (left) and 10 µm (right) were used.

In order to test the new optical arrangement, low- and high-resolution maps of a 15 µm thickness PVDF-TrFE film with deposited aluminium electrodes (thickness of 160 nm) are presented (Fig. 4.18). The finger-electrode width after deposition was 220 µm. On the low-resolution scan (spot size = 100 µm), the shape of the electrodes is very well reproduced. Notice that the areas without electrodes remain unpolarized, as expected. On the high-resolution tomography (spot size = 10 µm), the inhomogeneities on the finger electrode are easily detectable and also the defects during the deposition. The highest polarization is observed near to edge at $x = 1$ mm.

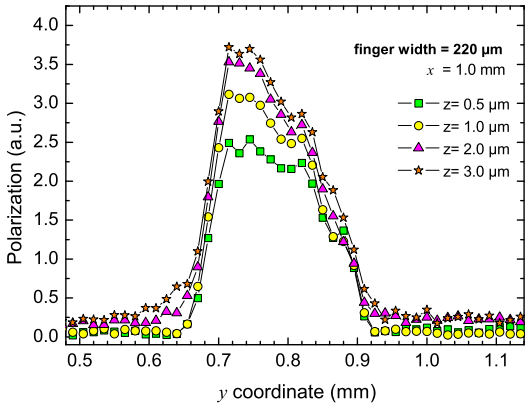

Figure 4.19: Polarization profile in P(VDF-TrFE) film with deposited finger electrode (width = 220 µm).

The polarization profile as a function of the y coordinate contains information about the width of the finger. In Fig. 4.19 the profile of the finger shows the highest value of the polarization at $x = 1$ mm, for several depths z. In the one-dimensional view, the profile does show a fast increment of the polarization and the transition between poled and non-poled regions is sharper. The width of the finger is reproduced even below the width of the curve in the polarization profile. This demonstrates the improvement of the TPT method. In order to determine the lateral resolution of the optimized setup, similar calculations as those reported by Mellinger et al. [65] were performed. The obtained value remains almost constant at depths of $z = 0.5 - 1.0$ µm, i.e. 55 µm. For depths between $z = 2$ to 3 µm, the calculated value was 85 µm. Possibly the values were not accurate enough due to the lack of sharp-edged electrodes. One possibility for future measurements would be the use of a commercial mask with better defined edges or a deposition of polymer electrodes by means of inkjet printing.

Conclusions

The switching phenomena in thin PVDF films have been imaged. Laser-cut masks have been obtained and showed a possibility to inspect interfacial effects. TPT and FLIMM have been demonstrated as key techniques to determine the polarization profile of thin dielectrics. The information that both methods yield complement each other. Two methods used to perform the deconvolution process of the LIMM equation, Regularization and Scale Transformation, have been implemented. Both methods yield similar results.

Chapter 5

TPT in Polymer-Dispersed Liquid Crystals (PDLCs)

This chapter includes a publication, which discusses the detailed sample preparation and settings used for the thermal probing on films of 10 w% liquid crystal dispersed in a P(VDF-TrFE) matrix. TPT measurements in commercial and laboratory-prepared P(VDF-TrFE) films were performed. The results exclude artifacts since the polarization profiles in both films show only the characteristic inhomogeneities of the polymer matrix (Fig. 5.1). In the commercial film, a small non-poled spot at $(x, y) = (0.4 \text{ mm}, 0.5 \text{ mm})$ appears due to a defect (breakdown) caused during poling. The edge of the circular top electrode at the bottom right corner can be seen as well. The polarization profiles in the PDLC films showed liquid crystal clusters. Among the limitations to resolve the features of individual LC droplets are the laser-beam spot size and possible electrostatic interactions [12] between functional groups in the polymer matrix and in the liquid crystal.

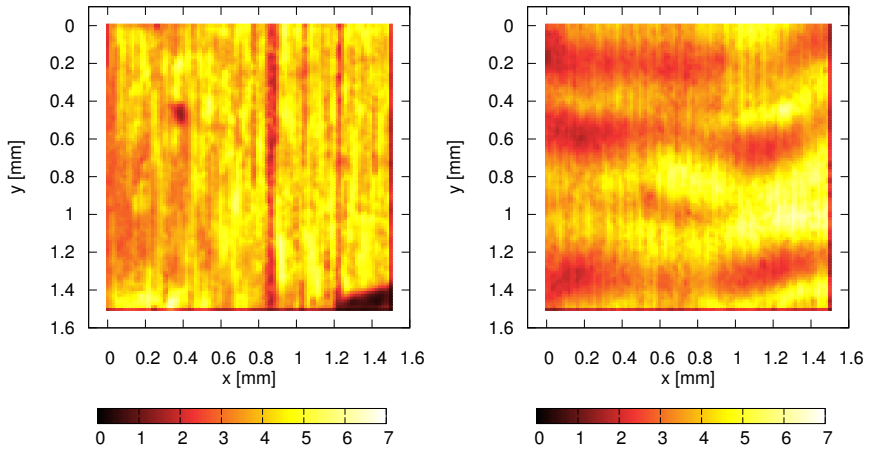

Figure 5.1: Polarization maps at $z = 1$ µm of the polymer matrix P(VDF-TrFE), commercial (right) and laboratory prepared films (left).

Publication

Imaging liquid crystals dispersed in a ferroelectric polymer matrix using Thermal-Pulse Tomography

R. Flores Suarez; L. M. Ganesan; W. Wirges; A. Mellinger and R. Gerhard
IEEE Transactions on Dielectrics and Electrical Insulation,
Vol. 17, 1123-1127 (2010)

Imaging Liquid Crystals Dispersed in a Ferroelectric Polymer Matrix by Means of Thermal-pulse Tomography

Rosaura Flores Suárez, Lakshmi Meena Ganesan, Werner Wirges, Reimund Gerhard
University of Potsdam
Department of Physics and Astronomy, Faculty of Science
14476 Potsdam-Golm, Germany

and **Axel Mellinger**
Central Michigan University
Department of Physics
Mount Pleasant, MI 48859, USA

ABSTRACT

A new arrangement of the optical elements in a Thermal-Pulse-Tomography (TPT) setup allows to scan micrometer structures in composite and heterogeneous samples such as polymer-dispersed liquid crystals (PDLCs). The non-destructive TPT technique allows the determination of three-dimensional profiles of polarization and space charge in dielectrics. The samples under study were 12 µm thick films of a copolymer of vinylidene fluoride with trifluoroethylene P(VDF-TrFE) (65/35) with embedded liquid-crystal droplets. The poling process was performed in direct contact well above the coercive field of the copolymer. The 3D map obtained from scanning with a 10 µm wide spot shows elliptically shaped areas with liquid-crystal droplets. Considering the droplets as oblate spheroids, their major axis lies in the *x*–*y* plane, while their minor axis in the *z* direction measures 0.5 µm or more. This result is in good agreement with scanning electron micrographs. It is believed that the major axis is overestimated due to imaging of liquid-crystal clusters.

Index Terms - **Thermal-pulse tomography, TPT, polarization profile, dielectrics, polymers, poly(vinylidene fluoride-co-trifluoroethylene), nematic liquid-crystal, PDLC, pyroelectric effect.**

1 INTRODUCTION

THE determination of space-charge and polarization distributions in dielectric materials is possible by means of two very well developed groups of techniques: acoustical and thermal [1]. The conventional thermal methods in the frequency [2] and time [3] domain have seen improvements in their lateral resolution down to 10 µm for the focused laser-intensity modulation method (FLIMM) and 38 µm for the thermal-pulse tomography (TPT) [4, 5]. These advances allow us to perform 3D imaging of space-charge and polarization profiles in dielectric materials. In a recent comparative study where both methods were implemented to investigate the same samples with a well-defined pattern, it was shown that both methods complement each other and deliver similar results within 10% [5]. The TPT method, up to 50 times faster than FLIMM, was shown to be suitable for cylindrical and planar geometries [6-8]. However, the fast thermal diffusion of the laser-induced pulses in the metal electrode limits the lateral resolution [5]. One possibility to mitigate this drawback is the use of conductive-polymer electrodes; however, this is still an ongoing project that requires investigation of the candidate polymer, its optimal deposition on the films, etc. In addition, the lateral resolution was limited by spherical aberration of the optical array which did not allow spot sizes below 30 µm.

As part of this work, the spherical lenses were replaced by a high numerical-aperture microscope objective. The upgraded system features a minimum spot size of 10 µm, which allows the imaging of smaller and more complex systems, such as liquid crystals embedded in a polymer matrix. These polymer-dispersed liquid crystals (PDLCs) [9] contain micrometer-sized spherical or elliptical droplets, depending on the preparation conditions [10]. In the present work, three-dimensional polarization imaging of liquid-crystal droplets was achieved with the improved TPT system.

Manuscript received on 11 December 2009.

2 EXPERIMENTAL DETAILS

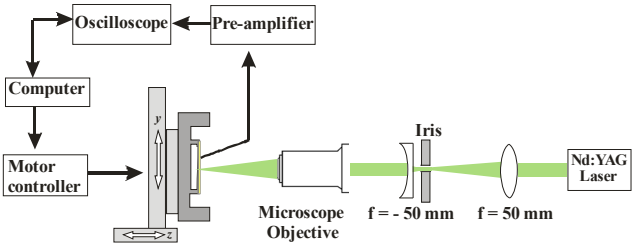

Figure 1. Experimental setup for the focused thermal-pulse technique.

PDLC films were prepared from a nematic LC (MDA-03-1767, Merck Chemicals, Germany) and P(VDF-TrFE) with a molar composition of 65/35. A homogeneous solution of the LC and the matrix polymer was prepared in a mixture of dimethyl formamide (DMF) and toluene (2:1). The PDLC film containing 10 wt% LC was prepared by drop casting. The solvent was evaporated at 70°C for 150 min and the annealing process was performed at 140°C for 4 h. Removal of the solvent induces a phase separation. The film thickness was in the range of 15 - 20 µm. For electrical poling well above the coercive field, 50 nm Al metal electrodes were evaporated onto both sides.

In the TPT experiment a Nd:YAG laser (New Wave Polaris III) is used to irradiate the sample which is positioned in the x–y plane with a motorized translation stage (ERLIC 85, OWIS GmbH). By manually adjusting the z position of the sample along the optical axis, the ($1/e^2$) laser-beam spot size could be varied between 10 and 400 µm. The short-circuit current is amplified with a FEMTO LCA-200K-20M current-to-voltage converter (20 MV/A) and recorded on an Agilent 54833A oscilloscope (Figure 1). For each beam pointing, 30 pulses were averaged.

3 DATA ANALYSIS

Data analysis was carried out in the frequency domain [11], after Fourier transformation of the transient signal. In order to find the polarization depth profile $P(z)$ at a given beam pointing, the LIMM equation (a Fredholm integral equation of the first kind) needs to be solved for $P(z)$:

$$\tilde{I}(f_n) = \frac{A}{d}\alpha_p \int_0^d P(z)\frac{\partial \tilde{T}(z,f_n)}{\partial t}dz \tag{1}$$

where $\tilde{I}$, A, α_p, d, $P(z)$ and $\tilde{T}$ are the complex pyroelectric current, electroded area, relative temperature dependence of the polarization, thickness, polarization distribution and complex temperature, respectively.

Several methods have been proposed for solving this ill-posed problem: scale-transformation method (ST) [12], regularization [13, 14] and more recently a Monte-Carlo technique [15, 16]. In the present work, we determined the pyroelectric coefficient $p(z)$ via ST:

$$p(z) = \frac{dc\rho}{A\eta j}\left[(\Re - \Im) I\left(\omega = 2D/z^2\right)\right] \tag{2}$$

where $c\rho$, h, j, and $(\Re - \Im)$ I are the heat capacity per volume, absorbance, laser intensity, and difference between the real and the imaginary part of the current signal, respectively. The pyroelectric coefficient is directly related to the polarization P via $p = \partial P/\partial T = \alpha_p P$

4 RESULTS AND DISCUSSIONS

Taking advantage of the reduced TPT spot size of 10 µm that may allow us to image micrometer structures, high-resolution measurements were performed on a PDLC film. A scanning-electron-microscope image of the PDLC film shows the oblate spheroidal liquid-crystal domains as relatively distinct droplets within the polymer matrix (Figure 2). The major axis of the LC droplets is parallel to the film surface and varies from 2 to 5 µm, whereas the minor axis (perpendicular to the film surface) varies between 0.5 and 2 µm. Polarization tomography of a P(VDF-TrFE) matrix-polymer film (prepared in the same way as the PDLC film) showed some inhomogeneities, as expected and as reported elsewhere [6-8].

Apart from the inhomogeneities caused by the polymer matrix, a non-poled area is found in the polarization-tomography image of the PDLC film, as seen in Figure 3. The non-poled area detected between depths of z = 0.5 and 0.9 µm can be attributed to the LC droplets dispersed in the polymer matrix.

One limitation for identifying individual LC droplets on the polarization maps (x–y plane) at different depths z (Figure 3) stems from scanning with a still relatively large spot size. The smallest beam diameter achievable with the present TPT setup is around 10 µm. This implies that the laser spot may illuminate up to five LC droplets when they are near to each other as seen in Figure 2.

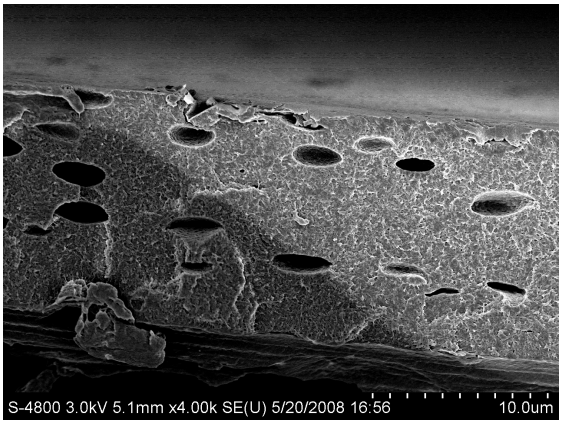

Figure 2. SEM image of the PDLC film with 10 wt% LC [10].

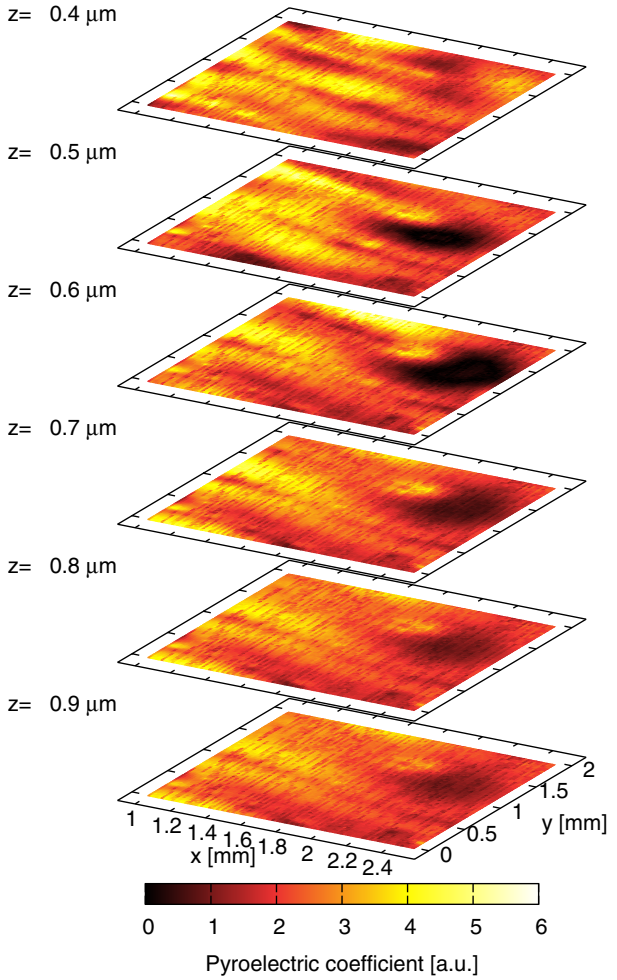

Figure 3. Three-dimensional polarization profile in a PDLC film. The dark area represents the liquid-crystal droplets**.**

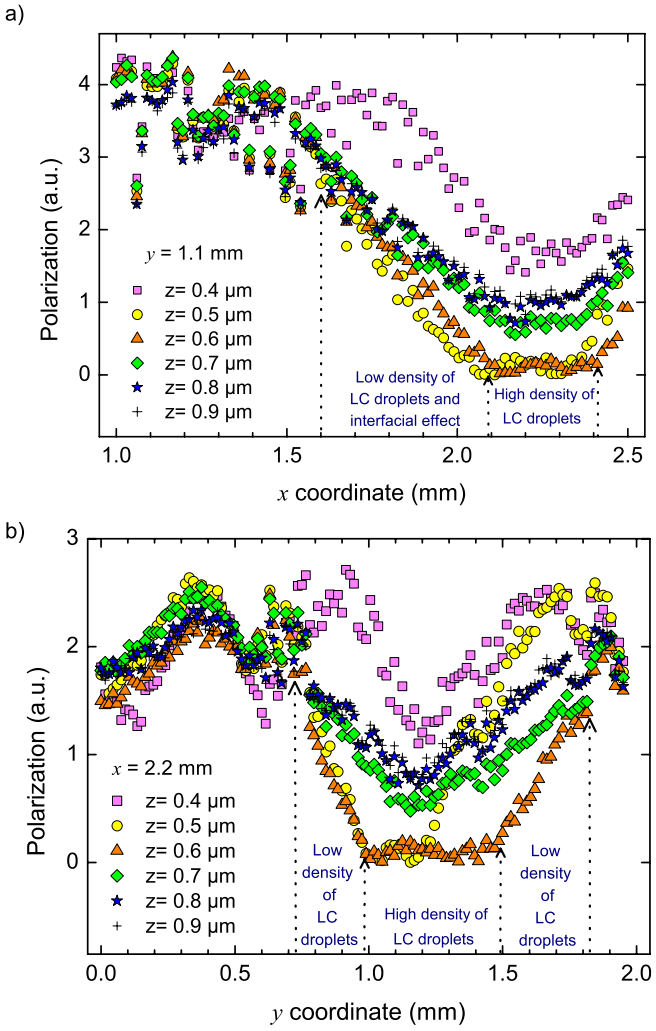

Figure 4. One-dimensional cut from the 3D profile of the PDLC film at a) y = 1.1 mm and (b) x = 2.2 mm. The width of the zone with $P \approx 0$ is attributed to the presence of several LC droplets within each spot.

It follows that the non-poled areas along the x–y plane may represent a group of droplets. In order to quantify the density of droplets along each coordinate, one-dimensional profiles were extracted from the data of Figure 3. In the polarization profile at y = 1.1 mm (Figure 4a), there are variations between x = 1 and x = 1.6 mm probably associated with inhomogeneities in the polymer matrix. A small number of LC droplets and their interaction with the polymer matrix at the interface [16] may cause the smooth transition between x = 1.6 and 2.1 mm, whereas the high density of droplets results in a non-poled zone of ≈ 300 µm width. Similar profiles as a function of x coordinate were determined at y = 2.2 mm (Figure 4b). The non-poled zone with a high density of droplets is ≈ 500µm wide, preceded and followed by a smooth transition. Thus, the presence of several LC droplets and the interfacial effect explain the enlargement in the non-poled area and the smooth transition between the poled polymer matrix and the droplets. A smaller spot size (< 10 µm) not necessarily make the task easier to distinguish individual droplets, but would also decrease the signal-to-noise ratio.

7 CONCLUSION

In conclusion, an upgraded thermal-pulse tomography setup with a tight focus allows the imaging of microstructures in pyroelectric materials. It is also proposed that the laser-spot size makes it difficult to distinguish individual droplets in the x–y plane. The depth resolution, however allows the identification of LC droplets in the z direction.

ACKNOWLEDGMENT

The authors are indebted to the Liquid Crystals Divison of Merck KGaA in Darmstadt for kindly providing the LC samples investigated in this study. The authors are especially grateful to Dr. Brigitte Tiersch (University of Potsdam) for the SEM pictures. We thank the European Union for partial financial support of our laboratory within the ERDF program.

REFERENCES

[1] R. J. Fleming, "Space Charge Profile Measurements Techniques: Recent Advances and Future Directions", IEEE Trans. Dielectr. Electr. Insul., Vol. 12, pp. 967-978, 2005.

[2] S. B. Lang and D. K. Das-Gupta, "Laser-intensity-modulation method: A Technique for determination of spatial distributions of polarization and space charge in polymer electrets", J. Appl. Phys., Vol. 59, pp. 2151-2160, 1986.

[3] R. E. Collins, "Analysis of spatial distribution of charges and dipoles in
electrets by a transient heating technique", J. Appl. Phys., Vol. 47, pp. 804-4808, 1976.

[4] D. Marty-Dessus, L. Berquez, A. Petre and J.L. Franceschi, "Space-charge cartography by FLIMM: a three-dimensional approach", J. Phys. D: Appl. Phys., Vol. 35, pp. 3249-3256, 2002.

[5] A. Mellinger, R. Singh, M. Wegener, W. Wirges, R. Gerhard-Multhaupt and S. B. Lang, "Three-dimensional mapping of polarization profiles with thermal pulses", Appl. Phys. Lett., Vol. 86, 082903, 2005.

[6] C.-D. Pham, A. Petre, L. Berquez, R. Flores-Suárez, A. Mellinger, W. Wirges and R. Gerhard, "3D high-resolution mapping of polarization profiles in thin poly(vynilidenefluoride-co-trifluoroethylene) (PVDF-TrFE) films using two thermal techniques", IEEE Trans. Dielectr. Electr. Insul., Vol. 16, pp. 676-681, 2009.

[7] R. Flores Suárez, A. Mellinger, M. Wegener, W. Wirges, R. Gerhard-Multhaupt and R. Singh, "Thermal-Pulse Tomography of Polarization Distributions in a Cylindrical Geometry", IEEE Trans. Dielectr. Electr. Insul., Vol. 13, pp. 1030-1035, 2006.

[8] A. Mellinger, R. Flores-Suárez, R. Singh, M. Wegener, W. Wirges, R. Gerhard and S. B. Lang, "Thermal-Pulse Tomography of Space-charge and Polarization Distributions in Electret Polymers", Intern. J. Thermophys., Vol. 29, pp. 2046-2054, 2008.

[9] H. S. Kitzerow, "Polymer-dispersed liquid crystals from the nematic curvilinear aligned phase to ferroelectric films", Liq. Cryst., Vol. 16, pp. 1-31, 1994.

[10] L. M. Ganesan, W. Wirges, A. Mellinger and R. Gerhard, "Piezo-optical and electro-optical behaviour of nematic liquid crystals dispersed in a ferroelectric copolymer matrix", J. Phys. D: Appl. Phys., Vol. 43, 015401, 2010.

[11] A. Mellinger, R. Singh and R. Gerhard-Multhaupt, "Fast thermal-pulse measurements of space-charge distributions in electret polymers", Rev. Sci. Instrum., Vol. 76, 013903, 2005.

[12] B. Ploss, R. Emmerich, and S. Bauer, "Thermal wave probing of pyroelectric distributions in the surface region of ferroelectric materials: A new method for the analysis", J. Appl. Phys., Vol. 72, pp. 5363-5370, 1992.

[13] S. Bauer and S. Bauer-Gogonea, "Current practice in space charge and polarization profile measurements using thermal techniques", IEEE Trans. Dielectr. Electr. Insul., Vol. 10, pp. 883-902, 2003.

[14] S. B. Lang, "Fredholm Integral equation of the laser intensity modulation method (LIMM): Solution with the polynomial regularization and L-curve methods", J. Mater. Sci., Vol. 41, pp. 147-153, 2006.

[15] E. Tuncer and S. B. Lang, "Numerical extraction of distributions of space-charge and polarization from LIMM", Appl. Phys. Lett., Vol. 86, 071107, 2005.

[16] S. B. Lang and R. Fleming, "A comparison of the three techniques for solving the Fredholm Integral equation of the laser intensity modulation method (LIMM)", IEEE Trans. Dielectr. Electr. Insul., Vol. 16, pp. 809-814, 2009.

[17] L. M. Ganesan, P. Frübing, A. Mellinger and R. Gerhard, "Dielectric relaxation behaviour of nematic liquid crystals dispersed in poly(vinylidene fluoride-trifluoroethylene)", J. Phys. D: Appl. Phys., Vol. 42, 092006, 2009.

Rosaura Flores Suárez was born in Mexico City, Mexico, on 29 April 1980. She received the Bachelor degree in physics and mathematics from the National Polytechnic Institute of México (IPN) and the M.Sc. degree in polymer science jointly from the University of Potsdam and the Free University, Humboldt University and Technical University in Berlin, with a thesis on polarization profiles in poled PVDF sensor cables. She is currently a Ph.D. Student at the University of Potsdam. Her research interests include the investigation of ferroelectric polymers through thermal techniques such as thermal-pulse tomography and applications of these polymers in sensors and actuators.

Lakshmi Meena Ganesan was born in Chennai, India, on 9 March 1981. She received the Bachelor of Technology degree in polymer technology from the University of Madras, India and the M.Sc. degree in polymer science jointly from the University of Potsdam and the Free University, Humboldt University and Technical University in Berlin, with a thesis on optical switching and dielectric response of nematic liquid crystals dispersed in a ferroelectric poly(vinylidene fluoride-trifluoroethylene) matrix. She obtained her Ph.D. degree in 2010 and her Ph.D. work was performed at the University of Potsdam. Her research activities are focused on the coupling of the electrical, mechanical and optical response in polymer/liquid crystal composites. .

Axel Mellinger was born in Munich, Germany, on 25 August 1967. He studied physics at the Technical University in Munich, where he obtained his diploma and the Ph.D. degree in 1992 and 1995, respectively (his Ph.D. work was performed at the Max-Planck-Institute for Extraterrestrial Physics). In 1996/7 he held a two year postdoctoral position at UC Berkeley in the Department of Chemistry. From December 1997 until July 2008 he was a senior scientist at the University of Potsdam, Germany, where he obtained the highest German university degree, the Habilitation, in 2005. Since 2008 he is an Assistant Professor in the Physics Department at Central Michigan University. His present work focuses on charge storage mechanisms in polymer electrets, optically induced charge-detrapping, and multi-dimensional mapping of polarization and space-charge distributions. From 1987 until 1992 he was a scholar of the German National Academic Foundation. He received the 2004 VDE/ITG award for a publication on dielectric resonance spectroscopy and the 2006 "Best Paper Award" by the German IEEE Instrumentation & Measurements chapter for his work on polarization tomography. In his spare time, he enjoys taking high-resolution mosaic images of astronomical objects for use in planetariums around the world.

Werner Wirges was born on 23 January 1962 in Bonn (Germany). He was trained as a plumber before studying physical engineering at the Aachen University of Applied Sciences. He graduated as Dipl.-Ing. in April 1988. Between 1988 and 1992 he worked at the Heinrich-Hertz Institute für Nachrichtentechnik, where he was in charge of the production and coating of viscoelastic control layers. From 1992 to 1997 he worked on the technology of thin film polymer systems for non-linear optical applications. This work was focused on the production and poling of polymer multilayers. At the same time he started his work on plasma deposition of new fluoropolymers for optical communication. Until 2000, he was employed in two industrial projects on passive optical components (thermo-optical switches and polymeric waveguide filter elements). His work is being continued in Potsdam since 2000 in the group of Prof. R. Gerhard, where he focuses on production and characterization of non-polar fluoropolymers.

Reimund Gerhard (S'80–M'84–SM'85–F'93) studied mathematics and physics at the Darmstadt University of Technology in Germany from 1972 until 1978. After graduating as Diplom-Physiker, he spent one year as research fellow at the Collège Militaire Royal in St-Jean, Québec, Canada. From 1979 until 1984, he did his Ph.D. thesis with Professor Gerhard M. Sessler in Darmstadt. From 1985 until 1994, he was research scientist and project manager at the Heinrich-Hertz Institute for Communications Technology in Berlin. Since 1994 he has been an associate professor and since 1997 a full professor in the Department of Physics and Astronomy of the University of Potsdam in Germany. Presently, he is Dean of the Science Faculty at his university. The main research areas of Prof. Gerhard are polymer electrets and ferroelectrets, in particular the mechanisms of space-charge storage and dipole polarization in dielectric polymers and polymer composites, their ferro-, pyro- and piezoelectrical properties, and their applications in sensors and actuators, as well as the nonlinear optical properties of polymers, and more recently also the physics of musical instruments. From 1974 until 1979, he was a fellow of the Studienstiftung des Deutschen Volkes. In 1988, he was awarded an ITG-Preis by the Informationstechnische Gesellschaft im VDE. In 1989, he received a Silver medal from the Stiftung Werner-von-Siemens-Ring. In 2001, he was awarded the first Technologietransfer-Preis by the Technologie- Stiftung Brandenburg and the Prof.-Adalbert-Seifriz-Preis by the Verein Technologie-Transfer Handwerk for his technological collaborations with small industrial companies. Reimund Gerhard is a member of the American, European and German Physical Societies. From 2002 to 2009 he served as Digest Editor of the IEEE Dielectrics and Electrical Insulation society.

Chapter 6

TPT in Polymer Ferroelectrets

It was previously demonstrated that the TPT method was suitable for measuring space-charge distributions in electrets (see publication in section 4.1). The multilayer systems were introduced for the first time in 2007; mainly the piezoelectric coefficients were measured [18]. The sandwiches consist of two fluorinated ethylene propylene (FEP) layers that cover a perforated middle layer of polytetrafluoroethylene (PTFE). Perforations were made by hand and by means of a Nd:YAG laser. Charging was performed using corona discharge and the direct method. The samples with laser-drilled holes yielded higher piezoelectric responses than the others. In the present chapter, a publication with three-dimensional maps of the field distribution in a new three-layer system is included. The system under investigation is a sandwich of an adhesive tape and two polymer films (Fig. 6.1). This sample preparation is easier to implement than the fabrication of three-layer ferroelectrets reported before [18]. The electric field between the charges inside the adhesive surfaces and their counter charges on the top electrode was shown [96]. The unexpected non-uniform distribution of this field encourage the search for new materials that may improve the stability of the ferroelectret system.

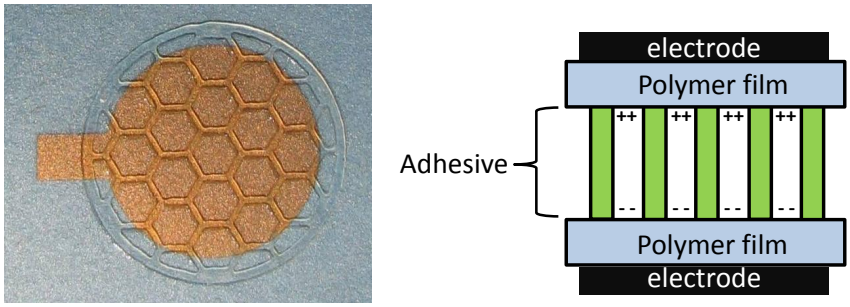

Figure 6.1: (a) Digital image of the adhesive honeycomb structure and a polymer-film with a gold electrode; (b) cross section of the three-layer ferroelectret; the voids were internally charged by means of dielectric barrier discharges (DBDs).

Publication

Polarization from dielectric-barrier discharges in ferroelectrets: Mapping of the electric-field profiles by means of Thermal-Pulse Tomography

X. Qiu; L. Holländer; R. Flores Suarez; W. Wirges and R. Gerhard

Applied Physics Letters,

Vol. 97, 072905-1-3 (2010)

Polarization from dielectric-barrier discharges in ferroelectrets: Mapping of the electric-field profiles by means of thermal-pulse tomography

Xunlin Qiu,[a] Lars Holländer, Rosaura Flores Suárez, Werner Wirges, and Reimund Gerhard

Applied Condensed-Matter Physics, Faculty of Science, University of Potsdam, Karl-Liebknecht-Strasse 24-25, 14476 Potsdam-Golm, Germany

(Received 25 June 2010; accepted 3 August 2010; published online 20 August 2010)

A polymer-ferroelectret system is fabricated by attaching two uniform polycarbonate films to a grid produced from double-sided adhesive tape by means of computer-controlled laser cutting. The openings of the grid structure result in well-defined voids inside the three-layer system, which can be internally charged through dielectric barrier discharges. The negatively charged internal void surfaces can be made visible by means of xerographical toner, and the electric-field distribution inside such ferroelectrets can be studied with thermal-pulse tomography. Both techniques exhibit polarization patterns that are consistent with the grid structure. Possible reasons for the observed non-uniform charge distributions are discussed. © *2010 American Institute of Physics*.
[doi:10.1063/1.3481802]

Polymer foams and layer systems with internally charged voids (so-called ferroelectrets) exhibit high piezoelectric activity combined with high mechanical flexibility and compliance.[1–5] So far, the standard material in ferroelectret studies and applications has been cellular polypropylene (PP), which is usually produced by means of blow extrusion or by stretching filler-loaded polymer sheets under suitable conditions.[6,7] Depending on the structure and the charging conditions, cellular PP ferroelectrets often show piezoelectric d_{33} coefficients of several hundred picocoulomb per newton. However, a wider application of cellular PP ferroelectrets is hindered by the relatively low thermal stability of their piezoelectricity, which decays dramatically between 60 and 80 °C.[8] In addition, cellular PP ferroelectrets have a void structure with a broad distribution of void sizes and shapes, and therefore only a limited number of the voids are optimal for charging and for transducer operation. In order to achieve ferroelectrets with better thermal stability of the piezoelectricity and/or with more uniform void structures, various other polymers have been employed recently as ferroelectrets.[5]

On the other hand, the understanding of the fundamental properties of ferroelectrets is still not sufficiently complete. It is known that the voids must be internally charged by means of dielectric barrier discharges (DBDs) in order to render cellular or void-containing polymer structures piezoelectric. Charges of both polarities are generated in the plasma of a DBD and subsequently trapped at the internal surfaces of the dielectric polymer.[9,10] The charged voids can be considered as macroscopic dipoles that consist of charges of opposite polarity on the internal surfaces. Theoretical analysis indicates that the piezoelectricity of ferroelectrets is linearly related to the effective polarization (i.e., the density of the macroscopic dipoles).[11,12] Early on, the existence of injected near-surface homocharge and of DBD-generated internal heterocharge in corona-poled cellular-PP ferroelectret films was confirmed by means of thermal-wave experiments (sometimes also called laser-intensity modulation method or LIMM).[13] A direct proof of the internal charges was obtained with scanning electron microscope (SEM) images.[14] SEM images of obliquely cut cellular PP ferroelectrets show the negative charges, because the secondary electron emission yield from negatively charged areas is higher than that from positively charged areas. However, this technique requires cutting of the sample and is thus destructive. For developing new ferroelectrets and for optimizing their properties, a nondestructive technique for assessing the effective polarization is highly desired.

In this paper, a new technique for the fabrication of ferroelectrets is proposed, and the electric-field profiles in the resulting ferroelectret samples are mapped by means of thermal-pulse tomography (TPT). TPT is a nondestructive thermal time-domain technique for detecting three-dimensional (3D) profiles of space charge and dipole polarization.[15–17] Electric-field maps resulting from TPT were shown to agree with those obtained by means of the focused LIMM (FLIMM).[18] In a preliminary study, TPT experiments on the same ferroelectret system revealed electric-field patterns that are closely related to the honeycomb structure of the sample.[19] Here, the earlier investigations were re-examined and re-evaluated as well as supplemented by new experiments and interpretations.

For sample preparation, polycarbonate (PC) films (Makrofol DE 6–2, BMS) with a thickness of 30 or 50 μm were metallized on one surface with either 50 nm thick aluminum or 20 nm thick gold electrodes. A grid of double-sided adhesive tape (468MP 200MP Adhesive, 3M) with a thickness around 100 μm was prepared by means of computer-controlled laser cutting. After peeling off the nonadhesive protective layers (which also have a thickness of about 100 μm), the adhesive-tape grid was sandwiched with two PC films via their nonmetalized surfaces. In this way, well-defined voids are formed at the openings of the adhesive-tape grid. Figure 1(a) schematically shows the sample preparation, while Fig. 1(b) is a digital image of part of such a sample in which the adhesive tape grid has a honeycomb structure with a length of 1.5 mm for one side of each hexa-

[a]Electronic mail: xunlin@canopus.physik.uni-potsdam.de.

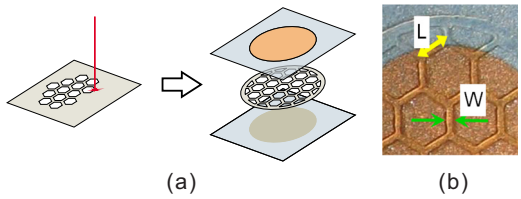

FIG. 1. (Color online) (a) Sample preparation: A grid of double-sided adhesive tape is produced by means of computer-controlled laser cutting. PC films are metalized on one side. The nonmetalized surfaces of two PC films stick to both sides of the adhesive-tape grid, respectively, forming well-defined voids. (b) A digital photo of part of a sample. The PC films are metalized with 20 nm thick semitransparent gold electrodes. The honeycomb structure of the adhesive-tape grid is clearly visible.

gon and with a width of 0.5 mm for the remaining adhesive-tape stripes.

In order to charge the sample by means of DBDs across the voids, a dc voltage is applied between the sample electrodes for 30 s by means of a high-voltage supply (Trek model 610D). The d_{33} coefficient of the sample as a function of the charging voltage is plotted in Fig. 2. The d_{33} coefficients were determined dynamically as described in more detail elsewhere.[20] The voltage dependence of d_{33} clearly shows a threshold behavior similar to that found previously on cellular-PP ferroelectrets.[21] For the present samples, d_{33} remains nearly zero for charging voltages below 1 kV. Thereafter, d_{33} increases strongly with the charging voltage and reaches a saturation value of about 30 pC/N at about 2 kV.

It is known that the DBDs in ferroelectrets are accompanied by light emission that can be recorded with a digital camera. Figure 3(a) shows the spatially resolved light emission from a sample under a positively biased sinusoidal voltage with a peak-to-peak value V_{pp} of 3 kV and a frequency of 100 Hz. The image was recorded by means of a computer-controlled electron-multiplying charge-coupled-device camera (EM-CCD, iXon, Andor Technology). For the measurement, the sample was metalized on both sides with semitransparent Au electrodes. In order to block any light emission from corona discharges at the electrode edges, the sample was covered by a mask with a circular hole of 8.5 mm diameter. In the image, the honeycomb structure is clearly visible, while the difference between the light intensities of individual voids might be caused by small differences in the void parameters that cannot be avoided in the laboratory.

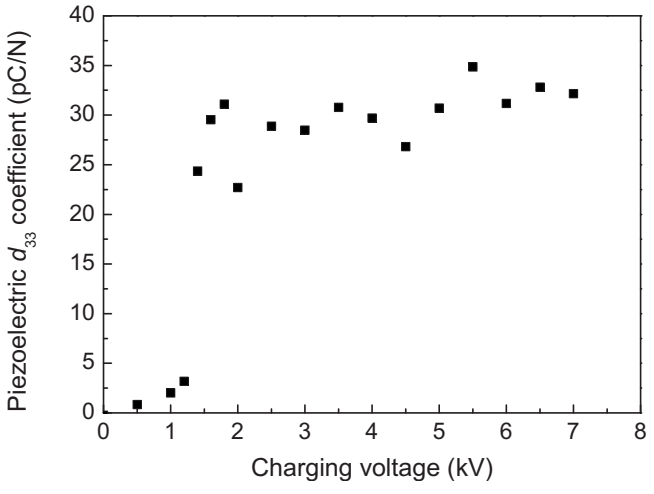

FIG. 2. The piezoelectric d_{33} coefficient of PC ferroelectrets as a function of the charging voltage.

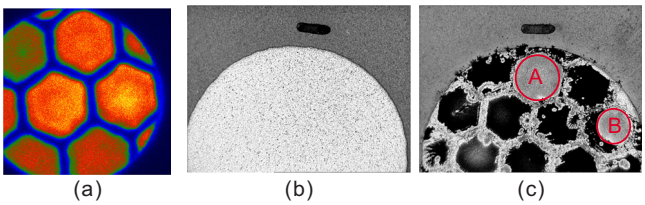

FIG. 3. (Color online) (a) Color-coded EM-CCD image of a PC ferroelectret with honeycomb voids under positive sinusoidal voltages. The EM-CCD camera was internally triggered with an exposure time of 5 s. (b) Digital photograph of the PC film serving as negatively charged internal void surface. The double-sided adhesive-tape template is removed after charging with a dc voltage of 3 kV for 30 s. The uniform aluminum electrode deposited on the other side of the film is clearly seen. (c) Toner pattern obtained by developing the latent charge image on the surface shown in (b) by means of xerographic toner. The negative charges deposited during the DBDs attract the toner, thus revealing the honeycomb void structure. Circles A and B represent areas with positive charges induced by back discharges.

In order to visualize the charge pattern deposited on the inner surfaces of the voids, an adhesive-tape template with its protective layers was used so that the PC films did not stick to the template. The PC-template-PC sandwich was charged with +3 kV for 30 s. According to a widely accepted model, the two internal surfaces of the charged voids carry positive and negative charges, respectively. After charging, the sandwich layers were separated, and the nonmetalized surface of the PC film whose electrode was connected with the positive side of the high voltage during charging was photographed [Fig. 3(b)]. The uniform aluminum electrode on the back side is seen through the transparent PC film. The latent charge image on the non-metallized surface of the PC film was developed with xerographic toner from a laser-printer cartridge, and a photograph was taken. The negative charges deposited during the DBDs attract the toner, thus exposing the honeycomb structure of the voids [Fig. 3(c)]. It is also seen in the figure that the surfaces of some of the voids (marked as circles A and B) did not attract the toner. With the same procedure, an inverse toner pattern was obtained on the other PC film, i.e., only the areas facing A and B attract the toner, while the other areas do not. Our results agree with the fact that the xerographic toner is positively charged.

The polarity reversal of areas A and B is attributed to back discharges during and after DBD charging (also known as choking effect in conventional DBDs). The internally deposited charges induce an electric field opposite to the externally applied one. Back discharges may be triggered when the charging voltage is turned off, leading to drastic reduction of the effective polarization and to a polarity reversal of some of the voids.[10]

The electric-field profiles in the resulting ferroelectret samples are mapped by means of TPT with a setup described in Ref. 16. For each beam pointing, the data from 30 laser-pulse experiments were averaged. A map of the electric-field distribution measured 87 days after charging is shown in Fig. 4. A rather high electric-field strength is seen very near to the electrode (depth $z=0.5$ μm from the laser-heated electrode). For depths beyond $z=1$ μm, however, the electric field does not change much with depth anymore. As can be seen from the figure, the honeycomb shapes of the voids are reproduced by the electric-field patterns. The difference between the

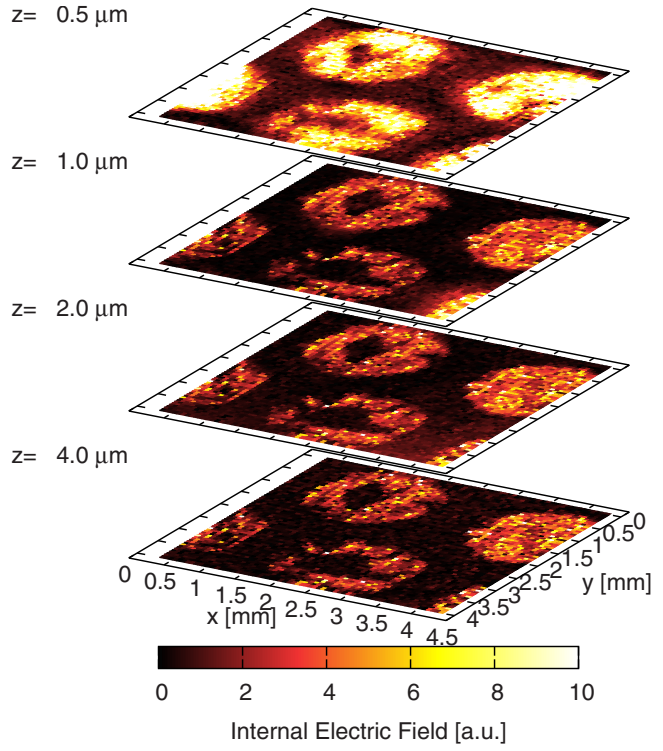

FIG. 4. (Color online) 3D electric-field profile in a three-layer PC-spacer-PC ferroelectret.

electric-field strengths at depths of z=0.5 and of 1 μm indicates a certain amount of space charge that partially compensates the electric field between the macroscopic dipoles and the electrode. The existence of this space-charge layer indicates a rather high conductivity of the PC films at high electric fields, while there seems to be a blocking layer near the electroded PC surface. The charge layer did stabilize the field distribution inside the sample so that it could still be recorded after almost three months.

Figure 4 also shows that the charge density is not always uniform across a honeycomb cell. Sometimes, the charge density is much higher near the edges of a honeycomb than at its center, which might be caused by void-height differences that cannot be avoided in the laboratory, but should be overcome in an industrial-scale production. Near the adhesive-tape stripes, there seems to be almost no charge. These observations probably indicate that both the internal surfaces of the polymer films at the top and the bottom of each void and the adhesive tape forming the side walls of the voids are too conductive for stable ferroelectret systems.

The relatively high conductivity of the double-sided adhesive tape was confirmed in surface-potential-decay measurements. A piece of the adhesive tape was charged in a point-to-grid corona setup with a point voltage V_p of 15 kV and a grid voltage V_g of 2 kV. A surface potential V_s of about 1 kV is found right after charging. Then the decay of the V_s was monitored under laboratory conditions. It is observed that V_s decreases to nearly zero within 10 min. Therefore, adhesive tape grids with lower conductivity as well as polymer films with better electret properties should be used in order to achieve ferroelectrets with higher stabilities of their piezoelectricity. Comprehensive information on the evolution of the electric field distribution in the polymer layers requires more detailed investigations. Other polymers as well as film systems with various void patters are under investigation.

In conclusion, ferroelectret systems have been fabricated by attaching two PC films to a double-sided adhesive-tape grid cut via a computer-controlled laser. The space-charge or effective-polarization patterns produced during charging by means of internal DBDs were demonstrated through exposure to xerographic toner and via three-dimensional mapping of the electric field by means of TPT, both revealing the honeycomb structure of the voids. From the electric-field profiles, we suspect that the charge stability on the top and bottom polymer films of the voids is deteriorated by conduction on and within the polymer films and the adhesive-tape stripes. Furthermore, it seems that a heterocharge layer may have formed near the top metalization of the electrode-poled three-layer PC-spacer-PC ferroelectrets because of the high conductivity of the polymer. Following and extending the early example of LIMM experiments on ferroelectrets,[13] it could thus be shown that TPT is a very useful method for investigating electric-field profiles at least in the uniform layers of ferroelectret systems and for drawing conclusions about space-charge distributions.

[1]R. Gerhard-Multhaupt, IEEE Trans. Dielectr. Electr. Insul. **9**, 850 (2002).
[2]S. Bauer, R. Gerhard-Multhaupt, and G. M. Sessler, Phys. Today **57**(2), 37 (2004).
[3]M. Wegener and S. Bauer, ChemPhysChem **6**, 1014 (2005).
[4]S. Bauer, IEEE Trans. Dielectr. Electr. Insul. **13**, 953 (2006).
[5]X. Qiu, J. Appl. Phys. **108**, 011101 (2010).
[6]K. Kirjavainen, "Electromechanical film and procedure for manufacturing same," U.S. Patent No. 4654 546 (March 31, 1987).
[7]J. Raukola, N. Kuusinen, and M. Paajanen, *Proceedings of the 11th International Symposium on Electrets, Melbourne*, Australia, 1–3 October 2002 (IEEE Service Center, Piscataway, NJ, 2002), pp. 195–198.
[8]A. Mellinger, M. Wegener, W. Wirges, R. Reddy Mallepally, and R. Gerhard-Multhaupt, Ferroelectrics **331**, 189 (2006).
[9]M. Lindner, S. Bauer-Gogonea, S. Bauer, M. Paajanen, and J. Raukola, J. Appl. Phys. **91**, 5283 (2002).
[10]X. Qiu, A. Mellinger, M. Wegener, W. Wirges, and R. Gerhard, J. Appl. Phys. **101**, 104112 (2007).
[11]M. Paajanen, H. Välimäki, and J. Lekkala, *Proceedings of the 10th International Symposium on Electrets*, Delphi, Greece, 22–24 September 1999 (IEEE Service Center, Piscataway, NJ, 1999), pp. 735–738.
[12]G. M. Sessler and J. Hillenbrand, Appl. Phys. Lett. **75**, 3405 (1999).
[13]J. van Turnhout, R. E. Staal, M. Wübbenhorst, and P. H. de Haan, *Proceedings of the 10th International Symposium on Electrets*, Delphi, Greece, 22–24 September 1999 (IEEE Service Center, Piscataway, NJ, 1999), pp. 785–788.
[14]J. Hillenbrand and G. M. Sessler, *Annual Report, Conference Electrical Insulation and Dielectric Phenomena*, Victoria, Canada, 15–18 October 2000 (IEEE Service Center, Piscataway, NJ, 2000), pp. 161–165.
[15]A. Mellinger, R. Singh, M. Wegener, W. Wirges, R. Gerhard-Multhaupt, and S. B. Lang, Appl. Phys. Lett. **86**, 082903 (2005).
[16]A. Mellinger, R. Flores-Suárez, R. Singh, M. Wegener, W. Wirges, R. Gerhard, and S. B. Lang, Int. J. Thermophys. **29**, 2046 (2008).
[17]R. Flores Suárez, A. Mellinger, M. Wegener, W. Wirges, R. Gerhard-Multhaupt, and R. Singh, IEEE Trans. Dielectr. Electr. Insul. **13**, 1030 (2006).
[18]C.-D. Pham, A. Petre, L. Berquez, R. Flores-Suárez, A. Mellinger, W. Wirges, and R. Gerhard, IEEE Trans. Dielectr. Electr. Insul. **16**, 676 (2009).
[19]R. F. Suárez, X. Qiu, L. Holländer, R. A. P. Altafim, W. Wirges, R. Gerhard, W. Jenninger, and J. Wagner, Annual Report, *Conference on Electrical Insulation and Dielectric Phenomena*, Virginia Beach, USA, 18–20 October 2009 (IEEE Service Center, Piscataway, NJ, 2009).
[20]R. A. P. Altafim, X. Qiu, W. Wirges, R. Gerhard, R. A. C. Altafim, H. C. Basso, W. Jenninger, and J. Wagner, J. Appl. Phys. **106**, 014106 (2009).
[21]M. Wegener, M. Paajanen, W. Wirges, and R. Gerhard-Multhaupt, *Proceedings of the 11th International Symposium on Electrets*, Melbourne, Australia, 1–3 October 2002 (IEEE Service Center, Piscataway, NJ, 2002), pp. 54–57.

Chapter 7

Conclusion

I- The polarization reversal in ferroelectric polyvinylidene fluoride copolymer with trifluoroethylene P(VDF-TrFE) films was measured with Thermal-Pulse Tomography. The depth-resolution was better than 0.5 µm, and a lateral resolution of 38 µm was previously reported. For the first time, there is a three-dimensional evidence of the inhomogeneous switching of polarization in films that supports the idea of a nucleation-growth process. Pinning of the layers near the electrode at depths of $z = 0.5$ µm may be related with an interaction between space charges and the crystalline domains of the PVDF-TrFE near the electrode. This behavior of having depolarized layers near the electrode surface has been reported previously with acoustic methods and is considered to be a typical characteristic of PVDF and its copolymers. Films whose thickness ranges between 300 and 400 nm and which exhibit this pinning have a bigger problem than those in the µm range.

II- After parallel measurements with the Focused Laser Intensity Modulation method (FLIMM) and the Thermal-Pulse Tomography (TPT) technique in copolymer films of PVDF having patterned electrodes, a qualitative similarity between the polarization maps was demonstrated. The advantage of implementing TPT was evident, since TPT is up to 50 times faster. Both methods are non-destructive and complement each other, however the claimed advantages of a higher lateral resolution with the FLIMM than with the TPT method, after a simple quantification of the polarization shape in one dimension, were not confirmed. Regardless of the method used for the data analysis, either Regularization or Scale transformation (ST), the qualitative information was the same. This shows TPT as the most reliable thermal technique for measuring polarization and space-charge profiles.

III-The TPT setup was improved by excluding spherical aberrations in the optics. This allows measurements with a laser-beam spot size down to 10 µm. The three-dimensional polarization imaging of liquid-crystal droplets (LCs) dispersed in a polymer matrix was partially successful. The in-depth information from TPT measurements was accurate. The minor axis of the droplets measured in images from scanning electron microscopy (SEM)

coincides with the one in the polarization distribution. Measuring LC droplets whose major axis is smaller than 10 µm, together with a strong electrostatic interaction between the ferroelectric matrix and the functional groups in the LC droplets, excludes the possibility of detecting single droplets. Instead, a density of droplets was observed. Nevertheless, the TPT method helped to realize that a strongly ferroelectric matrix is not optimal for preparing polymer-dispersed liquid crystals. The preparation of new composite films with a different polymer matrix and a compatible liquid crystal is out of the scope of this work, but is being performed elsewhere.

IV- Likewise, the electric field distribution measured with the TPT in a new multilayer ferroelectret system showed successfully the patterned macroscopic dipoles. An evident inhomogeneous space-charge distribution can be observed. The details in the TPT maps at different depths demonstrated a preferred accumulation of charges near the edges of every hexagonal structure. Besides, the presence of some space charges near the electrode area suggested a high conductivity of both the top and bottom polymer films and the adhesive material between them. This is a motivation to look for different materials and geometries in order to build a more stable and functional ferroelectret system.

V- The thermal probing can be improved if the metal electrodes are replaced by conductive polymers such as poly(3, 4−ethylenedioxythiophene) poly(styrenesulfonate) (PEDOT-PPS). A material-conserving deposition technique like inkjet printing is suggested for printing the organic electrodes. Another route to improve the profiling of charge and polarization distribution is directly connected to the data analysis. Thus, a general solution for the three-dimensional LIMM equation (considering the lateral thermal diffusion) should be developed. In this way, an increase in the lateral resolution is expected.

Bibliography

[1] J. van Turnhout. *Thermally* S*timulated discharge of* P*olymer* E*lectrets*. Elsevier, Amsterdam, 1975.

[2] S. B. Lang. Pyroelectricity: From ancient curiosity to modern imaging tool. *Physics Today (August)*, 58 (8):31–36, 2005.

[3] D. A. Berlincourt, D. R. Currand, and H. Jaffe. *Physical* A*coustics-*P*rinciples and* M*ethods. Vol. 1 Part A*. edited by W. P. Mason (Academic Press, New York), 1967.

[4] H. Kawai. The piezoelectricity of poly(vinylidene fluoride). *Japanese Journal of Applied Physics*, 8:975–976, 1969.

[5] T. Furukawa. Ferroelectric properties of vinylidene fluoride copolymers. *Phase Transitions*, 18:143–211, 1989.

[6] T. Nakajima, Y. Takahashi, and T. Furukawa. Intrinsic switching characteristics of ferroelectric ultrathin vinylidene fluoride/trifluoroethylene copolymer films revealed using Au electrode. *Japanese Journal of Applied Physics*, 44:L1385–L1388, 2005.

[7] F. S. Foster, K. A. Harasiewicz, and M. D. Sherar. A history of medical and biological imaging with polyvinylidene fluoride PVDF transducers. *IEEE Transactions on Ultrasonics, Ferroelectrics and Frecuency Control*, 47:1363–1371, 2000.

[8] G. R. Harris, R. C. Preston, and A. S. DeReggi. The impact of piezoelectric PVDF on medical ultrasound exposure measurements, standars, and regulations. *IEEE Transactions on Ultrasonics, Ferroelectrics and Frecuency Control*, 47:1321–1335, 2000.

[9] A. J. Tuzzolino, R. B. McKibben, J. A. Simpson, S. BenZvi, H. D. Voss, and H. Gursky. The space dust (SAPDUS) instrument aboard the earth-orbiting ARGOS spacecraft:I- instrument description. *Planetary and Space Science*, 49:689–703, 2001.

[10] A. J. Tuzzolino, R. B. McKibben, J. A. Simpson, S. BenZvi, H. D. Voss, and H. Gursky. The space dust (SAPDUS) instrument aboard the earth-orbiting ARGOS spacecraft:II- results from the first 16 months of flight. *Planetary and Space Science*, 49:705–729, 2001.

[11] H. S. Kitzerow. Polymer-dispersed liquid crystals. from the nematic curvilinear aligned phase to ferroelectric films. *Liquid Crystals*, 16:1–31, 1994.

[12] T. Koda, Y. Morito, and S. Ikeda. Liquid crystal droplets dispersed in ferroelectric copolymer vinylidene fluoride and trifluoroethylene. *Polymer Journal*, 33 (6):475–480, 2001.

[13] L. M. Ganesan, P. Frübing, A. Mellinger, and R. Gerhard. Dielectric relaxation behaviour of nematic liquid crystals dispersed in poly(vinylidene fluoride-trifluoroethylene). *Journal of Physics D: Applied Physics*, 42:092006, 2009.

[14] M. Wegener, M. Paajanen, W. Wirges, and R. Gerhard-Multhaupt. Corona-induced partial discharges, internal charge separation and electromechanical transducer properties in cellular polymer films. In *Proceedings of the 11th International Symposium on Electrets, Melbourne, Australia. IEEE Service Center, Piscataway, NJ*, pages 54–57, 2002.

[15] R. Gerhard-Multhaupt. Less can be more. Holes in polymers lead to a new paradigm of piezoelectric materials for electret transducers. *IEEE Transactions on Dielectrics and Electrical Insulation*, 9:850–859, 2002.

[16] S. Neugschwandtner, R. Schwödiauer, S. Bauer-Gogonea, S. Bauer, M. Paajanen, and J. Lekkala. Piezo- and pyroelectricity of a polymer-foam space-charge electret. *Journal of Applied Physics*, 89:4503–4511, 2001.

[17] S. Bauer, R. Gerhard-Multhaupt, and G. Sessler. Ferroelectrets: Soft electroactive foams for transducers. *Physics Today*, 57 (2):37–43, 2004.

[18] H. C. Basso, R. A. P. Altafim, R. A. C. Altafim, A. Mellinger, P. Fang, W. Wirges, and R. Gerhard. Three-layer ferroelectrets from perforated Teflon-PTFE films fused between two homogeneous Teflon-FEP films. In *2007 Annual report Conference on Electrical Insulation and Dielectric Phenomena (Vancouver, Canada, 2007)*, pages 453–456, 2007.

[19] S. Bauer and S. Bauer-Gogonea. Current practice in space charge and polarization profile measurements using thermal techniques. *IEEE Transactions on Dielectrics and Electrical Insulation*, 10:883–902, 2003.

[20] G. M. Sessler, J. E. West, and R. Gerhard-Multhaupt. Measurements of charge distribution in polymer electrets by a new Pressure-Pulse method. *Polymer Bulletin*, 6:109–111, 1981.

[21] W. Eisenmenger and M. Haardt. Observation of charge compensated polarization zones in polyvinylindenefluoride (PVDF) films by piezoelectric acoustic step-wave response. *Solid State Communications*, 41 (12):917–920, 1982.

[22] S. B. Lang and D. K. Das-Gupta. A technique for determining the polarization distribution in polymer electrets using periodic heating. *Ferroelectrics*, 39:1249–1252, 1981.

[23] R. E. Collins. Distribution of charge in electrets. *Applied Physics Letters*, 26:675–677, 1975.

[24] D. Marty-Dessus, L. Berquez, A. Petre, and J. L. Franceschi. Space charge cartography by FLIMM: a three dimensional approach. *Journal of Physics D: Applied Physics*, 35:3249–3256, 2002.

[25] A. Mellinger, R. Singh, M. Wegener, W. Wirges, R. Gerhard-Multhaupt, and S. B. Lang. Three-dimensional mapping of polarization profiles with thermal pulses. *Applied Physics Letters*, 86:082903–1–3, 2005.

[26] A. S. DeReggi, C. M. Guttman, F. I. Mopsik, G. T. Davis, and M. G. Broadhusrt. Determination of charge or polarization distribution across polymer electrets by the thermal pulse mehod and Fourier analysis. *Physical Review Letters*, 40:413–416, 1978.

[27] H. von Seggern. Thermal-pulse technique for determining charge distributions: effect of measurement accuracy. *Applied Physics Letters*, 33:134–137, 1978.

[28] S. B. Lang and D. K. Das-Gupta. A new technique for determination of the spatial distribution of polarization in polymer electrets. *Ferroelectrics*, 60:23–36, 1984.

[29] R. Emmerich, S. Bauer, and B. Ploss. Temperature distribution in a film heated with a laser spot: Theory and measurements. *Applied Physics A*, 54:334–339, 1992.

[30] S. B. Lang. Laser intensity modulation method (LIMM): review of the fundamentals and a new method for data analysis. *IEEE Transactions on Dielectrics and Electrical Insulation*, 11:3–12, 2004.

[31] E. Tuncer and S. B. Lang. Numerical extraction of distributions of space-charge and polarization from laser intensity modulation method. *Applied Physics Letters*, 86:071107–1–3, 2005.

[32] R. J. Fleming. Space-charge profile measurements techniques: recent advances and future directions. *IEEE Transactions on Dielectrics and Electrical Insulation*, 12:967–978, 2005.

[33] S. B. Lang. A 2400 year history of pyroelectricity: from ancient Greece to exploration of the solar system. *British Ceramics Transactions*, 103:65–70, 2004.

[34] B. Dickens, E. Balizer, A. S. DeReggi, and S. C. Roth. Hysteresis measurements of remanent polarization and coercive field in polymers. *Journal of Applied Physics*, 72:4258–4264, 1992.

[35] H. Ohigashi and T. Hattori. Improvement of piezoelectric properties of poly(vinylidene fluoride) and its copolymers by crystallization under high pressures. *Ferroelectrics*, 171:11–32, 1995.

[36] E. Fukada and T. Sakurai. Piezoelectricity in polarized poly(vinylidene fluoride) films. *Polymer Journal*, 2:656–662, 1971.

[37] K. Tashiro, H. Tadokoro, and M. Kobayashi. Structure and piezoelectricity of poly(vinylidene fluoride). *Ferroelectrics*, 32:167–175, 1981.

[38] C. J. Constantino, A. E. Job, R. D. Simoes, J. A. Giacometti, V. Zucolotto, O. N. Oliveira Jr., G. Gozzi, and D. L. Chinaglia. Phase transition in poly(vinylidene fluoride) investigated with micro-Raman spectroscopy. *Applied Spectroscopy*, 59:275–279, 2005.

[39] T. Furukawa, H. Matsuzaki, M. Shiina, and Y. Tajitsu. Nanosecond switching in thin films of vinylidene fluoride trifluoroethylene copolymers. *Japanese Journal of Applied Physics*, 24:L661–L662, 1985.

[40] S. Sakai, M. Date, and T. Furukawa. Development of polarization distribution in fatigued films of ferroelectric vinylidene fluoride/trifluoroethylene copolymer. *Japanese Journal of Applied Physics*, 41:3822–3828, 2002.

[41] T. Furukawa, S. Kanai, A. Okada, Y. Takahashi, and R. Yamamoto. Ferroelectric switching dynamics in VDF/TrFE copolymer thin films spin coated on Si substrate. *Journal of Applied Physics*, 105:061636, 2009.

[42] M. Wegener and S. Bauer. Microstorms in Cellular Polymers: A Route to Soft Piezoelectric Transducer Materials with Engineered Macroscopic Dipoles. *Journal of Chemical Physics and Physical Chemistry*, 6 (6):1014–1025, 2005.

[43] S. Bauer. Pyro-, piezo- and ferroelectrets: SOft transducer materials for electromechanical energy conversion. *IEEE Transactions on Dielectrics and Electrical Insulation*, 13:953–962, 2006.

[44] X. Qiu. Patterned piezo-, pyro-, and ferroelectricity of poled polymer electrets. *Journal of Applied Physics*, 108 (1):011101, 2010.

[45] K. Kirjavainen. Electromechanical film and procedure for manufacturing same. U.S. Patent No. 4654 546 (March 31), 1987.

[46] J. Raukola, N. Kuusinen, and M. Paajanen. Cellular electrets: from polymer granules to electromechanically active films. In *Proceedings of the 11th International Symposium on Electrets. Melbourne, Australia. (IEEE Service Center, Piscataway, NJ)*, pages 195–198, 2002.

[47] J. Hillenbrand and G. M. Sessler. *Piezoelectric properties of polypropylene/air and poly(vinylidene fluoride)/air composites.* IEEE Conf. Electr. Insul. Dielectr. Phenomena, Piscataway, NJ: IEEE Service Center, pages 161-165, 2000.

[48] M. Lindner, S. Bauer-Gogonea, S. Bauer, M. Paajanen, and J. Raukola. Dielectric barrier microdischarges: Mechanism for the charging of cellular piezoelectric polymers. *Journal of Applied Physics*, 91:5283–5287, 2002.

[49] J. van Turnhout, R. E. Staal, M. Wübbenhorst, and P. H. de Haan. Distribution and stability of charges in porous polypropylene films. In *Proceedings, 10th International Symposium on Electrets, IEEE Service Center, Piscataway, NJ*, pages 785–788, 1999.

[50] X. Qiu, A. Mellinger, M. Wegener, W. Wirges, and R. Gerhard. Barrier discharges in cellular polypropylene ferroelectrets: How do they influence the electromechanical properties? *Journal of Applied Physics*, 101:104112, 2007.

[51] J. Lewiner, S. Hoé, and T. Ditchi. Pressure wave propagation methods: a rich history and a bright future. *IEEE Transactions on Dielectrics and Electrical Insulation*, 12:114–126, 2005.

[52] G. M. Sessler. Charge distribution and transport in polymers. *IEEE Transactions on Dielectrics and Electrical Insulation*, 4:614–628, 1997.

[53] A. G. Rozno and V. V. Gromov. Measurements of the space-charge distribution in a solid dielectric. *Soviet Technical Physics Letters*, 5:266–267, 1979.

[54] M. Haardt and W. Eisenmenger. High-resolution technique for measuring charge and polarization distributions in dielectrics by Piezoelectrically Induced Pressure Step Waves. *1982 Annual Report, Conference on Electrical Insulation and Dielectric Phenomena*, pages 46–51, 1982.

[55] T. Takada, T. Maeno, and H. Kushibe. An electrical stress Pulse technique for the measurement of charges in a plastic plate irradiated by an Electron Beam. In *Proceedings of the 5th International Symposium of Electrets, ISE (Heidelberg, Germany 1985)*, pages 450–453, 1985.

[56] T. Maeno, H. Kushibe, T. Takada, and C. M. Cooke. Pulse Electo-Acoustic method for the measurement of volume charges in E-Beam irradiated PMMA. *1985 Annual Report, Conference on Electrical Insulation and Dielectric Phenomena*, pages 389–397, 1985.

[57] G. M. Sessler. *Distribution and transport of charge in polymers.* in R. Gerhard-Multhaupt (ed.) Electrets, 3rd ed. Vol. 2, Laplacian Press, 1998.

[58] G. M. Sessler, J. E. West, and R. Gerhard-Multhaupt. High-resolution Laser-Pulse method for measuring charge distributions in dielectrics. *Physical Review Letters*, 48:563–566, 1982.

[59] J. B. Bernstein. Improvements to the Electrically Stimulated Acoustic Wave method for analyzing bulk space charge. *IEEE Transactions on Dielectrics and Electrical Insulation*, 27:152–161, 1992.

[60] T. Maeno and K. Fukunaga T. Takada. High-resolution PEA charge distribution measurement system. *1984 Annual Report, Conference on Electrical Insulation and Dielectric Phenomena*, pages 200–205, 1994.

[61] T. Maeno and K. Fukunaga. High-resolution PEA charge distribution measurement system. *IEEE Transactions on Dielectrics and Electrical Insulation*, 3:754–757, 1996.

[62] M. Wegener and R. Gerhard-Multhaupt. Electric poling and electromechanical characterization of 0.1-mm-thick sensor films and 0.2-mm-thick cable layers from piezoelectric poly(vinylidene fluoride-trifluoroethylene). *IEEE Transactions on Ultrasonics, and Ferroelectrics Insulation*, 11:255–263, 2004.

[63] R. Gerhard-Multhaupt, W. Künstler, G. Eberle, W. Eisenmenger, and G. Yang. *High space-charge densities in the bulk of fluoropolymer electrets detected with piezoelectrically generated pressure steps.* J. C. Fothergill and L. A. Dissado (eds.) Space Charge in Solid Dielectrics. pp. 123-132. The Dielectric Society, 1997.

[64] R. E. Collins. Practical applications of the thermal pulsing technique to he study of electrets. *Journal of Applied Physics*, 51:2973–2986, 1980.

[65] A. Mellinger, R. Singh, and R. Gerhard-Multhaupt. Fast thermal-pulse measurements of space-charge distribution in electret polymers. *Review of Scientific Instruments*, 76:013903, 2005.

[66] F. I. Mopsik and A. S. DeReggi. Numerical evaluation of the dielectric polarization distribution from thermal-pulse data. *Journal of Applied Physics*, 53:4333–4339, 1982.

[67] S. B. Lang and D. K. Das-Gupta. Laser-intensity modulation method: A technique for determination of spatial distributions of polarization and space charge in polymer electrets. *Journal of Applied Physics*, 59:2151–2160, 1986.

[68] R. Flores Suárez and C-H. Yin. Advanced laboratory. Electrical and Optical Properties Laboratory: Pyroelectric Depth Profiles, June 2004.

[69] S. Bauer and B. Ploss. A method for measurement of the thermal, dielectric, and pyroelectric properties of thin pyroelectric films and their applications for integraded heat sensors. *Journal of Applied Physics*, 68:6361–6367, 1990.

[70] D. K. Das-Gupta and J. S Hornsby. Laser-intensity modulation method (LIMM)-an analytical and numerical modification. *IEEE Transactions on Electrical Insulation*, 26:63–68, 1991.

[71] B. Ploss. The resolution of thermal profiling techniques. In *11th International Symposium on Electrets (ISE 11) Proceedings,(Melbourne, Australia, 2002)*, pages 177–180, 2002.

[72] B. Ploss, W. Hassler, H. Hulz, and G. Kobernik. Investigation of the polarization depth distribution of PZT thick films by LIMM. In *Proceedings of the 11th IEEE International Symposium on Applications of Ferroelectrics, ISAF XI (Montreux, Switzerland 1998)*, pages 207–210, 1998.

[73] X. Qin, K. Suzuki, Y. Tanaka, and T. Takada. Three-dimensional space charge measurement in a dielectric using the acoustic lens and PWP method. *Journal of Physics D: Applied Physics*, 32:15–160, 1999.

[74] T. Maeno. Three-dimensional PEA charge measurement system. *IEEE Transactions on Dielectrics and Electrical Insulation*, 8:845–848, 2001.

[75] A. Petre, D. Marty-Dessus, L. Berquez, and J. L. Franceschi. A comparison of different mathematical treatments for solving the inverse problem in Focused Laser Intensity Modulation Method. *Japanese Journal of Applied Physics*, 43:2572–2579, 2004.

[76] A. Petre, D. Marty-Dessus, L. Berquez, and J. L. Franceschi. Space charge cartographies by FLIMM on thin PTFE films irradiated by Scanning Electron Microscope. *Journal of Electrostatics*, 64:492–497, 2006.

[77] P. C. Hansen and D. P. O'Leary. The use of the L-curve in the regularization of discrete ill-posed problems. *SIAM Journal on Scientic Computing*, 14:1487–1503, 1992.

[78] A. van der Ziel. Pyroelectric response and D^* of thin pyroelectric films on a substrate. *Journal of Applied Physics*, 44:546–549, 1973.

[79] M. Frigo and S. G. Johnson. The design and implementation of FFTW3. In *Proceedings in IEEE*, volume 93, pages 216–231, 2005.

[80] B. Ploss, R. Emmerich, and S. Bauer. Thermal wave probing of pyroelectric distributions in the surface region of ferroelectric materials: A new method for the analysis. *Journal of Applied Physics*, 72:5363–5370, 1992.

[81] A. Mellinger. Unbiased iterative reconstruction of polarization and space-charge profiles from thermal-wave experiments. *Measurement Science and Technology*, 15:1347–1353, 2004.

[82] S. B. Lang and E. Tuncer. Comparison of techniques for solving the Laser Intensity Modulation Method (LIMM) equation. *Journal of Electroceramics*, 21:827–830, 2008.

[83] S. B. Lang and R. Fleming. A comparison of three techniques for solving the Fredholm integral equation of the Laser Intensity Modulation Method (LIMM). *IEEE Transactions on Dielectrics and Electrical Insulation*, 16:809–814, 2009.

[84] G. Eberle, E. Bihler, and W. Eisenmenger. Polarization dynamics of VDF-TrFE copolymers. *IEEE Transactions on Dielectrics and Electrical Insulation*, 26:69–77, 1991.

[85] S. Bauer, G. Eberle, W. Eisenmenger, and H. Schlaich. Second-harmonic generation with partially poled polymers. *Optics Letters*, 18 (1):16–18, 1993.

[86] T. Nakajima, Y. Takahashi, and T. Furukawa. Pulse train measurement of ferroelectric switching in thin films of vinylidene fluoride/trifluoroethylene copolymer. *Applied Physics A: Materials Science and Processing*, 91:33–39, 2008.

[87] M. Young. *Optics and Lasers. Including fibers and optical waveguides*. Springer-Verlag, 4th edition, 1993.

[88] B. N. Chichkov, C. Momma, S. Nolte, F. von Alvensleben, and A. Tünnermann. Femtosecond, picosecond and nanosecond laser ablation of solids. *Applied Physics A: Material Science Processing*, 63:109–115, 1996.

[89] V. H. Schmidt, L. Lediaevand J. Polasik, and J. Hallenberg. Piezoelectric actuators employing PVDF coated with flexible PEDOT-PPS polymer electrodes. *IEEE Transactions on Dielectrics and Electrical Insulation*, 13:1140–1148, 2006.

[90] R. C. Jaeger. *Lithography: Introduction to* M*icroelectronic* F*abrication*. Prentince Hall, Upper Saddle Middle River, New Jersey USA, 2nd edition, 2002.

[91] H. J. Levinson. *Principles of Lithography*. SPIE PRESS, Bellingham, Washington USA, first printing edition, 2001.

[92] E. Tekin, P. J. Smith, and U. S. Schubert. Inkjet printing as a deposition and patterning tool for polymers and inorganic particles. *Soft Matter*, 4:703–713, 2008.

[93] J. A. Lim, J. H. Cho, Y. D. Park, D. H. Kim, M. Hwang, and K. Cho. Solvent effect of inkjet printed source/drain electrodes on electrical properties of polymer thin-film transistors. *Applied Physics Letters*, 88:082102, 2006.

[94] J. Doggart, Y. Wu, P. Liu, and S. Zhu. Facile inkjet-printing self-aligned electrodes for organic thin-film transistors arrays with small and uniform channel length. *Applied Materials and Interfaces*, 2:2189–2192, 2010.

[95] M. Singh, H. M. Haverinen, P. Dhagat, and G. E. Jabbour. Inkjet Printing– Process and Applications. *Advanced Materials*, 22:673–685, 2010.

[96] R. Flores Suárez, X. Qiu, L. Holländer, R. A. P. Altafim, W. Wirges, and R. Gerhard. Annular space-charge rings in ferroelectrets with perforated central layers: Mapping of the resulting electric-field profiles by means of Thermal-Pulse Tomography (TPT). In *Proceedings Conference on Electrical Insulation and Dielectric Phenomena, IEEE Service Center, Piscataway, NJ*, pages 1–4, 2009.

[97] R. Flores Suárez. Polarization profiles in poled PVDF sensor cables. Master's thesis, Institute of Physics and Astronomy, University of Potsdam, Germany, 2005.

[98] M. R Spiegel and J. Liu. *Schaum's Mathematical Handbook of Formulas and Tables*. McGraw-Hill, 1999.

[99] M. Wegener, J. Hesse, T. Wegener, and R. Gerhard-Multhaupt. Patterned ferro-, pyro- and piezoelectricity in poly(vinylidene fluoride) by means of a laser-induced irreversible β to α phase transformation. *Journal of Applied Physics*, 91:3193–3196, 2002.

Appendix A

Ablation threshold

Mellinger et al. [65] observed damage in the metal electrode when high laser fluence (energy per area) was used to obtain data from the Thermal-Pulse Tomography. Therefore, a detailed inspection was carried out on evaporated aluminum electrodes on a homogeneously corona-charged PVDF film [97]. The experimental data were analyzed using the regularization method and the L-curve method. The resulting pyroelectric coefficient, at a depth $z = 3$ µm, was plotted as a function of the x position, at different laser-energy settings. Since the laser settings are not absolute values, a conversion curve was needed (Fig.A.1 left). The generated profiles show the transition between the poled and the non-poled region of the sample (Fig.A.1 right). A homogeneous polarization along the scanned line can be observed at a fixed energy. The detection sensitivity of the TPT method increases evidently with the laser power.

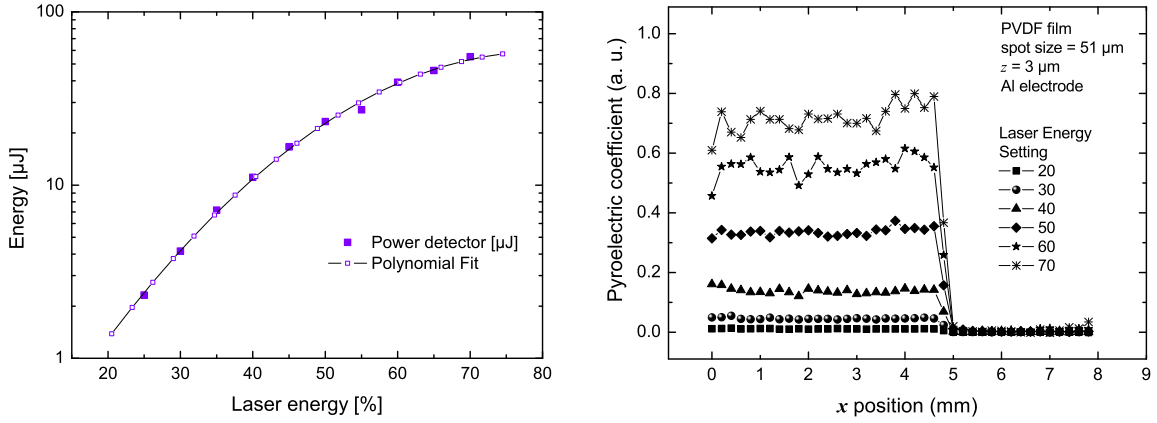

Figure A.1: Energy conversion curve and profiles of polarization at different laser pulse energies from PVDF film coated with an Al electrode

Let us consider the laser-beam as a Gaussian curve. This assumption is possible since there is a spatially filtering by means of lenses and a small iris apperture [87]. Thus, the energy fluence Φ can be written as:

$$\Phi(r) = \Phi_0 \exp\left\{-2\left(\frac{r}{r_0}\right)^2\right\} \tag{A.1}$$

r is the radius position and r_0 is the beam waist. The total laser pulse energy U is expressed as

$$U = \int_0^\infty \Phi(r) 2\pi r dr. \tag{A.2}$$

If $2r_0 = W = laser - beamspotsize$ and by substituting (A.1) in (A.2), then

$$U = \Phi_0 2\pi \int_0^\infty r \exp\left(-\frac{8}{W^2} r^2\right) dr. \tag{A.3}$$

To solve the integral in equation (A.3) we use [98]:

$$\int_\infty^0 r^m exp\left(ar^2\right) dr = \frac{\Gamma\left(\frac{m+1}{2}\right)}{2a^{\frac{m+1}{2}}} \tag{A.4}$$

If $m = 1$ then $\Gamma(1) = 1$, and the energy U is

$$U = \frac{\Phi_0 \pi W^2}{8} \tag{A.5}$$

with $W = 51$ µm. On the other hand, the energy U is also expressed in terms of the absorption coefficient η of the electrodes, the area A and the peak fluence Φ_0, these values can be deduced from reflectivity values at 532 nm (A.6). And U is a function also of the temperature in the electrode ΔT, the heat capacity c, and the density ρ of the metal electrode (A.7).

$$U = \eta \Phi_0 A \tag{A.6}$$

$$U = c\rho A d \Delta T \tag{A.7}$$

Then, by combining (A.6) and (A.7), the temperature in the electrode is:

$$\Delta T = \frac{\eta \Phi_0}{c\rho h}. \tag{A.8}$$

The averaged pyroelectric signal from the plateau (from 0 mm to 5.5 mm in x position) in Fig A.1 was plotted as a function of the peak energy fluence Φ_0, which was calculated using equation A.5 (Fig. A.2 left).

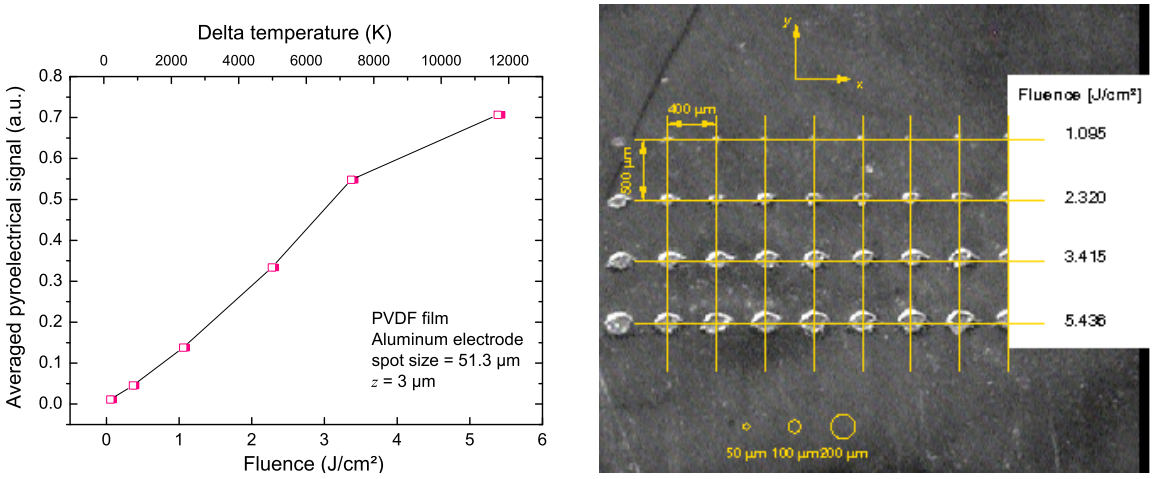

Figure A.2: Averaged pyroelectric signal in a PVDF film as a function of the peak energy fluence and temperature increment at the Al electrode. Ablation on a PVDF film coated with an Al electrode.

The plotted curves show a linear increase until $\Phi_0 \approx 0.5$ J/cm^2. No ablation is caused in the electrode up to these peak energy fluence values. However, beyond the linear behavior of the averaged pyroelectric signal, ablation occurs on Al electrodes; holes less than 50 µm in diameter appear in the electrode at $\Phi_0 \approx 1$ J/cm^2 (Fig. A.2 right). It must be remarked that a better signal-to-noise ratio in the polarization distribution profiles is achieved when higher values of peak fluence are reached or electrodes with higher absorption coefficient are used [65]. Mellinger et al. suggested a possible damage on the polymer surface layers near the irradiated electrode. This can be confirmed by means of the calculated temperature rise in the Al electrode (Fig. A.2 left). At the temperatures at which the ablation occurs (∼2300 K) the polymer layer near to the electrode is already melted (T_m = 480 K for PVDF). Wegener et al. [99] reported that for a laser irradiated PVDF films, a phase transition from β to α and therefore a loss of polarization can occur. Thus, some layers near the irradiated electrode could be depolarized. Based on these arguments, it is possible to find a compromise between a good signal-to-noise ratio and non-damage polymer samples by using Al electrodes.

Glossary

Notation	Description
A	electroded area
D	thermal diffusivity: $D = \kappa/c\rho$
$D\tau_L$	square of heat-difussion length
E	electric field
$E_{\mathbf{c}}$	coercive field
$I(t)$	short circuit pyroelectric current
N	number of recorded data points during a meaurement
$P_{\mathbf{r}}$	remanent polarization
$P_{\mathbf{s}}$	spontaneous polarization
T	temperature
$T_{\mathbf{c}}$	Curie temperature
$T_{\mathbf{g}}$	glass transition temperature
$V_{\mathbf{th}}$	threshold voltage
V_c	charging voltage
V_{pp}	peak-to-peak amplitude of voltage
Δt	sampling interval during a measurement
Ω	specific enthalpy
Φ	energy fluence
Φ_{th}	ablation threshold $= \rho\Omega\sqrt{D\tau_L}$
α	TGT$\overline{G}$ conformation, amorphous phase of the polyvinylidene fluoride
$\alpha_{\mathbf{p}}$	relative temperature dependence of the polarization: $\alpha_{\mathrm{p}} = (1/P)dP/dT$
$\alpha_{\mathbf{z}}$	relative thermal expansion coefficient in the z direction: $\alpha_{\mathrm{z}} = (1/z)dz/dT$
α_ϵ	relative temperature dependence of the permittivity: $\alpha_\epsilon = (1/\epsilon)d\epsilon/dT$
β	TT conformation, polar phase phase of the polyvinylidene fluoride
ϵ	permittivity of the sample material
ϵ_0	permittivity of the vacuum
η	absorption coefficient

Notation	Description
$\eta(r)$	roughness residual
γ	$T_3GT_3\overline{G}$ conformation, polar phase phase of the polyvinylidene fluoride
κ	thermal conductivity
λ_i	coefficients from a polynomial; $i = 1...8$
μ	dipole moment
ω	angular frequency
$\partial Q/\partial T$	change of surface charge after a temperature change
$\phi(r)$	fit residual
ρ	density
σ	elastic stress
$\sigma_{\mathbf{eff}}$	effective charge density
τ_L	laser-pulse duration
τ_i	lattice heating time
$\widetilde{j}e^{i\omega t}$	light intensity
$\widetilde{I}$	complex amplitude of the pyroelectric current; $\Re$: real and $\Im$: imaginary part
$\widetilde{J}(f_n)$	pyroelectric current in the frequency domain
$\widetilde{J}_{\mathbf{calc}}$	calculated pyroelectric current
$\widetilde{J}_{\mathbf{exp}}$	measured pyroelectric current
$\widetilde{T}$	complex temperature amplitude
$\widetilde{\alpha}$	gain spectrum from the preamplifier
$c\rho$	heat capacity per volume
d	sample thickness
d_{33}	piezoelectric coefficient
f_n	frequency points
$f_a(z, z_r)$	normalized scanning function with the expectation value x_r for the pyroelectric coefficient
k	complex thermal-wave-vector $= (1 + i)k_r$
k_r	magnitude of $k = 1/z_r$
p	pyroelectric coefficient
p_a	approximation function for the distribution of the pyroelectric coefficient
r	weight factor, regularization parameter
$r(z)$	polarization distribution function (due to space charges and/or polarization)
t	time
z	coordinate that corresponds to the sample thickness direction
z_i	spatial coordinates of the surfaces of the sample; $i = 1, 2$

Notation	Description
$BaTiO_3$	Barium titanate
EMCCD	Electron-Multiplying Charge-Coupled Device
FEP	Fluorinated ethylene-propylene copolymer
NaOH	Sodium hydroxide
P(VDF-TrFE)	Copolymer of polyvinylidene fluoride and trifluoroethylene
PE	Polyethylene
PEDOT-PPS	Poly$(3,4-$ethylenedioxythiophene) poly(styrenesulfonate)
PMMA	Polymethylmetacrylate
PP	Polypropylene
PTFE	Teflon: Polytetrafluoroethylene
PVDF	Polyvinylidene fluoride
PZT	Lead-zirconate-titanate: $Pb(Zr_{0.95}Ti_{0.05}O_3)$
PZTPMN	Lead zirconate titanate-lead magnesium niobate: $Pb[Zr_{1-x}Ti_x]O_3$-$PbMg_{1/3}Nb_{2/3}O_3$

Publications

Parts of this work have been published in journals, conference proceedings as well as presented in the listed conferences as oral presentation or poster. The main publications were included in this Thesis; please refer to the corresponding pages.

Journal Articles

Polarization from dielectric-barrier discharges in ferroelectrets: Mapping of the electric-field profiles by means of Thermal-Pulse Tomography

X. Qiu; L. Holländer; R. Flores Suarez; W. Wirges and R. Gerhard
Applied Physics Letters,
Vol. 97, 072905-1-3 (2010) (ref. to pages 91-93 in Thesis)

Imaging liquid crystals dispersed in a ferroelectric polymer matrix using Thermal-Pulse Tomography

R. Flores Suarez; L. M. Ganesan; W. Wirges; A. Mellinger and R. Gerhard
IEEE Transactions on Dielectrics and Electrical Insulation,
Vol. 17, 1123-1127 (2010) (ref. to pages 84-88 in Thesis)

3D High-resolution mapping of polarization profiles in thin poly(vinylidenefluoride-trifluoroethylene) (PVDF-TrFE) films using two thermal techniques

C.-D. Pham; A. Petre; L. Berquez; R. Flores Suarez; A. Mellinger
W. Wirges and R. Gerhard
IEEE Transactions on Dielectrics and Electrical Insulation,
Vol. 16, 676-681 (2009) (ref. to pages 70-75 in Thesis)

Thermal-Pulse Tomography of space-charge and polarization distributions in electret polymers

A. Mellinger; R. Flores Suarez; R. Singh, M. Wegener; W. Wirges
R. Gerhard and S. B. Lang
International Journal of Thermophysics,
Vol. 29, 2046-2054 (2008) (ref. to pages 51-59 in Thesis)

Zerstörungsfreie Tomographie von Raumladungs- und Polarisationsverteilungen mittels Wärmepulsen

A. Mellinger; R. Flores Suarez; R. Singh; M. Wegener;
W. Wirges and R. Gerhard-Multhaupt
tm-Technisches Messen,
Vol. 74, 437-444 (2007) (ref. to pages 29-36 in Thesis)

Thermal-Pulse Tomography of polarization distributions in a cylindrical geometry

R. Flores Suarez; M. Wegener; W. Wirges; A. Mellinger
R. Gerhard-Multhaupt and R. Singh
IEEE Transactions on Dielectrics and Electrical Insulation,
Vol. 13, 1030-1035 (2006) (ref. to pages 23-28 in Thesis)

Publications in Conference Proceedings

Annular space-charge rings in ferroelectrets with perforated central layers: Mapping of the resulting electric-field profiles by means of Thermal-Pulse Tomography (TPT)

R. Flores Suarez; X. Qiu; L. Holländer; R. A. P. Altafim; W. Wirges
R. Gerhard; W. Jenninger and J. Wagner
Annual Report, IEEE Conference on Electrical Insulation
and Dielectric Phenomena (2009),
IEEE Service Center, Piscataway, NJ.

High-resolution space-charge and polarization tomography with thermal pulses

A. Mellinger; R. Flores Suarez; R. Singh; M. Wegener; W. Wirges
S. B. Lang and R. Gerhard-Multhaupt
Tagungsband der ITG/GMA-Fachtagung "Sensoren und Messsysteme"
(VDE Verlag GmbH, Offenbach 2006), pp. 511-514 (2006)
Die Arbeit wurde am 13.03.2006 mit dem "Best Paper Award" des deutschen
IEEE Instrumentation and Measurement (I&M) Chapter ausgezeichnet

High-resolution three-dimensional space-charge and polarization mapping with thermal pulses

A. Mellinger; R. Singh; M. Wegener; W. Wirges; R. Flores Suarez
S. B. Lang; L. F. Santos and R. Gerhard-Multhaupt
12th International Symposium on Electrets (ISE 12), Proceedings, 212 (2005)

Conference Presentations

Annular space-charge rings in ferroelectrets with perforated central layers: Mapping of the resulting electric-field profiles by means of the Thermal-Pulse Tomography (TPT)

R. Flores Suarez; X. Qiu; L. Holländer; R. A. P. Altafim; W. Wirges; R. Gerhard; W. Jenninger and J. Wagner.
Presented as a **poster** by R. Gerhard on October 18-21, 2009.
IEEE Conference on Electrical Insulation and Dielectric Phenomena (CEIDP), Virginia Beach, USA.

Time- and frequency-domain polarization imaging on poly(vinylidene fluoride-trifluoroethylene) films

R. Flores Suarez; A. Mellinger; W. Wirges R. Gerhard-Multhaupt and C.-D. Pham A. Petre; L. Berquez; and D. Marty Dessus.
Presented as a **talk** by R. Flores Suarez on August 26-29, 2008.
5th International Conference on Dielectric and Related Phenomena and 10th Conference on Dielectric and Related Phenomena (IDS and DRP), Lyon, France.

High-Resolution Imaging of a Defined Polarization Pattern un PVDF Films using Thermal-Pulse Tomography

R. Flores Suarez; A. Mellinger; W. Wirges and R. Gerhard.
Presented as a **poster** by R. Flores Suarez on September 3-7, 2007.
11th European Meeting on Ferroelectricity (EMF),
Bled, Slovenia, 2007

Thermal-Pulse Tomography: A Tool to perform 3D Mapping of Polarization profiles and Polarization Switching Processes

R. Flores Suarez; A. Mellinger; M. Wegener; W. Wirges; and R. Gerhard-Multhaupt
Presented as a **poster** by R. Flores Suarez on September 3-7, 2006.
4th International Conference on Dielectric and Related Phenomena and 9th Conference on Dielectric and Related Phenomena (IDS and DRP), Poznan, Poland, 2006

Pyroelectric Tomography: Non destructive 3D Mapping of Polarization Profiles in Poled Polyvinylidene Fluoride Copolymer Sensor Cables

R. Flores Suarez; M. Wegener; W. Wirges and A. Mellinger.
Presented as a **poster** by R. Flores Suarez on March 26-31, 2006.
Deutsche Physikalische Gesellschaft (DPG),
Dresden, Germany 2006